The Journal of
Gemmology
2013 / Volume 33 / Nos. 5–6

The Gemmological Association of Great Britain

The Gemmological Association of Great Britain

21 Ely Place, London EC1N 6TD, UK
T: +44 (0)2 0 7404 3334 **F:** +44 (0)20 7404 8843
E: information@gem-a.com **W:** www.gem-a.com

Registered Charity No. 1109555
Registered office: Palladium House, 1–4 Argyll Street, London W1F 7LD

The Journal of Gemmology

The Editor is glad to consider original articles shedding new light on subjects of gemmological interest for publication in *The Journal of Gemmology*. A guide to the preparation of typescripts for publication in *The Journal* is given on our website, or contact the Production Editor at the Gemmological Association of Great Britain.

Any opinions expressed in *The Journal of Gemmology* are understood to be the views of the contributors and not necessarily of the publishers.

The Journal of Gemmology / 2013 / Volume 33 / No. 5–6

Synthetic alexandrites grown by the HOC method in Russia: internal features related to the growth technique and colorimetric investigation

Dr Karl Schmetzer, Dr Heinz-Jürgen Bernhardt, Walter A. Balmer and Thomas Hainschwang

Abstract: Mineralogical and gemmological properties of synthetic alexandrites grown by the horizontally oriented crystallization (HOC) method are described. The method is used to grow crystal plates weighing up to 450 g. The morphology of the rough crystals is dependent on the form of the molybdenum boat used as a container for crystal growth. The most significant inclusions for gem identification are curved growth striations and flat, irregularly-shaped somewhat elongated cavities. Microprobe analyses revealed distinct amounts of chromium and vanadium but extremely low iron contents. Spectra in the UV-Vis range are consistent with published work. Six differently sized cubes were cut from an HOC alexandrite crystal and used to show pleochroism in combination with two optical phenomena: the alexandrite effect and the Usambara effect. Colorimetric parameters were calculated from the spectra of the cubes and plotted in the CIELAB colour space to demonstrate the alexandrite and Usambara effects graphically for different directions of view. The absorption bands in the infrared are polarized and assigned to structural OH-groups.

Keywords: alexandrite effect, colorimetry, inclusions, melt growth, microprobe analyses, pleochroism, synthetic alexandrite, Usambara effect, UV-Vis-IR spectra

Crystal of synthetic alexandrite produced by the HOC technique in Novosibirsk; the original crystal weighing 39.2 g and measuring about 38 × 23 × 14.5 mm, was cut into slices for further examination. Incandescent light. Photo by K. Schmetzer.

Introduction

Synthetic alexandrites which had been grown by a method designated as 'horizontally oriented crystallization' (HOC), have been available since the late 1980s (Gurov *et al.,* 1988; Gurov and Kirdyashkin, 2001; Gurov *et al.,* 2003). The method was recently mentioned by Malsy and Armbruster (2012) in a paper describing chemical properties of various types of synthetic alexandrites, but a complete gemmological description of the gem material grown using this technique is not yet available. The present paper tries to fill this gap.

In contrast to the 'vertical floating zone' method, which was applied by Seiko for the growth of synthetic alexandrites (see e.g. Schmetzer, 2012), we can describe the HOC method as the 'horizontal floating zone' technique. The synthetic alexandrites produced with this method in Novosibirsk typically show an intense bluish green to blue green coloration in daylight and a colour change to violet purple or purple in incandescent light *(Figure 1)*. Thus, the coloration of these alexandrites is

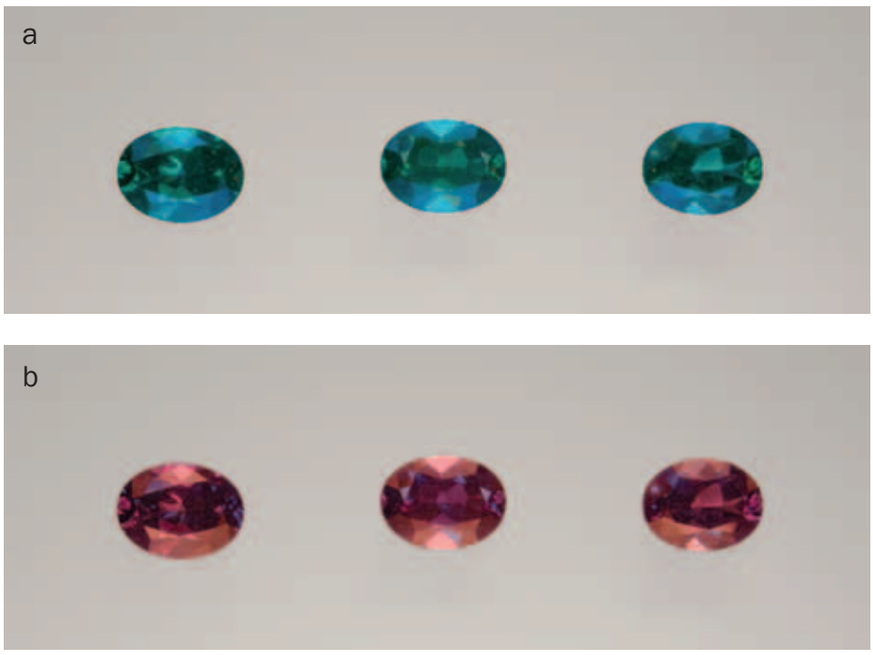

Figure 1 a,b: Faceted synthetic alexandrites grown by the HOC technique in Novosibirsk (a) in daylight and (b) in incandescent light; weight of samples from 1.63 to 1.75 ct, size 8.3 × 6.4 or 8.3 × 6.3 mm. Photo by K. Schmetzer.

Figure 2: Portrait of Vladimir V. Gurov (2011) who developed the technique for the growth of large alexandrite crystals by the HOC method at the Institute of Geology and Geophysics, Siberian Branch of the USSR Academy of Sciences in Novosibirsk; Dr Gurov is now growing synthetic alexandrites for jewellery purposes at the Institute of Geology and Mineralogy, Siberian Division, Russian Academy of Sciences, Novosibirsk, Russia, in cooperation with the Tairus company, Novosibirsk.

comparable to the natural alexandrites originating from Hematita, Minas Gerais, Brazil, which has been the most productive mine since the 1980s.

Growth of alexandrite by the HOC method

The apparatus used at the Institute of Geology and Mineralogy, Siberian Division, Russian Academy of Sciences, Novosibirsk, Russia, is described in detail by Gurov *et al.* (2003) *(Figure 2)*. The principal components of the crystallization apparatus are similar to those used in the facilities developed in the 1970s (see Box A). Because the crystallization of chrysoberyl progresses through a metastable phase, the known apparatus used mainly for growth of large sapphires needed some specific modification for the stable growth of large alexandrite crystals (V.V. Gurov, pers. comm., 2012).

In general $BeAl_2O_4$ crystallizes from a melt as the high temperature phase (β-$BeAl_2O_4$) and on cooling, undergoes a polymorphic transition to a low temperature phase (α-$BeAl_2O_4$, chrysoberyl) at 1826°C which is then stable down to and at room temperature.

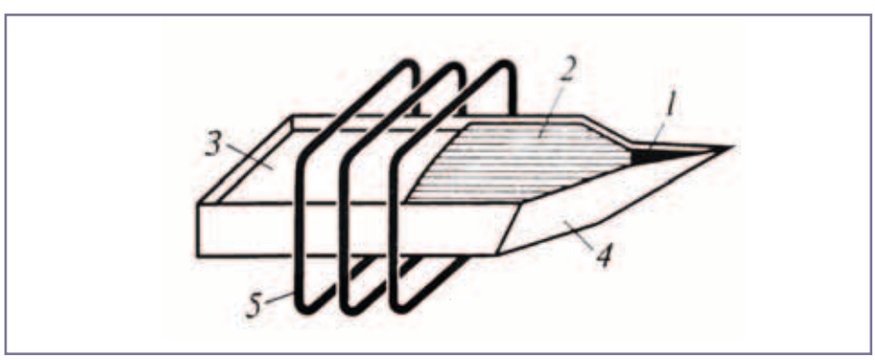

Figure 3: Crystallization container for the growth of alexandrite crystals by the HOC method; (1) seed crystal, (2) synthetic alexandrite, (3) melt, (4) molybdenum boat, (5) heater. Courtesy of V.V. Gurov.

However, under special conditions, the α-phase (chrysoberyl) can be formed directly from the melt and chromium- and vanadium-bearing chrysoberyl crystals can be grown (Gurov *et al.,* 1986, 2003; Gurov and Tsvetkov, 1998, 2008; V.V. Gurov, pers. comm., 2012). Detailed knowledge of the role of dopants such as chromium and vanadium is essential for the growth of high quality crystals for optical applications, e.g. laser crystals, as well as of gem-quality alexandrite crystals.

Interest in the production of materials for jewellery purposes started in the late 1980s and samples have been grown since the mid-1990s at the Institute of Geology and Mineralogy (part of the former Institute of Geology and Geophysics) in a joint venture with the Tairus company, Novosibirsk. The first commercial samples were released to the market in mid-1994 (V.V. Gurov, pers. comm., 2011, 2012).

The practical growth of alexandrite single crystals is performed in boat-like molybdenum containers in an atmosphere of purified argon. Dimensions of the containers are at present 150–160 mm long and up to 70 mm wide *(Figure 3)*. The containers are filled with a mixture of

Box A: The HOC growth technique

The horizontally oriented crystallization technique (HOC), also designated by some authors as 'horizontally directed crystallization' (HDC) or as 'horizontal directed solidification', is considered as a variant of the floating zone method and closely related to the technical development by Khachik Saakovich Bagdasarov and his research group (Bagdasarov *et al.,* 1975, 1977, 1978, 1981). The method is used for the growth of large crystal plates of compounds with high melting temperature such as corundum or rare-earth aluminium garnets, especially for laser or other optical applications. The crystals are grown in containers of molybdenum or tungsten, which avoids the use of expensive crucibles made of platinum or iridium. Some relevant extracts from Bagdasarov *et al.* (1975) are:

"The herein-proposed method of growing oriented monocrystals of corundum from a melt, say, in the shape of plates, is explained as follows [see *Figure A1*].

"A crystal seed 2 is placed into a container 1 having the required orientation. The container is then charged with a stock blend 3. The thus-charged container 1 is placed onto a pulling mechanism 4 of a crystallization chamber 5 and introduced into a heater 6 so that part of the crystal seed 2 goes into an expected temperature zone 7 of the melting of corundum.

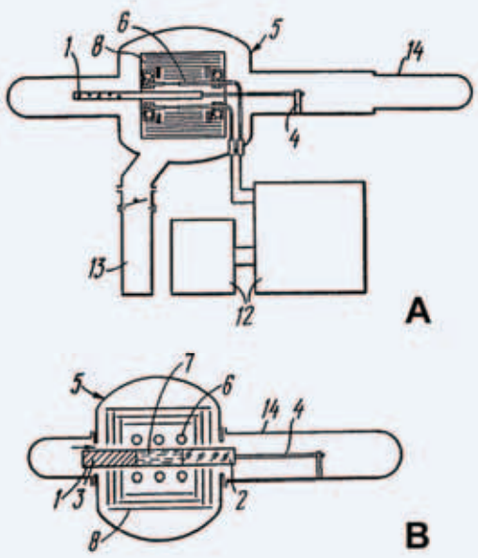

Figure A1: (A) Diagrammatic view of an apparatus for growth of large single crystals of materials with high melting temperatures; (B) a somewhat enlarged part of Figure A seen from above: (1) container, (2) seed crystal, (3) charge, (4) pulling mechanism, (5) crystallization chamber, (6) heater, (7) melt in high temperature zone, (8) heat screens, (12) electrical transformers, (13) vacuum pumps, (14) receptacle. From British patent GB 1 383 400, inventors: K.S. Bagdasarov et al.*, applicant: Institut Kristallografii Akademii Nauk SSSR, Moscow.*

Figure A2 : Production hall with numerous HOC facilities for the growth of large single crystals of compounds with high melting temperatures; Institute of Geology and Mineralogy, Siberian Division, Russian Academy of Sciences, Novosibirsk, Russia. Photo courtesy of V.V. Gurov.

"The heater 6 is fashioned as a bifilar rectangular coil whose ends are fixed to water-cooled current leads. In order to provide a more efficient operation for the heater and increase the consistency of the temperature field thereof, the heater is surrounded by a system of rectangular screens 8 arranged all around except for two opposite sides through which the container 1 is moved ... The electric power supply of the device is from transformers 12, while the required vacuum is established by corresponding vacuum pumps 13.

"Once a rarefaction of not higher than 5×10^{-5} Torr has been attained in the crystallization chamber 5, the blend 3 is subjected to melting. Due to the provision of the heater 6 using Joule heating and the system of the screens 8 a temperature gradient of from 5° to 40° per cm is attained across the crystallization zone. Further, the container 1 with the melt and a part of the crystal seed 2 is pulled into a receptacle 14 at a velocity of 4 to 10 mm/hr. When the growth process is completed, the resultant monocrystal is cooled and withdrawn from the receptacle 14."

A somewhat modified and improved apparatus is specified by Bagdasarov *et al.,* 1977, 1978, to which the reader is referred for further details. A photo of a production hall for HOC-grown synthetic single crystals is given in *Figure A2*, showing several growth facilities used for alexandrite synthesis.

Synthetic alexandrites grown by the HOC method in Russia

Figure 4: Complete alexandrite crystal grown by the HOC technique in a molybdenum container in Novosibirsk. Weight of the crystal approx. 420 g. Photo courtesy of V.V. Gurov.

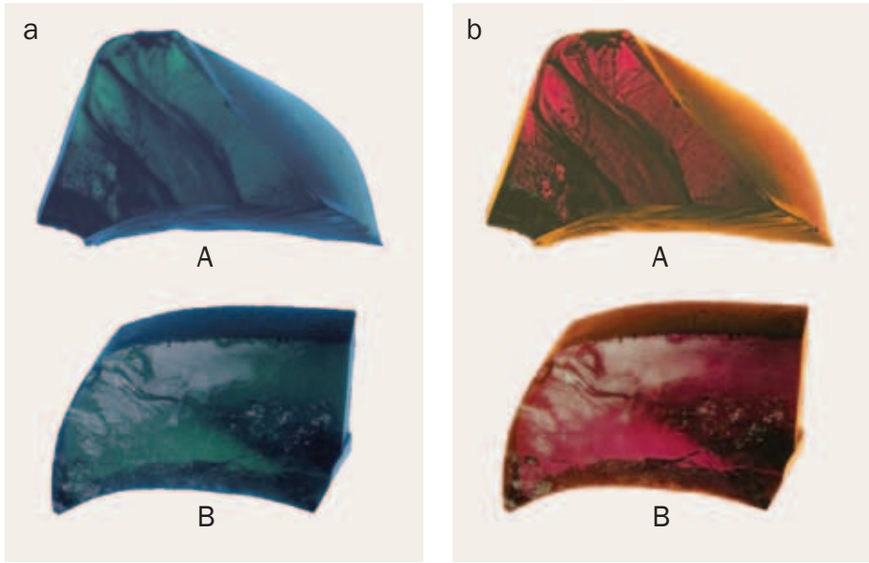

Figure 5 a,b: The two synthetic alexandrite crystals grown by the HOC technique in Novosibirsk investigated in this study; the samples are shown in daylight (a) and incandescent light (b); sample A measures approx. 48 × 24 mm, thickness variable up to 23 mm, weight 51.6 g; sample B measures about 38 × 23 mm, thickness 14.5 mm, weight 39.2 g. Photo by K. Schmetzer.

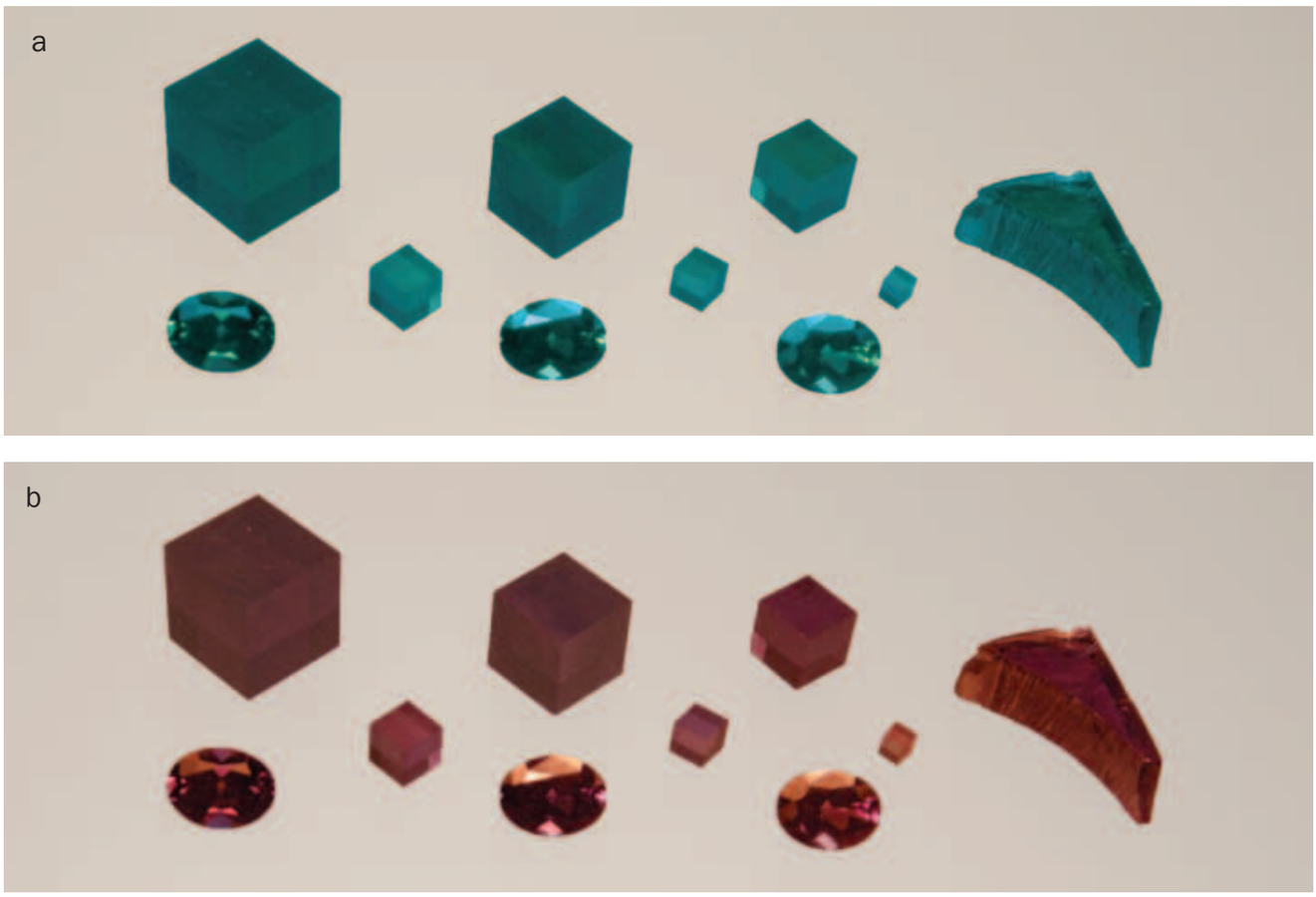

Figure 6 a,b: From sample B depicted in Figure 5 various research stones were prepared; the photos, (a) in daylight and (b) in incandescent light, show a slice from the crystal, three faceted alexandrites cut with the table facets exactly perpendicular to either the a-, b- or c-axis of the crystal (weighing 1.63 to 1.75 ct), and six cubes cut with their faces exactly perpendicular to the a-, b- and c-axes of the crystal (weighing 0.17 to 18.05 ct, edges of the cubes 2, 3, 4, 6, 8 and 10 mm). Photo by K. Schmetzer.

Figure 7 a,b: Faceted synthetic alexandrites purchased from the Tairus company, Bangkok, Thailand, (a) in daylight and (b) in incandescent light; the weights range from 1.38 to 1.74 ct; the rectangular sample at the right (1.74 ct) measures 8.7 × 5.1 mm. Photo by K. Schmetzer.

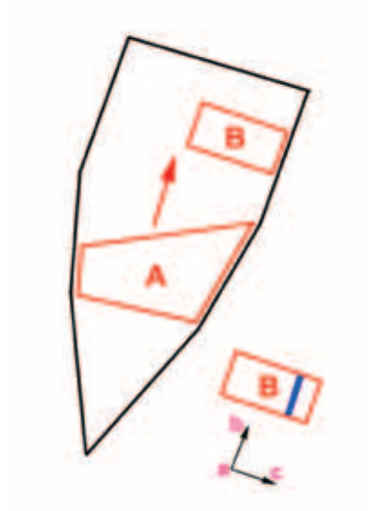

Figure 8: This schematic drawing shows the position of the two alexandrite crystals depicted in Figure 5 in the molybdenum container applied for crystal growth as indicated by the producer; the growth direction (red arrow) is almost parallel to the b-axis and perpendicular to the c-axis of the alexandrite crystal (indicated schematically below right with black arrows); the position and orientation of the slab cut parallel to the ab-plane and used for chemical analysis (five scans by electron microprobe) is indicated in blue.

beryllium and aluminium oxide and oxides of colour-causing trace elements, especially chromium. A special attachment allows the introduction of an oriented seed into the melt filling the nose of the container. The rates of moving the molybdenum boat through the heating zone are 1.5–3 mm per hour. Under these experimental conditions, single crystals are obtained which closely reflect the form of the boat-shape of the container *(Figure 4)*.

Various aspects of chrysoberyl and alexandrite synthesis have been discussed in the papers of V.V. Gurov and his co-authors, and the properties of alexandrites grown by the HOC method were compared to samples grown by the Czochralski technique (Gurov *et al.,* 1986, 1988, 2003, 2008; Gulev *et al.,* 1990; Gurov and Tsvetkov, 1998, 2008; Gurov and Kirdyashkin, 2001, 2012). The principal features of gemmological interest resulting from these discussions are:

- the orientation of seeds and the orientation of the free surface of the grown crystal;
- the nature and distribution of inclusions and the concentration and zoning of chromium and vanadium dopants;
- the sector zoning of the crystals.

Research materials

Two rough crystals of 51.6 g and 39.2 g were directly obtained from Dr Gurov in Novosibirsk via the Tairus company *(Figure 5 a,b)*. The smaller of these crystals was sliced and several faceted alexandrites and seven exactly oriented alexandrite cubes were prepared from these slices *(Figure 6 a,b)*. In addition, we studied seven faceted alexandrites which had been purchased from the Tairus company in Bangkok by Dr D. Schwarz of Lucerne, Switzerland *(Figure 7 a,b)*.

Observations on the crystals and the cut stones

a. Morphology

Both rough crystals *(Figure 5 a,b)* showed larger plane faces which are cleavage planes parallel to **b** (010). The positions of both crystals in the molybdenum container used for crystal growth were given schematically by the producer *(Figure 8)*. A photo of crystal A shows the contact faces with the bottom and the two sidewalls of the container *(Figure 9a)*. The growth direction of the crystal was slightly inclined to the b-axis (based on a morphological cell with a 4.42, b 9.39, c 5.47), and the free surface of the crystal (growing in contact with the argon atmosphere) and the face in contact with the bottom of the crucible were more or less parallel to the **a** (100) pinacoid *(Figure 9b)*.

This applies also to crystal B (Fig*ure 10)*. The two plane faces represent cleavage planes parallel to **b** (010), and the face in contact with the bottom of the container as well as the free surface of the crystal are almost parallel to the **a** (100) pinacoid. With this information, we were able to produce several alexandrite cubes with an exact orientation of the faces perpendicular to the a-, b- and c-axes of the crystal and a number of faceted alexandrites whose table facet was cut perpendicular to one of the three crystal axes *(Figure 6 a,b)*.

b. Microscopic features

Only limited information has hitherto been available about inclusion features of synthetic alexandrites grown in

Synthetic alexandrites grown by the HOC method in Russia

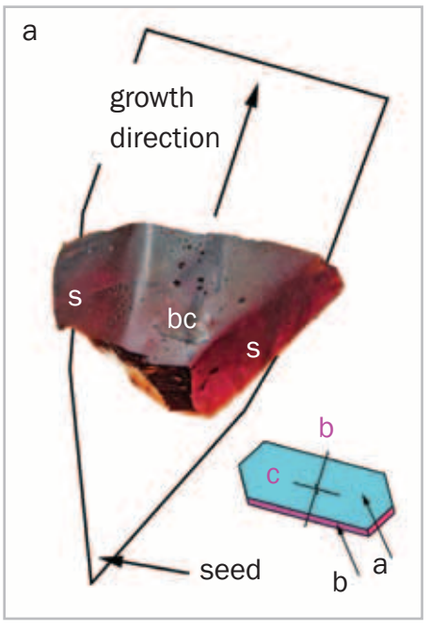

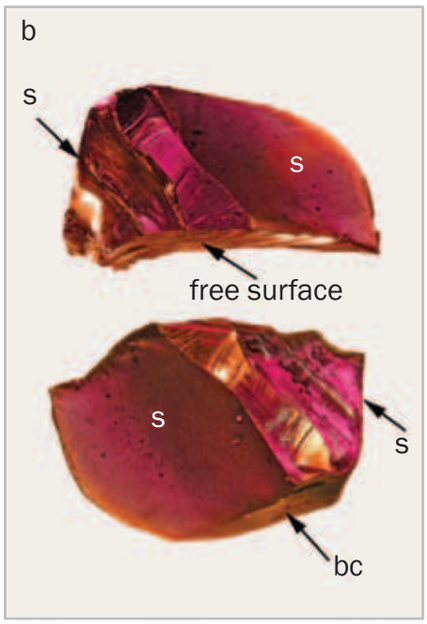

*Figure 9 a,b: View of sample A of Figure 8 parallel to the crystallographic a-axis (a) and parallel to the crystallographic b-axis (b). Photo (a) shows the sample from below and its approximate position in the molybdenum boat used for crystal growth; the position of the seed and the growth direction are also given. The sample shows two faces **s** which were in contact with the side walls of the container, and one face **bc** which was in contact with the bottom of the container; this latter face is parallel to the **a** pinacoid of an alexandrite crystal drawn schematically at the lower right, the growth direction is almost parallel to the b-axis, and perpendicular to the **b** pinacoid. Photo (b) shows the sample from the side, resting on a cleavage plane parallel to the **b** pinacoid, the two faces **s** in contact with the side walls of the container and the face **bc** in contact with the bottom of the container are indicated; the free surface of the crystal was grown in contact with the argon atmosphere within the crystallization chamber. Size of the crystal 48 × 23 × 24 mm, incandescent light. Photos by K. Schmetzer.*

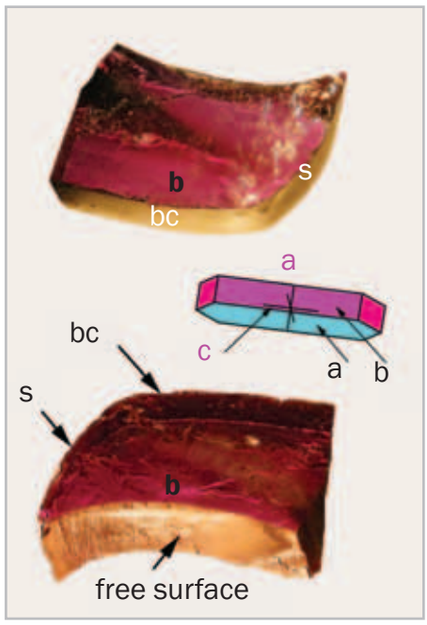

*Figure 10: Two different views of sample B of Figure 8 almost parallel to the crystallographic b-axis. The photos show the sample from each side, resting on a cleavage plane parallel to the **b** pinacoid (see schematic crystal drawing in the centre), the face **s** in contact with the side wall of the container and the face **bc** in contact with the bottom of the container are indicated. Size of the crystal about 38 × 23 mm, thickness 14.5 mm, incandescent light. Photos by K. Schmetzer.*

Novosibirsk by the HOC method. Gurov *et al.* (1988, 2003, 2008), Gulev *et al.* (1990) as well as Gurov and Tsvetkov (2008) mentioned the presence of growth striations and described small molybdenum platelets and molybdenum microparticles. Malsy and Armbruster (2012) pictured small cavities of unknown nature.

The microscopic features in both the samples obtained from V.V. Gurov and those found in the faceted samples purchased directly from Tairus, Bangkok, are identical, so they are now described together.

Structural features:

More or less curved growth striations, which represent the interface between the melt and the growing crystals *(Figure 11 a–d)*, are common. In some samples, numerous small bubbles or particles are related to the curved growth striations.

In one part of the rough crystal an additional defect was present, which could be described as numerous irregularly oriented fissures and fibres *(Figure 12a)*. In areas with a lower concentration of these defects, the fibrous nature of the inclusions is clearly seen *(Figure 12b)*. Under crossed polarizers, no interference effects in adjacent parts of the alexandrite crystals were seen, so structural features such as twinning are ruled out as a cause *(Figure 12 c,d)*. At present, the formation mechanism of these inclusions, which could represent grain boundary defects within the alexandrite crystals, is not understood. These defects are only occasionally developed in the crystals (V. Gurov, pers. comm., 2012).

Irregularly shaped or elongated cavities:

In most slices of the rough crystals and in the faceted alexandrites, irregularly shaped, somewhat elongated cavities are present. In a view parallel to the b-axis, these cavities are normally transparent, but most appear opaque in a view parallel to the a-axis *(Figure 13)*. This morphology and especially the thickness in different directions indicates relatively flat and thin cavities, with their flat surface oriented perpendicular to the b-axis, i.e. perpendicular to the growth direction.

Under crossed polarizers, there was no microscopic evidence to suggest the presence of any solid phases, and only some reflections of the rims of these cavities were observed *(Figure 14 a,b,c)*. Upon rotation of the sample with that particular inclusion in the immersion microscope, total internal reflection for the complete surface of the flat cavities becomes visible *(Figure 14 d,e,f)*, which also indicates a homogeneous gaseous filling of the voids.

Very few birefringent small crystals were seen in the samples; some were

Synthetic alexandrites grown by the HOC method in Russia

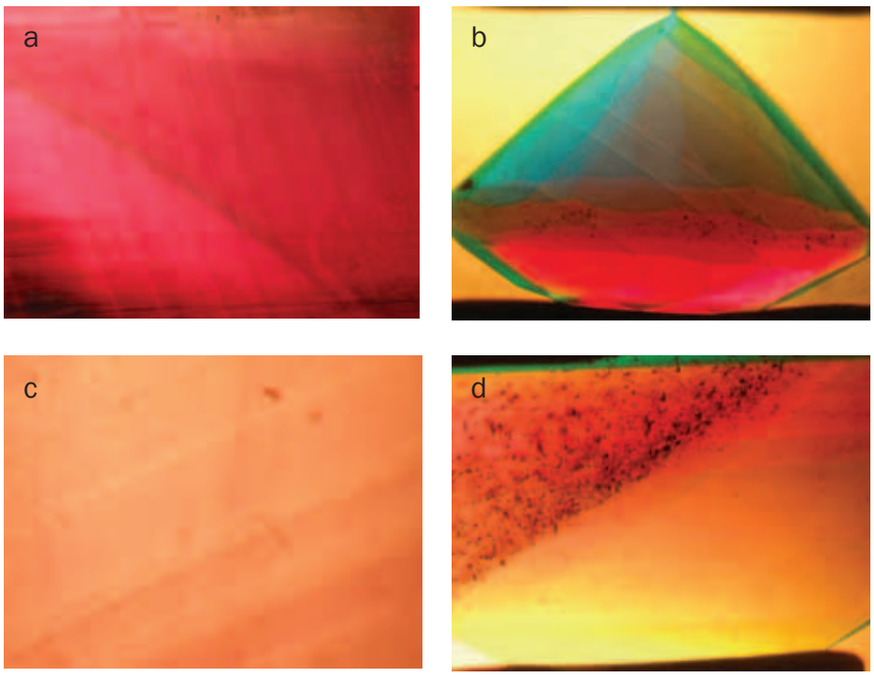

Figure 11: Various forms of growth striations in synthetic alexandrites produced by the HOC technique (a–d). Some samples contain numerous small particles concentrated along the growth striations (c); in others, the curved growth striations separate a part with extremely high concentrations of inclusions from more or less clean parts within the crystal (d). Immersion, field of view (a) 7.3 × 5.4 mm, (b) 6.3 × 4.7 mm, (c) 4.2 × 3.2 mm, (d) 6.7 × 5.0 mm. Photos by K. Schmetzer.

but others were not in contact with the flat voids described above (*Figure 15*). In plane polarized light, these birefringent tiny crystals are difficult to see, which indicates refractive indices close to the chrysoberyl host. Thus, these small crystals might be chrysoberyl or corundum.

In different samples, somewhat elongated voids or channels with partly transparent, partly opaque 'fillings' were seen *(Figure 16)*. After closer inspection of these inclusions in different orientations, the pattern can be attributed to flat cavities, which are transparent in a view parallel to the b-axis *(Figure 17B)*. In a view parallel to the a-axis, i.e. parallel to the thin rim of these cavities, and parallel to the flat side of the cavities, the formerly transparent parts become opaque, but additional transparent 'tails' or 'elongations' become visible at one or both ends of these elongated cavities *(Figure 17A)*. In a view along the c-axis *(Figure 17C)*, i.e. parallel

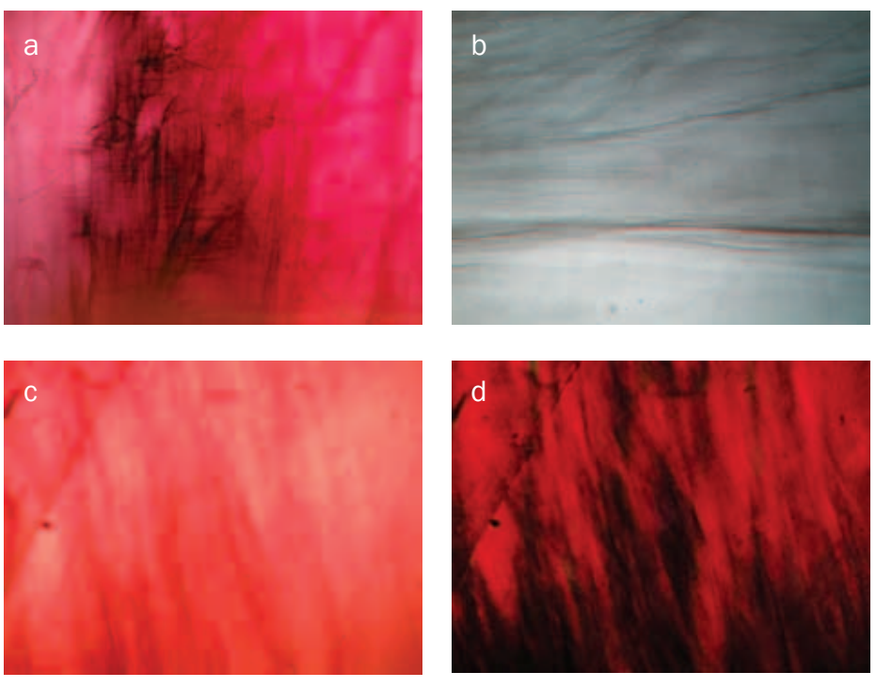

Figure 12: A few HOC alexandrites contain numerous irregularly oriented fissures and fibres (a–d); if a crystal with these features is viewed in plane polarized light (c) and then with crossed polarizers (d) it does not show any interference effects, which could indicate microtwinning if present. Immersion, field of view (a) 9.1 x 6.8 mm, (b) 7.6 x 5.7 mm, (c,d) 9.5 x 7.2 mm. Photos by K. Schmetzer.

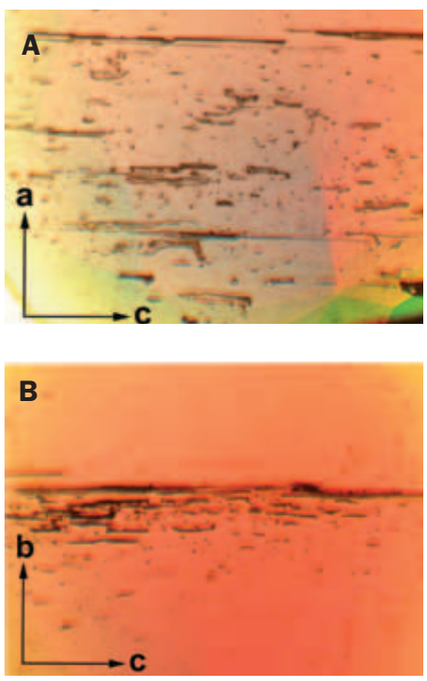

Figure 13: Elongated and occasionally somewhat irregularly-shaped flat cavities; viewed parallel to the crystallographic b-axis (A), the cavities appear transparent, whilst in a view parallel to the a-axis (B), they appear opaque. Immersion, field of view 4.2 × 3.1 mm. Photos by K. Schmetzer.

Synthetic alexandrites grown by the HOC method in Russia

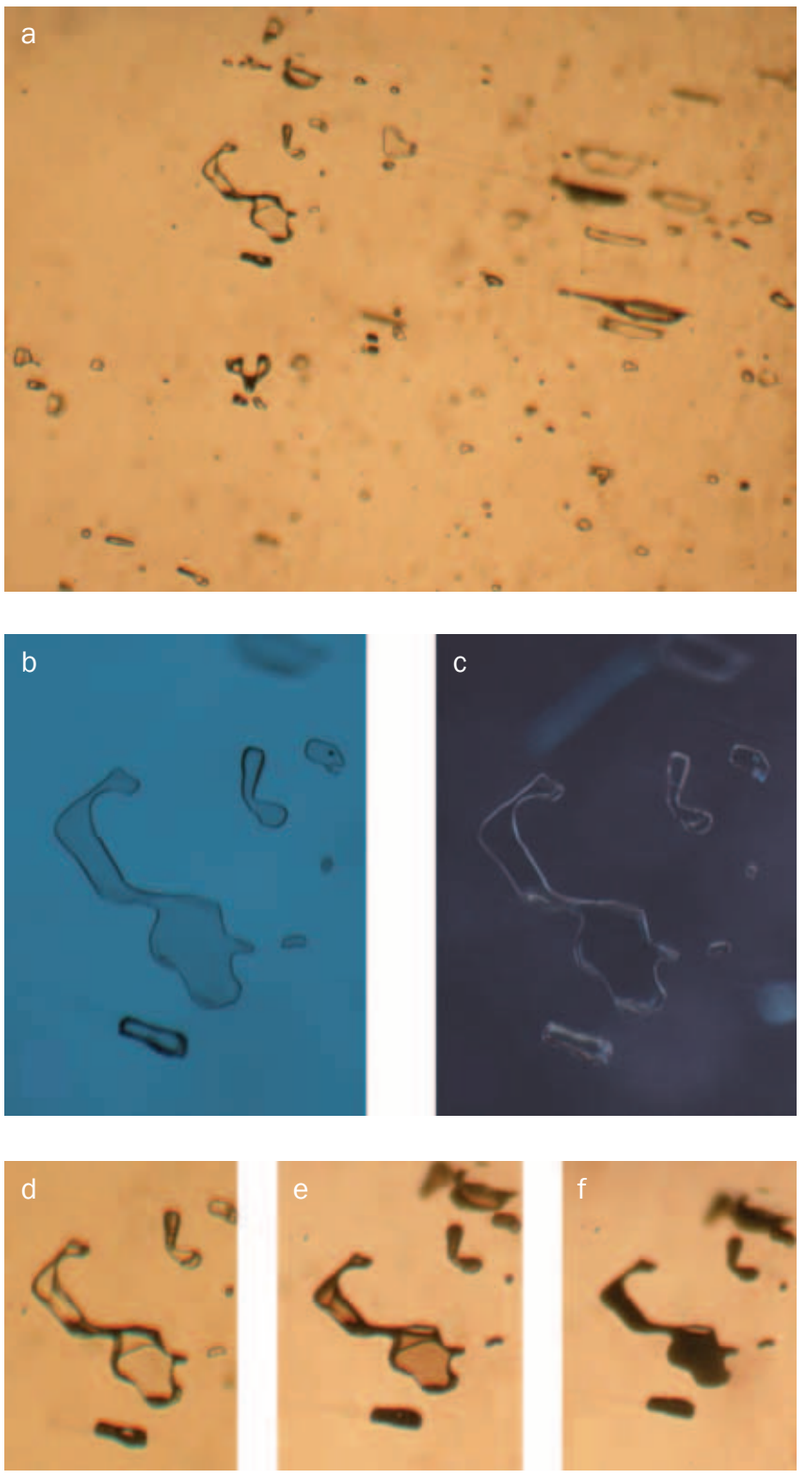

Figure 14: Irregularly-shaped flat cavities in an HOC alexandrite: (a) overview in the direction parallel to the b-axis; (b) in plane polarized light and (c) between crossed polarizers; in (c) only small reflections of the edges of the cavities are visible, but no birefringent solid phase is present; in immersion (d–f), under various angles to the illuminating light beam, the cavities appear transparent (d), semitransparent (e) or opaque (f). Field of view (a) 3.8 × 2.8 mm; (b–f) 1.05 × 0.8 mm. Photos a and d–f by K. Schmetzer; b and c by T. Hainschwang.

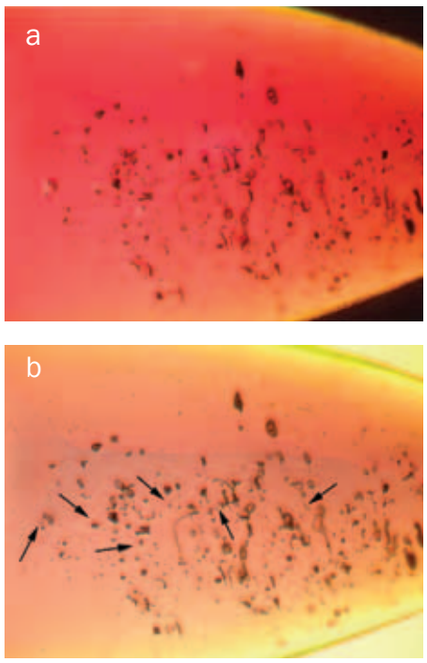

Figure 15: Rarely small birefringent inclusions are detectable under crossed polarizers (a), but these inclusions were extremely difficult to recognize in plane polarized light (b, see arrows); most of these birefringent crystalline inclusions were associated with flat cavities, but some were without contact with any internal cavity. Immersion, field of view 5.8 × 4.4 mm. Photos by K. Schmetzer.

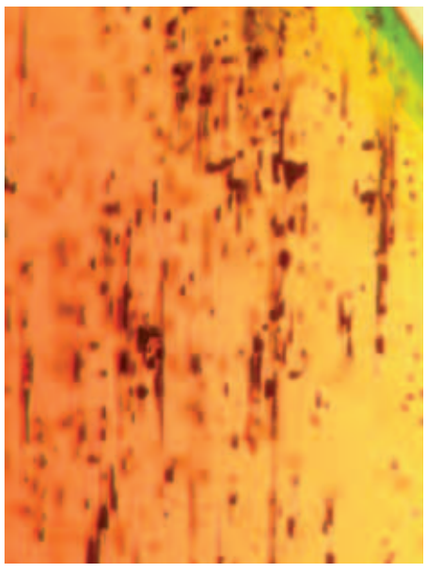

Figure 16: Some elongated voids or channels show partly transparent and partly opaque 'fillings'. Immersion, field of view 1.8 × 1.4 mm. Photo by K. Schmetzer.

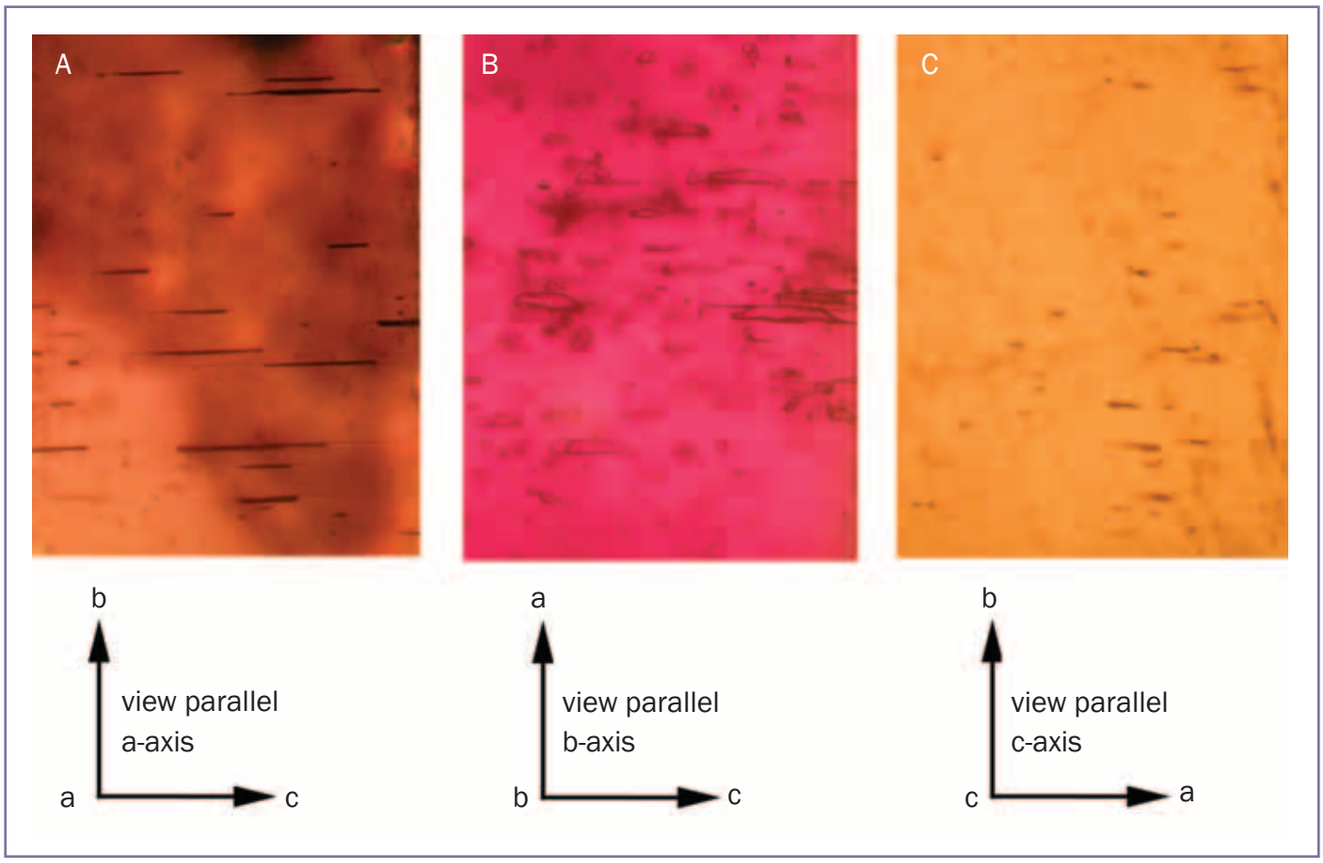

Figure 17: In different directions, the same flat cavities may appear transparent (B) or opaque with transparent 'tails' or 'elongations' (A), which are invisible in other directions; in a view parallel to the axes of these elongated cavities (C), only small flat inclusions are visible. Immersion, field of view (A–C) 2.3 × 1.7 mm. Photos by K. Schmetzer.

to the elongation of these flat cavities, only slightly elongated, flat channels or cavities are apparent. It seems that the 'tails' described above could represent the tracks of gases moving parallel to the c-axis to form the larger cavities and could be due to diffusion processes along the c-axis accompanying crystal growth from the melt.

Chemical properties

A slab of crystal B (see *Figures 5* and *8*) parallel to the **c** (001) face, i.e. parallel to the a- and b-axes of the crystal, was prepared. The dimensions were 18 mm from the free surface to the bottom of the container (parallel to the a-axis) and 14 mm in the growth direction (parallel to the b-axis; see also *Figure 10*). Five scans, each with 20 point analyses, were performed in the direction from the free surface to the bottom of the container along lengths from 12 to 16 mm, and at intervals between the different scans along the b-axis (parallel to the growth direction) of about 2 mm.

The results are presented in *Table I*. The dominant colour-causing element is chromium (0.30–0.43 wt% Cr_2O_3), with smaller amounts of vanadium also being present (0.07–0.14 wt% V_2O_3). The only other transition elements detected were Fe, Mn and Ti, near or at the limit of detection (0.01 wt% oxide) for the method. No systematic variation of these elements within the different scans nor between the five scans was observed *(Figure 18)*. These results show a relatively homogeneous distribution with no correlation between chromium and vanadium contents *(Figure 19)*. According

Table I: Trace element contents of synthetic alexandrites grown by the HOC technique (in wt%).

	This paper[1]		Malsy and Armbruster[2]	
	range	average	range	average
TiO_2	0.0–0.03	0.01	not detected	
V_2O_3	0.07–0.14	0.10	0.06–0.08	0.07
Cr_2O_3	0.30–0.43	0.38	0.25–0.46	0.38
MnO	0.0–0.03	0.01	below detection limit	
Fe_2O_3	0.0–0.03	0.01	below detection limit	

1. electron microprobe analyses, five scans each of 20 point analyses.
2. LA-ICP-MS analyses of five samples.

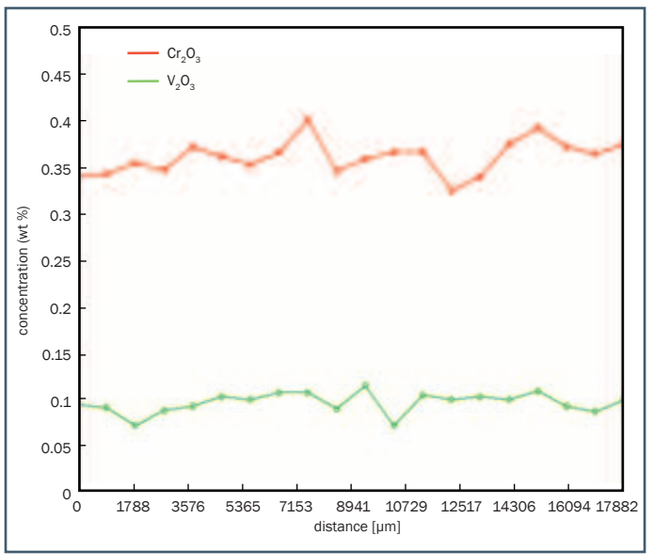

Figure 18: Plot of chromium (red) and vanadium (green) concentration measured by one electron microprobe scan across a polished slice of a synthetic alexandrite crystal which had been sawn parallel to the ab-plane (see Figures 5, sample B, and Figure 10); the chemical data reveal no specific pattern of chemical zoning in different parts of the crystal.

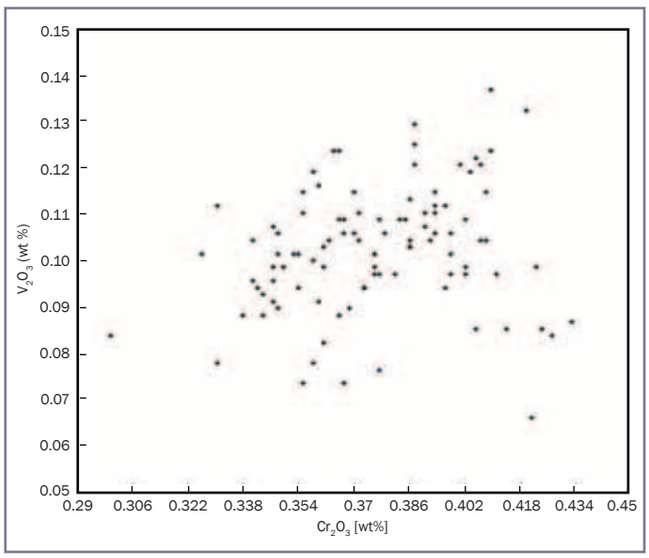

Figure 19: Chromium/vanadium binary diagram showing the variability of these trace elements in five scans of 20 analysis points each across a polished slice of synthetic alexandrite, sawn parallel to the ab-plane (see Figures 5 and 10); the scatter of points appears random, showing no correlation.

to information from the producer, any variation of trace element contents, especially of chromium, is found only at the beginning of crystal growth (close to the seed) and close to the end of growth next to the molybdenum container (V. Gurov, pers. comm., 2012). The contents of vanadium and chromium determined by Malsy and Armbruster (2012) for five samples grown by the same technique in Novosibirsk (material originating from Tairus, Bangkok) were in the same range (see *Table I*).

The colour of HOC alexandrites and their visible and ultraviolet range spectra

Colour and colour change in alexandrites are dependent on several factors, the three main ones being:

a. the direction of observation of a faceted gemstone or a rough alexandrite crystal relative to its orientation to the crystallographic axes, a, b and c;
b. the contents of colour-causing trace elements, especially chromium, vanadium and iron; and
c. the length of the path of light within a sample, which relates to its thickness.

Hitherto, to evaluate the dependency on orientation, faceted samples with different orientations of the table facet or crystals with known morphology have been measured spectroscopically and colorimetric parameters have been calculated. A correlation between colour and trace element contents has been established for alexandrites of known compositions. To examine orientation dependence within the same crystal, it has also been possible to examine three carefully oriented alexandrite cubes with faces parallel to the crystal axes (Schmetzer and Bosshart, 2010; Schmetzer and Malsy, 2011; Schmetzer *et al.,* 2012). However, it has not so far been possible to examine samples in different known orientations, which showed either an identical composition and different thickness, or samples with identical thickness and different composition. Therefore, because of the established small variation in chemical composition found in the HOC alexandrites, our samples seemed to be the ideal research material for the evaluation of colour and investigation of pleochroism for different orientations and thicknesses.

Chromium-bearing tourmalines, which have an absorption spectrum resembling that of alexandrite, show a colour variation with variable thickness, a phenomenon first described by Halvorsen and Jensen (1997) as the 'Usambara effect'. This causes these tourmalines to appear green when thin and red when thick. Colorimetric calculations in the CIELAB colour space assuming different sample thicknesses showed that samples showing the Usambara effect can also show an alexandrite effect, i.e. a colour variation between daylight and incandescent light (Liu *et al.,* 1999; Nassau, 2001). In addition, minerals showing these effects can also show pleochroism, and the relative influence of the different effects can be hard to separate (Halvorsen, 2006).

Thus, to evaluate and distinguish these various optical phenomena for alexandrite, several cubes were cut from the same optically homogeneous crystal (sample B) with their faces exactly orientated perpendicular to the three crystallographic axes of the chrysoberyl. Seven alexandrite cubes were prepared with edge lengths: 2 mm, 3 mm (two

Synthetic alexandrites grown by the HOC method in Russia

Table II: Main features of the visible-range absorption spectra of HOC-grown synthetic alexandrites*

With polarization, absorption maxima and minima (in nm)

Polarization	X	Y	Z
Maxima	569	566	586
	414	420	422
Minima	483	494	489

Additional spin-forbidden chromium bands were observed at 680, 678, 655, 648, 645 and 472, 469, 467 nm.

Without polarization, absorption maxima and minima (in nm)

Orientation	a-axis	b-axis	c-axis
Maxima	570	572	569
	423	420	415
Minima	492	486	490

Additional spin-forbidden chromium bands were observed at 680, 678, 655, 648, 645 and 472, 469, 467 nm.

*Based on a morphological cell with a 4.42, b 9.39, c 5.47 and X || a, Y || b, Z || c.

cubes), 4 mm, 6 mm, 8 mm and 10 mm, all with polished faces. Their spectra were collected in the three directions parallel to the crystal axes, and colorimetric parameters were calculated for daylight and incandescent light in the CIELAB colour space. This information was plotted accordingly in the CIELAB hue circle (see Schmetzer *et al.,* 2009; Schmetzer and Bosshart, 2010).

Absorption spectra of X, Y and Z in polarized light for the cubes of 3 mm edge length are given in *Figure 20*, and spectra recorded in non-polarized light along the a-, b- and c-axis are depicted in *Figure 21*. The absorption maxima recorded *(Table II)* are consistent with literature data and assigned mainly to trivalent chromium with some influence of vanadium (see, e.g., Farrell and Newnham, 1965; Bukin *et al.,* 1980), because the absorption bands of vanadium and chromium cannot be distinguished in the spectra of vanadium- and chromium-bearing samples (Schmetzer and Bosshart, 2010); the influence of emission is commented on in Box B. No absorption bands of iron were detected, which is consistent with the

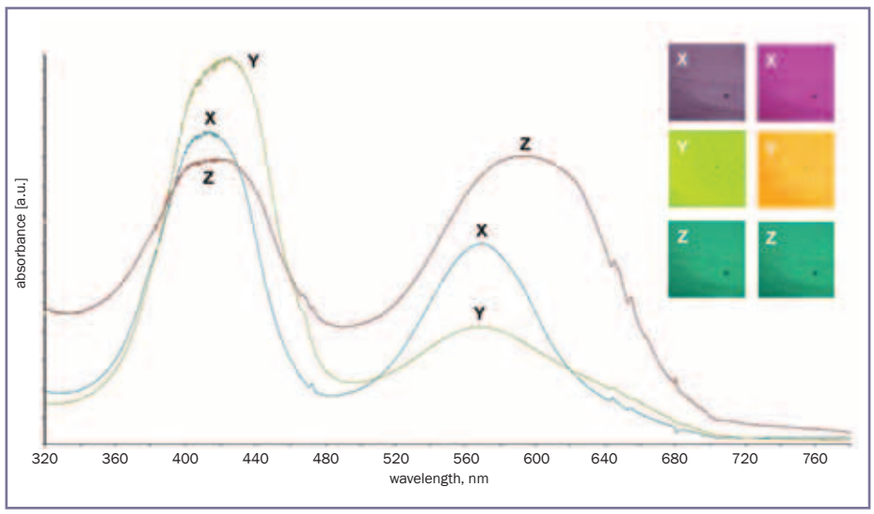

Figure 20: Absorption spectra of a synthetic alexandrite cube produced by the HOC technique (see Figure 6) for polarized light (with X || a, Y || b and Z || c); the colours of the cube in polarized light are depicted for daylight (left column) and incandescent light (right column).

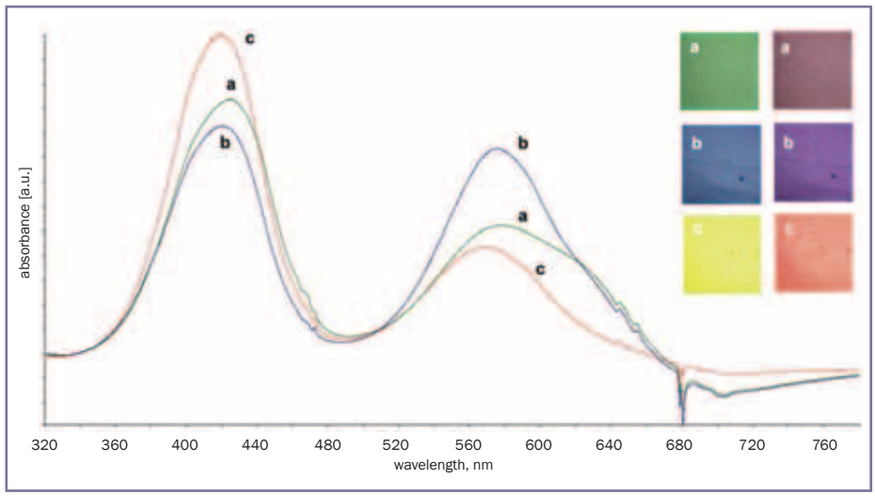

Figure 21: Absorption spectra of a synthetic alexandrite cube produced by the HOC technique (see Figure 6) for non-polarized light in different views parallel to the a-, b- and c-axes, the colours in these directions are depicted for daylight (left column) and incandescent light (right column).

Box B:

In addition to absorptions, there may be two principal Cr^{3+} emissions which are sometimes detected as 'negative' peaks in our spectra and, at the lower energy side (longer wavelength) of these peaks, additional luminescence bands may be present, also seen in the 'negative' direction. This effect is caused by the use of a CCD type Czerny-Turner spectrometer in combination with an integration sphere. Such a setup permits the detection of all wavelengths at the same time in contrast to a traditional scanning spectrometer. In samples with strong luminescence, the light source used to record spectra also excites fluorescence, which is detected at the same time. When the absorption dominates the emission, the peaks will point in the 'positive' direction while in the case of dominant emission, the absorption/luminescence peaks will point in the 'negative' direction.

Synthetic alexandrites grown by the HOC method in Russia

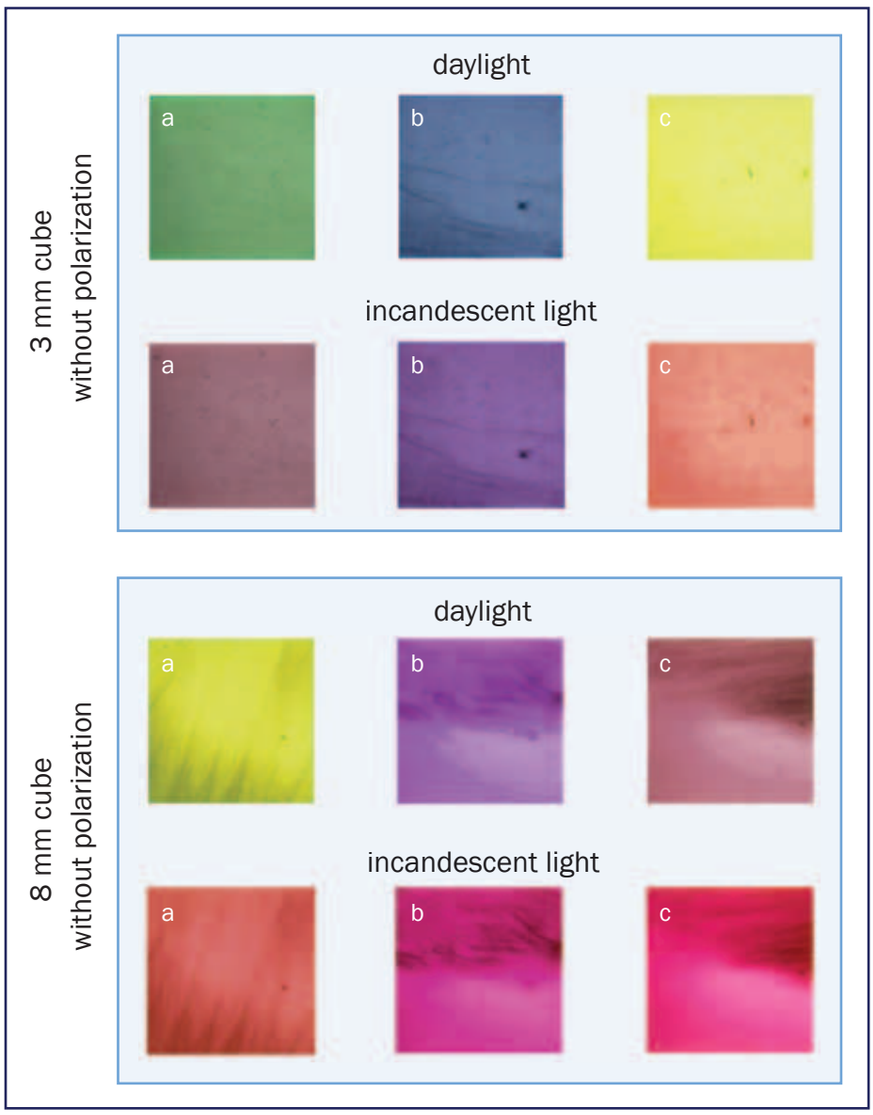

Figure 22: Schematic representation of colour and pleochroism in two cubes of HOC synthetic alexandrite with edges of 3mm and 8mm, in daylight and incandescent light; the cube faces are exactly perpendicular to the a-, b- and c-axes of the alexandrite crystal; with the unaided eye (in non-polarized light) different views parallel to the these three axes are depicted. The illustration demonstrates a combination of pleochroism, the alexandrite effect in daylight and incandescent light and the Usambara effect for different path lengths of light. Photos and artwork by K. Schmetzer.

low iron contents determined by electron microprobe.

In polarized light, there is a distinct change of colour from daylight to incandescent light for X and Y, but an almost identical bluish green is apparent in the Z direction for daylight and incandescent light *(Figure 20)*. This distinct pleochroism enables one to determine the approximate orientation of a rough crystal or a faceted gemstone in the immersion microscope, using a tungsten bulb or a light source with daylight-equivalent illumination.

In non-polarized light the colours and spectra along the three crystal axes a, b, and c are always dependent on two of the three vibration directions X, Y and Z *(Figure 21)*. The pleochroism indicates that the most brilliant green in daylight is visible parallel to a, but a more distinct colour change is seen in the direction parallel to c. Furthermore, in the direction parallel to b, the colour change is also distinct — from an intense greenish blue to violet purple. This indicates that there is no orientation of the alexandrite in which one can see both the most brilliant green and the most spectacular colour change from the same direction.

In *Figure 22* the colour and pleochroism of two alexandrite cubes (with edge lengths of 3 mm and 8 mm) are depicted for non-polarized daylight and incandescent light. The colours are summarized for non-polarized light in *Table III*. Also, the colorimetric parameters for the seven alexandrite cubes have been calculated from spectra for non-polarized light and are plotted in *Figure 23* to demonstrate the colorimetric parameters obtained graphically.

A strong dependence of colour and colour change on the length of the light path (Usambara effect) within the samples is evident. In particular, with increasing sizes of the alexandrite cubes, an increase of redness is observed for the colour in daylight and also for the colour in incandescent light. However, together with this increasing redness, there is a slight increase of blueness for the view parallel to the a-axis, a moderate increase of yellowness for the view parallel to the b-axis, and a distinct increase of blueness in the view parallel to the c-axis *(Figures 23, 24)*.

In chromium-bearing tourmaline showing the Usambara effect, absorption spectra reveal two areas with high transmission, namely in the red and in the yellowish green (around 540 nm). With increasing sample thickness, the transmittance in both areas is reduced, but the rate of decrease is greater in the green range compared to that in the red area. This effect is used to explain the increasing redness in tourmaline with increasing path length of light through the sample (Liu *et al.,* 1999; Nassau, 2001). In alexandrite spectra also there are two areas with high transmission (see *Figures 20, 21*), but in these stones the shorter wavelength transmission maximum is shifted to bluish green. In addition, the absorption maxima for alexandrite and tourmaline are different. Nevertheless, the

Synthetic alexandrites grown by the HOC method in Russia

basic concept to explain the increase of redness with increasing sample thickness described for tourmaline might also apply to alexandrite.

Also, with increasing thickness, the lightness of the alexandrite cubes decreased in all three directions, e.g. from a range of L* 75–85 for the 2 mm cube to a range of L* 25–30 for the 10 mm cube. In other words, the larger samples were relatively dark. This effect explains why larger brilliant alexandrites with chromium contents in the region of 0.4 wt% Cr_2O_3 (as determined for our HOC-grown alexandrite) or above and that have good colour and colour change are extremely rare.

Although we could not measure exactly oriented cubes of the same size with different chromium contents, we would predict from basic spectroscopic and physical equations, that increasing chromium contents in samples with comparable light paths would cause a comparable alteration of colour as demonstrated in this paper for samples with identical chromium concentration and variable thickness (Usambara effect).

The samples examined for this paper are iron-free alexandrites. However, natural alexandrites from different sources as well as some flux-grown synthetic alexandrites contain various amounts of iron. Chromium- and vanadium-free, iron-bearing chrysoberyl is yellow and reveals only weak pleochroism. Thus, it is concluded that a distinct iron-content in an alexandrite increases its yellowness. Thus we selected samples with and without iron-contents but with other properties (thickness and trace element contents) which make them 'comparable'. If we plot the colorimetric parameters of the two 3 mm HOC cubes measured for this paper (average chromium contents 0.38 wt% Cr_2O_3) and the parameters of a flux-grown alexandrite cube produced by Creative Crystals with a 6 mm edge length (average chromium contents 0.20 wt% Cr_2O_3, average iron content 1.05 wt% Fe_2O_3, Schmetzer *et al.*, 2012) we observe an increase of yellowness for the iron-bearing sample for all three directions of view parallel to the crystal axes *(Figure 25)*. A similar effect, i.e. increase of yellowness, is predicted for natural iron-bearing samples.

The observed colour change shown in *Figure 22* and the schematic diagrams depicted in *Figures 23* and *24* illustrate the difficulty of finding the 'best' orientation for the table facet for alexandrites of different thickness or size as well as with different chromium contents. All three effects — pleochroism, alexandrite effect and Usambara effect — contribute to the colour of a faceted

Table III: Colours of two alexandrite cubes in daylight and incandescent light

Size (edge length)	Light source	Direction of view parallel to the		
		a-axis	b-axis	c-axis
3 mm	daylight D_{65}	green	greenish blue	greenish yellow
	incandescent light A	reddish grey	violet	slightly red orange
8 mm	daylight D_{65}	yellowish green	violet purple	reddish grey
	incandescent light A	red orange	red purple	purplish red

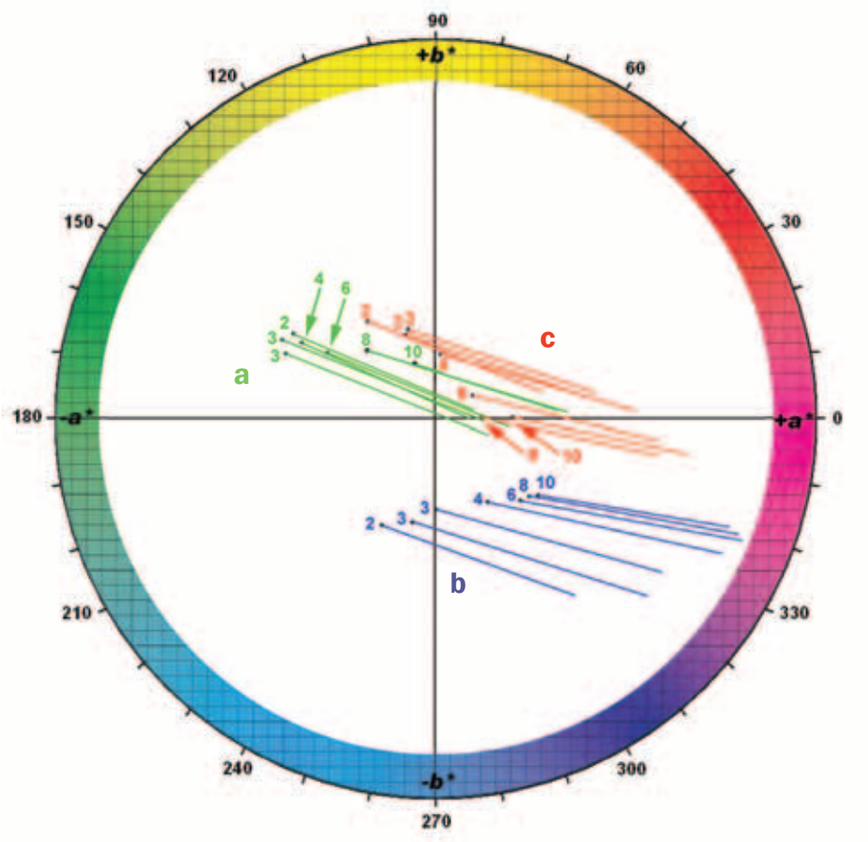

*Figure 23: Colorimetric parameters for seven exactly oriented alexandrite cubes with different sizes are plotted for daylight and incandescent light in the CIELAB colour circle; the neutral point (white point) is in the centre of the a*b* coordinate system, the black circles represent the coordinates in daylight D_{65} and the ends of the differently coloured bars represent the coordinates in tungsten light A; the outer circle represents a chroma of 40. The dependency of colour and colour change on stone orientation in views parallel to the a-axis (green bars), b-axis (violet bars) and c-axis (red bars) is evident. With increasing sizes of the cubes (edge lengths from 2 mm to 10 mm as indicated) a shift of colour is visible; for all three different orientations, the change from daylight to incandescent light is confined to an increase of redness and blueness (alexandrite effect); in addition, the larger the cube, the more red does the alexandrite appear in both daylight and incandescent light (Usambara effect).*

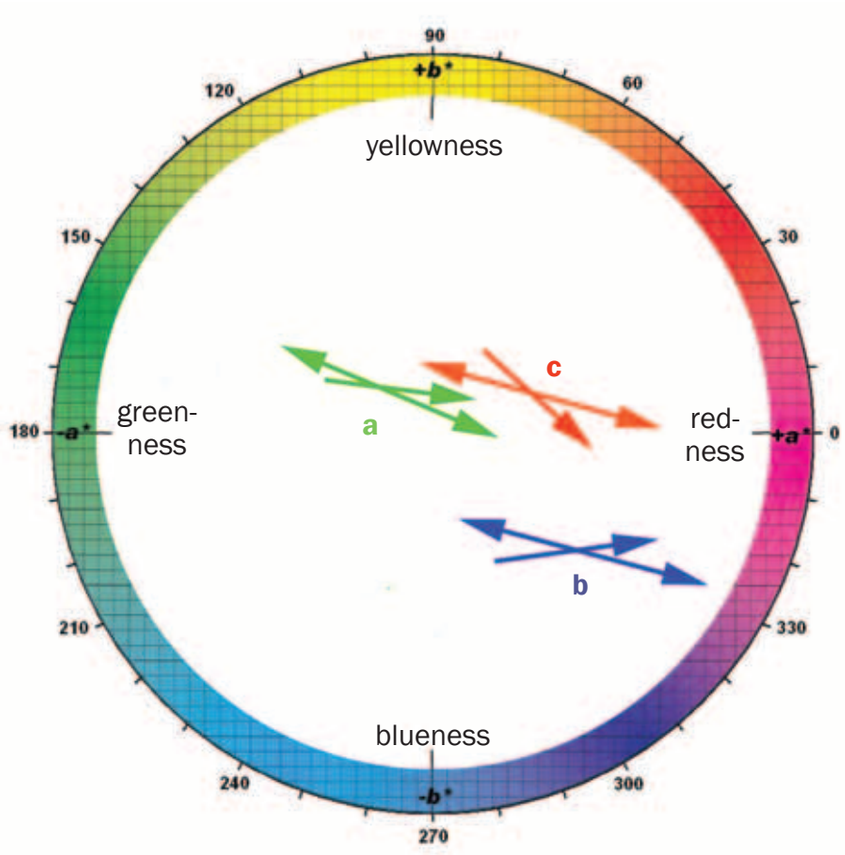

Figure 24: CIELAB colour circle with a schematic representation of the alexandrite effect (double-headed arrows) and Usambara effect (single-headed arrows) for the seven alexandrite cubes in directions of view parallel to the a-axis (green arrows), b-axis (violet arrows) and c-axis (red arrows). With a change of illumination between daylight and incandescent light, the alexandrite effect is based upon the increase of redness and blueness for all three directions of view. With a lengthening of the light paths within different cubes, the Usambara effect is caused by increasing redness of the samples, but with varying (increase or decrease) of blueness and yellowness for the three directions of view.

stone. This indicates why an orientation of the table facet that is appropriate for smaller samples or for samples with lower chromium contents can be inappropriate for larger samples or for samples with higher chromium contents for obtaining an alexandrite with the most desirable colours, green to bluish green in daylight and reddish purple to purple in incandescent light. It also clarifies why predicting the colour and colour change of a stone to be faceted from the rough is so difficult.

Infrared spectroscopy

Infrared spectra were recorded with beam directions parallel to the a-, b- and c-axes of the crystal, i.e. perpendicular to the faces of one oriented cube. The spectra showed absorption bands with maxima at 2970 and 2655 cm^{-1} and shoulders at 2030 and 1995 cm^{-1} *(Figure 26)*. Although the spectra were recorded without polarization of the primary beam, the two bands at 2970 and 2655 cm^{-1} showed a clear polarization dependency. They were recorded in the spectra parallel to the b-axis (representing a combination of X and Z) and parallel to the c-axis (representing a combination of X and Y), but not in the spectrum parallel to the a-axis (representing a combination of Y and Z). These results indicate a polarization of these absorptions parallel to X.

Spectra along the three crystal axes of a Czochralski-grown synthetic alexandrite were also recorded for comparison. The position and polarization of absorption bands found are identical with the spectra of the HOC crystal *(Figure 26)*. Similar spectra were recorded for a cube of flux-grown synthetic alexandrite produced by Creative Crystals. This sample, however, showed an additional band at 3225 cm^{-1} (Schmetzer *et al.,* 2012).

These results are consistent with infrared spectra published for different types of chromium-, vanadium- and iron-bearing synthetic alexandrites, which showed small absorption bands in the same spectral range (Henn, 1992; Schmetzer *et al.,* 1996; Malsy and Armbruster, 2012). The different intensities of infrared absorption bands in natural and synthetic alexandrites have already been mentioned by Stockton and Kane (1988). The polarization dependency indicates that absorptions are due to structural OH-groups, as described in detail for polarized spectra of natural chrysoberyl by Bauerhansl and Beran (1997) who also showed a polarization in the X direction, although the absorption maxima recorded in natural stones were in somewhat different positions compared to our synthetic samples.

Summary and Discussion

The HOC technique has been applied since the late 1980s in Novosibirsk for the growth of large alexandrite single crystals. The method allows the production of very homogeneous chromium- and vanadium-bearing crystals of 400 to 450 g in weight. There has been commercial production and release of rough and faceted material to the international market since 1994.

The examinations presented in our paper show that the internal properties of the gemstones closely reflect the growth conditions present during the HOC process. In most samples, with some searching, curved growth striations are visible, which represent the moving phase boundary between the melt and the growing alexandrite crystal. Flat elongated, sometimes irregularly shaped cavities are oriented parallel to the **b** (010) pinacoid, i.e. perpendicular to the main growth direction.

The large dimensions and homogeneity of the crystals have allowed

Synthetic alexandrites grown by the HOC method in Russia

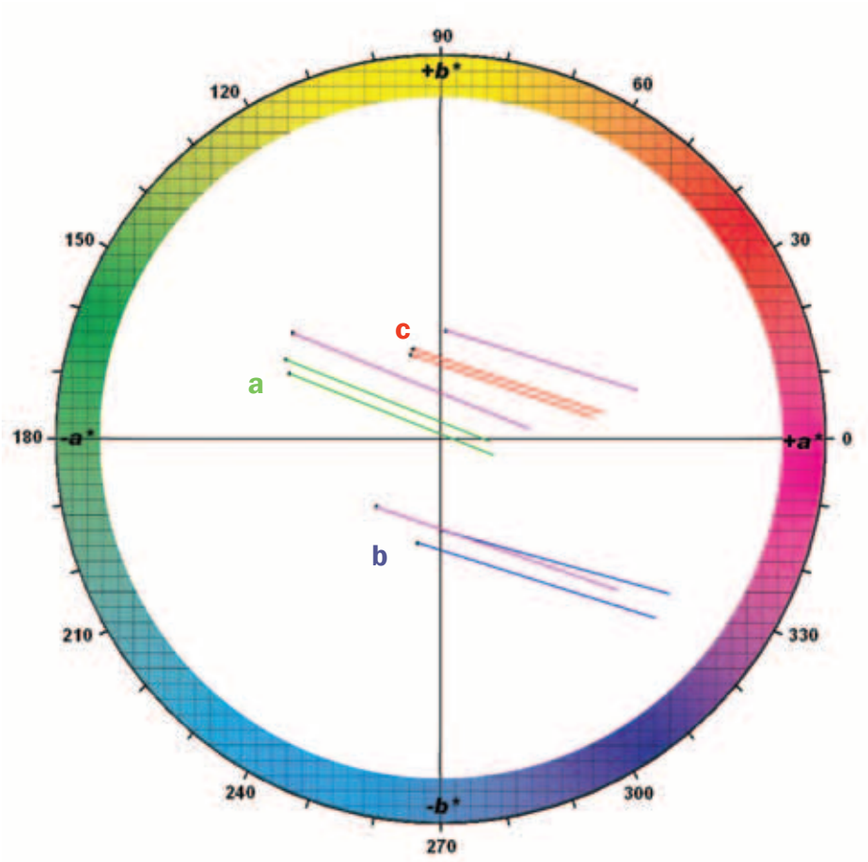

*Fig. 25: Colorimetric parameters for two exactly oriented iron-free alexandrite cubes grown by the HOC method with edge lengths of 3 mm are plotted for daylight and incandescent light in the CIELAB colour circle; the neutral point (white point) is in the centre of the a*b* coordinate system, the black circles represent the coordinates in daylight D_{65} and the ends of the differently coloured bars represent the coordinates in tungsten light A, the outer circle represents a chroma of 40. The dependency of colour and colour change on stone orientation in views parallel to the a-axis (green bars), b-axis (violet bars) and c-axis (red bars) is compared with colorimetric parameters of a flux-grown iron-bearing alexandrite cube (purple bars). This alexandrite crystal has edges of 6 mm, but its chromium content is about half that of the chromium contents measured in the two other alexandrite cubes. The influence of iron causes an increase of yellowness of the iron-bearing sample in all three directions of view.*

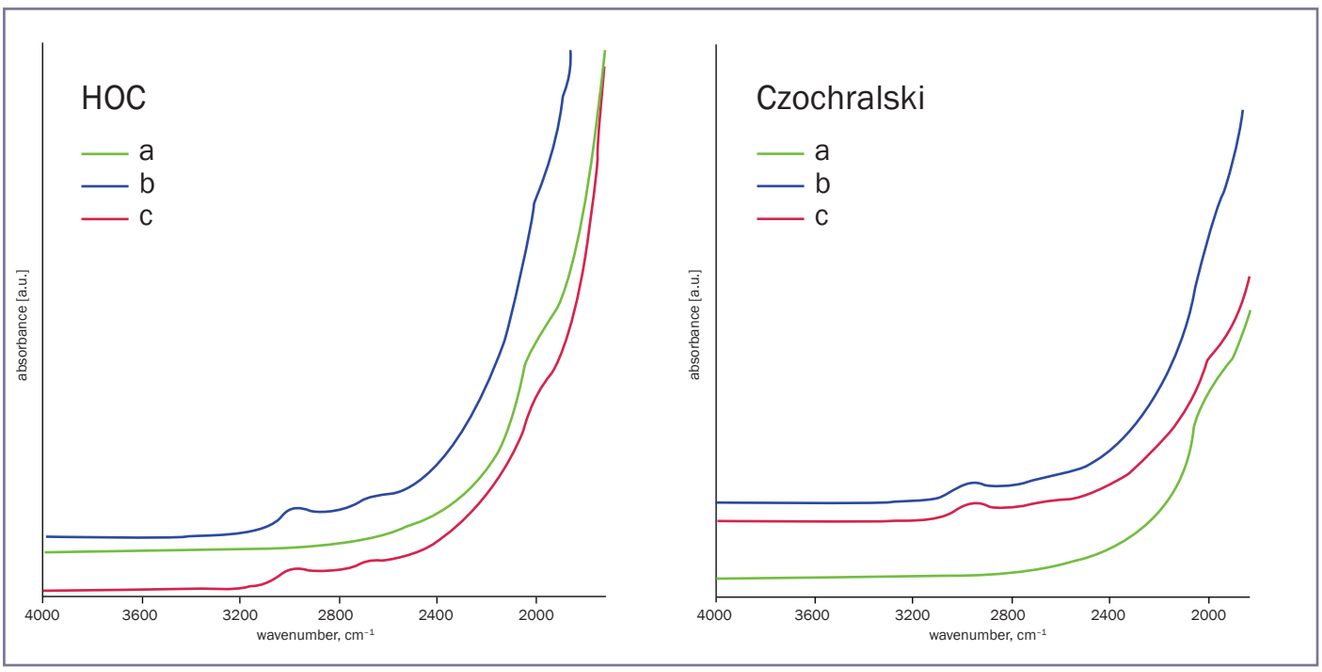

Figure 26: Infrared spectra of a HOC-grown synthetic alexandrite cube in non-polarized light in views parallel to the a-, b- and c-axes of the crystal (left): the small absorption maxima are observed only in spectra representing views parallel to the b- and c-axes which indicates a polarization of these weak absorption bands parallel to X. Spectra of a Czochralski-grown synthetic alexandrite, produced in Novosibirsk in the 1990s, are shown on the right for comparison and indicate no significant difference in this property from the HOC-grown stone.

the examination of several oriented cubes of different sizes. With this research material, the pleochroism, colour change (alexandrite effect) and colour variation with sample thickness (Usambara effect) in the crystals have been distinguished and clearly described.

In Czochralski-grown synthetic alexandrites, curved growth striations and gas bubbles are common and there can be a few somewhat elongated cavities. Thus, a clear separation of Czochralski- and HOC-grown alexandrites is not always possible using only the microscope, especially for the smaller faceted stones. However if a stone has cavities matching the description in this paper in detail, it is a good indicator that it is an HOC-grown stone.

In 1986, C. Trossarelli described three semi-rough (sawn) alexandrite crystals from a new production in the USSR. He mentioned curved striations associated with 'bubble streams', larger bubbles at or near the surface and various forms of flat irregularly-shaped and sometimes tailed cavities. He concluded in his paper that these samples were probably grown by the Czochralski method, but now he considers that they could have been actually produced using the HOC method (C. Trossarelli, pers. comm., 2012). Unfortunately, these were loan samples and are not available for re-examination but these three crystals could be samples of the first experimental state of crystal growth by the HOC method in Russia.

In the last two decades, at different times there have been rumours of the presence in the market of hydrothermally grown synthetic alexandrites. In 1992, U. Henn described several types of synthetic alexandrites which had been produced by different techniques (designated as flux-grown, hydrothermally-grown and Czochralski-grown samples) in various locations of the former USSR. The samples assigned to the hydrothermal production showed irregularly shaped, elongated flat cavities, which closely resemble the common inclusion type described in this paper for HOC-grown stones. The samples, which were loaned to Dr Henn with the designation 'hydrothermally-grown synthetic alexandrites' were only available for some days for examination and no similar material has since come to light (U. Henn, pers. comm., 2011, 2012). Another kind of synthetic alexandrite was briefly mentioned by Bank *et al.* (1997) and also designated as hydrothermally-grown, but this showed a quite different inclusion pattern.

Since then, the present authors have been informed that some limited research on hydrothermal synthesis of chrysoberyl and alexandrite was carried out at the Institute of Geology and Geophysics at the Siberian Branch of the USSR Academy of Sciences in Novosibirsk in the 1990s. Further research is now being performed at the Tairus company in Novosibirsk. However, according to the information available to the authors, no faceted or rough material of gem quality of hydrothermally-grown synthetic alexandrite has ever been released on to the market from Novosibirsk (V. Thomas, Tairus company, Novosibirsk, pers. comm., 2012). So the origin(s) of the samples described in 1992 and 1997 (see above), no longer being available for comparison, remain(s) in doubt.

Acknowledgements

The authors are grateful to Dr Vladimir V. Gurov, Novosibirsk, Russia, who provided the two large rough crystals for examination as well as valuable information regarding the growth process applied for the production of the synthetic alexandrites; he furthermore discussed the results of our study. The preparation of oriented alexandrite cubes and faceted stones from the rough was carefully performed by Wild & Petsch GmbH, Kirschweiler, Germany. The seven faceted samples purchased from Tairus company, Bangkok, were kindly loaned from the private collection of Dr D. Schwarz, Lucerne, Switzerland.

References

Bagdasarov, K.S., Ilin, N.P., and Starostin, J.A., 1977. Apparatus for growing single crystals of high-melting oxides. US Patent 4,013,421, Mar. 22, 1977

Bagdasarov, C.S., Ilin, N.P., and Starostin, J.A., 1978. Vorrichtung zum Züchten von Einkristallen schwer schmelzbarer Oxide. DE Patent 24 61 968, 3.8.1978

Bagdasarov, K.S., Khaimov-Malkov, V.Y., Ilin, N.P., Starostin, J.A., Fedorov, E.A., and Sedakov, N.I., 1975. The growth of monocrystals of corundum. GB Patent 1 383 400, 12 Feb. 1975

Bagdasarov, K.S., Khaimov-Malkov, V.Y., Ilin, N.P., Starostin, J.A., Fedorov, E.A., and Sedakov, N.I., 1981. Method of growing monocrystals of corundum from a melt. US Patent 4,303,465, Dec. 1, 1981

Bank, H., Henn, U., and Milisenda, C.C., 1997. Gemmological news. Synthetic alexandrites from Russia. Gemmologie. *Zeitschrift der Deutschen Gemmologischen Gesellschaft,* **46**(2), 70

Bauerhansl, P., and Beran, A., 1997. Trace hydrogen in the olivine-type minerals chrysoberyl, Al_2BeO_4 and sinhalite, $MgAlBO_4$ — a polarized FTIR spectroscopic study. *Schweizerische Mineralogische und Petrographische Mitteilungen,* **77**, 131–6

Bukin, G.V., Eliseev, A.V., Matrosov, V.N., Solntsev, V.P., Kharchenko, E.I., and Tsvetkov, E.G., 1980. The growth and examination of optical properties of gem alexandrite. In: Sidorenko, A.V., *et al.* (Eds.) *Inhomogeneity of minerals and crystal growth*. Proceedings of the XI General Meeting of IMA, Novosibirsk 1978, published Moscow 1980, 317–28 (in Russian)

Farrell, E.F., and Newnham, R.E., 1965. Crystal-field spectra of chrysoberyl, alexandrite, peridot, and sinhalite. *American Mineralogist,* **50**(11-12), 1972–81

Gulev, V.S., Gurov, V.V., and Yurkin, A.M., 1990. Generation of laser based on alexandrite grown by horizontally directed crystallization. *Proceedings SPIE,* **1223**, Solid State Lasers, 115–26

Gurov, V.V., Bukin, G.V., Yurkin, A.M., and Kovalenko, N.V., 1988. Growth of Cr- and Ti-activated chrysoberyl crystals by horizontal directional solidification. *VII All-Union Conference on Crystal Growth, Moscow 1988,* **3**, 245–7 (in Russian)

Gurov, V.V., and Kirdyashkin, A.G., 2001. Sectorial structure of chrysoberyl crystals grown by horizontal directional solidification. *Inorganic Materials,* **37**(1), 44–6

Gurov, V.V., and Kirdyashkin, A.G., 2012. Physical modelling of heat and mass transfer in large crystal growth by high-temperature horizontal directional crystallization. *Journal of Applied Mechanics and Technical Physics,* **53**(1), 83–9

Gurov, V.V., and Tsvetkov, E.G., 1998. Investigation of the high-temperature polymorphic transformation in chrysoberyl. *Inorganic Materials,* **34**(7), 719–21

Gurov, V.V., and Tsvetkov, E.G., 2008. Specific character of melt growth of low-temperature phase of aluminium beryllate. *Journal of Crystal Growth,* **310**(1), 229–33

Gurov, V.V., Tsvetkov, E.G., and Bukin, G.V., 1986. Study of the solid-state transformation in chrysoberyl. XI All-Union Conference on Experimental Studies in Mineralogy, Chernogolovka 1986, 54 (in Russian)

Gurov, V.V., Tsvetkov, E.G., and Kirdyashkin, A.G., 2003. Features of beryllium aluminate crystal growth by the method of horizontally oriented crystallization. *Journal of Crystal Growth,* **256**(3/4), 361–7

Gurov, V.V., Tsvetkov, E.G., and Yurkin, A.M., 2008. Laser alexandrite crystals grown by horizontal oriented crystallization technique. *Optical Materials,* **30**(9), 1399–404

Halvorsen, A., 2006. The Usambara effect and its interaction with other colour change phenomena. *Journal of Gemmology,* **30**(1/2), 1–21

Halvorsen, A., and Jensen, B.B., 1997. A new colour-change effect. *Journal of Gemmology,* **25**(5), 325–30

Henn, U., 1992. Über die diagnostischen Merkmale von synthetischen Alexandriten aus der Gemeinschaft Unabhängiger Staaten (GUS). *Zeitschrift der Deutschen Gemmologischen Gesellschaft,* **41**(2/3), 85–93

Liu, Y., Shigley, J.E., and Halvorsen, A., 1999. Colour hue change of a gem tourmaline from the Umba Valley, Tanzania. *Journal of Gemmology,* **26**(6), 386–96

Malsy, A.-K., and Armbruster, T., 2012. Synthetic alexandrite–growth methods and their analytical fingerprints. *European Journal of Mineralogy,* **24**(1), 153–62

Nassau, K., 2001. *The physics and chemistry of color. The fifteen causes of color. 2nd edn.* John Wiley & Sons, New York, 94–6

Schmetzer, K., 2012. Natural alexandrites and chrysoberyls from Madagascar with irregular and regular growth patterns. *Australian Gemmologist,* **24**(10), 243–48

Schmetzer, K., Bernhardt, H.-J., Bosshart, G., and Hainschwang, T., 2009. Colour-change garnets from Madagascar: variation of chemical, spectroscopic and colorimetric properties. *Journal of Gemmology,* **31**(5-8), 235–82

Schmetzer, K., Bernhardt, H.-J., and Hainschwang, T., 2012. Flux-grown synthetic alexandrites from Creative Crystals. *Journal of Gemmology,* **33**(1–4), 49–81

Schmetzer, K., and Bosshart, G., 2010. Colorimetric data of Russian alexandrite and yellowish green to green chrysoberyl. In: Schmetzer, K. *Russian alexandrites.* Schweizerbart Science Publishers, Stuttgart, 107–20

Schmetzer, K., and Malsy, A.-K., 2011. Alexandrite and colour-change chrysoberyl from the Lake Manyara alexandrite-emerald deposit in northern Tanzania. *Journal of Gemmology,* **32**(5–8), 179–209

Schmetzer, K., Peretti, A., Medenbach, O., and Bernhardt, H.-J., 1996. Russian flux-grown synthetic alexandrite. *Gems & Gemology,* **32**(3), 186–202

Stockton, C.M., and Kane, R.E., 1988. The distinction of natural from synthetic alexandrite by infrared spectroscopy. *Gems & Gemology,* **24**(1), 44–6

Trossarelli, C., 1986. Synthetic alexandrite from USSR. *La Gemmologia,* **11**(4), 6–22

The Authors

Dr Karl Schmetzer
D-85238 Petershausen, Germany
email: SchmetzerKarl@hotmail.com

Dr Heinz-Jürgen Bernhardt
ZEM, Institut für Geologie, Mineralogie und Geophysik, Ruhr-Universität, D-44780 Bochum, Germany
email: Heinz-Juergen.Bernhardt@rub.de

Walter A. Balmer
CH-3800 Unterseen, Switzerland
email: wb@quicknet.ch

Thomas Hainschwang
GGTL Laboratories, Gemlab (Liechtenstein)/GemTechLab, FL 9496 Balzers, Liechtenstein/CH 1227 Geneva, Switzerland
email: thomas.hainschwang@ggtl-lab.org

Gem-A

THE GEMMOLOGICAL ASSOCIATION
OF GREAT BRITAIN

Special offer

September offer available from the Gem-A shop

New Diamond Tester

This useful instrument is capable of testing all diamond simulants including synthetic moissanite.

- Metal detection facility
- Built-in longwave UV and LED
- Tester flashes following colours upon detection:
  Blue light: diamond
  Green light: synthetic moissanite
  Red light: other stone
  Yellow light: metal

SPECIAL PRICE
(Usual price: £135 + VAT)

£108 + VAT

SAVE 20%

Plus postage and packing

Offer available on orders placed before 1 October 2013 only; no further discounts apply.

Understanding Gems™

Visit www.gem-a.com

The Journal of Gemmology / 2013 / Volume 33 / No. 5–6

Structural features of new varieties of freshwater cultured pearls in China

Professor Li Liping and Wang Min

Abstract: Some new varieties of freshwater cultured pearls in different shapes have emerged onto the Chinese market, including both non-beaded and beaded special shape pearls, and second generation cultured pearls. The culturing process to produce the new-shaped pearls is investigated and many samples in pearl-culturing farms in the Shanxiahu area, Zhuji City, Zhejiang Province, China, were collected. The gemmological microscope, cathodoluminescence microscope and Raman spectroscope were used in detecting the structures of a comprehensive sample of the new varieties in special shapes, and X-ray diffraction was used to detect the composition of the central parts of the new varieties. The results reveal that the structures of the new varieties of freshwater cultured pearls compare closely with those of traditional varieties of freshwater cultured pearl: a series of concentric nacreous layers and, for beaded pearls, nacreous layers around the bead. The nacreous layers consist mainly of aragonite, a little vaterite and some organic substance, which is the same as that in traditional cultured freshwater pearls.

Keywords: composition, freshwater cultured pearls, new varieties, structure

Second generation pearls.

1. Introduction

The production of pearls in China has experienced rapid growth in the past five decades. Since 2005, the yield of freshwater cultured pearls in China has generally been more than 1200 tonnes, maintaining the highest national output in the world, and accounting for over 90% of the total annual yield (see *Table I*).

First and foremost, the achievement is attributed to optimization of the breeding of mussels, improvement of surgery techniques, and reinforcement of culturing management. By utilizing variety and quality appraisal, hybridization and other biological techniques, the Kang Le mussel, a new hybrid of *Hyriopsis schlegelii* and *Hyriopsis cumingii*, was successfully cultivated using a patented technique. Three years after the implant operation, compared with *Hyriopsis cumingii*, the average width and weight of Kang Le mussels increased by 25.66% and 46.98% respectively. Together with a 31.96% increase in yield, the average size of pearls produced increased 23.32% and the proportion of large and good quality pearls increased by a factor of 3.72[1].

Table I: The yield of Chinese freshwater cultured pearls in recent years.

Year	Yield (ton)	Percentage of the total yield worldwide
2005	1200	95%
2006	1550	96%
2007	1600	96%
2008	1400	94%
2009	1200	94%
2010	1000	93%

Traditional and simple ways of pearl processing – drilling and stringing – have evolved to include faceting, embedding and engraving[2]. Now, various kinds of beaded and non-beaded pearls can also be cultivated by changing the shape of the mantle implant and the position in which it is inserted.

Structural features of new varieties of freshwater cultured pearls in China

Figure 1: Long strip pearl.
Figure 2: Cross-shaped pearl.
Figure 3: Square flake beaded pearls.
Figure 4: Round disc-shape beaded pearls; the one indicated with the arrow is the round flake nucleus.
Figure 5: Rectangular flake beaded pearls.

Figure 6: Second generation flake or petal-shape pearls.

Figure 7: Soufflé pearls.

2. New varieties of freshwater pearl and their cultivation techniques

Roundness has traditionally played an important role in pearl quality appraisal — this also being an appreciation of the rarity of this shape in natural populations. Like the natural population, most non-beaded freshwater cultured pearls are off-round or elliptical, and their prices are rather low. The same is true for new varieties of baroque cultured freshwater pearls, which comprise:

a. Non-beaded cultured pearls of elongated bar shapes such as long strip pearl *(Figure 1)*, and cross-shaped pearls *(Figure 2)*.
b. Flat, beaded cultured pearls of rhombic shape *(Figure 3)*, circular or round (so-called coin pearls) *(Figure 4)*, and rectangular pearls *(Figure 5)*.
c. Second generation pearls of a thin flake or petal shape *(Figure 6)* and bubble-shaped so-called soufflé pearls *(Figure 7)*.

2.1 Appearance and culturing techniques of non-beaded cultured baroque-shaped pearls

Depending on the shape of the mantle tissue implant, non-beaded cultured pearls can accordingly take various shapes, such as elongated bars and crosses. Usually, additional characteristics will disturb the smoothness of the surface of the pearls and affect their appearance. Colours are typical for pearls of freshwater origin, mostly white, orange and purple. However, a colourful iridescence, leading to peacock, gold and purple hues, is quite common. Surfaces are usually wrinkled and folded to some degree and their lustre can vary over the surface of a single pearl; the larger non-beaded cultured pearls generally have a high lustre.

The culturing routine for non-beaded cultured pearls follows the established pattern of providing spat for the cultivation of parent mussels, followed by implantation and farming techniques prior to the pearl harvest. However, there are now stricter requirements in the selection and cultivation of parent mussels, and the method of implantation.

a. Donor mussels used for the grafting process should be high-quality *Hyriopsis cumingii* shells, one to two years old, with a length of over 10 cm, grown at the muddy bottom without fertilizers. They are moved into a pool and hung at a depth of 20–30 cm from the water surface for 10–15 days before they are operated on[3].
b. The mantle tissue (epidermal cells) of the donor mussel is cut into small pieces of different shapes. For instance, long-strip shapes are used if the desired pearl shape is an elongated bar.
c. For the grafting process, a shell opener and a cork are used to keep the shell open, and the inner soft body and the abdominal foot are pushed aside. Prepared tiny pieces of mantle tissue are now implanted into the mantle of the mussel. If the desired pearl is cross shaped, two strips of mantle tissue have to be implanted at a right angle to each other.
d. At the end, grafted mussels are put into the water to recover.

2.2 Appearance and culturing techniques of beaded cultured pearls displaying new shapes

The new shapes of beaded cultured pearls depend on the shapes of the beads. The surfaces of these new pearl varieties are usually not quite smooth, but the shapes are regular and their lustres are good.

Compared with the culturing routine for non-beaded pearls, there are differences in the implantation procedure. Beads are produced from freshwater shell. During the grafting process a round bead or a bead of another shape, such as a flat rhombus flake or a round disc, is implanted into the mantle, the visceral sac or the gonad of the recipient mussel, together with a prepared tiny piece of mantle tissue. The recipient mussel is then put back into the water for post-operative recovery.

Currently, most round beaded freshwater cultured pearls are gonad-grown as this technique produces a higher survival rate and higher yield.

2.3 Appearance and culturing techniques of second generation pearls

It is well-known that most freshwater cultured pearls have been obtained by killing the pearl mussel at the harvest, which means utilizing the mussel only

Figure 8: The cross section of a cross-shaped pearl.

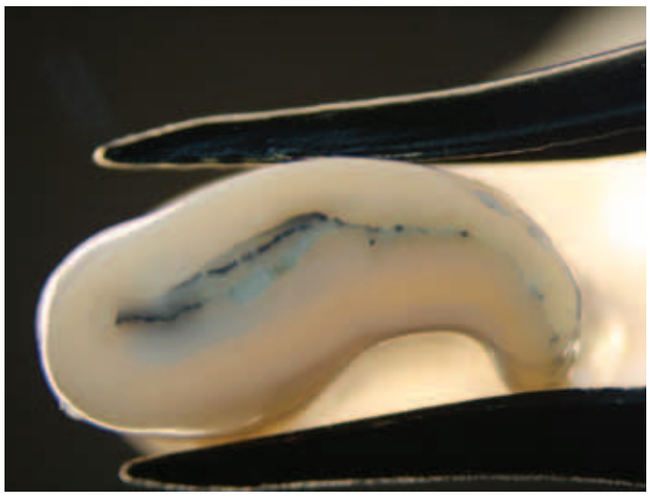

Figure 9: The cross section of an elongated bar-shaped pearl.

once. Second generation pearls are produced by operating on harvested mussels which have been kept alive. Immediately after the first harvest is finished, a bead or a piece of mantle tissue is implanted in the pearl sac from which a pearl has just been extracted, and then the mussel is put back in the water. After two or three years, a second generation pearl can be obtained. It may be beaded or non-beaded.

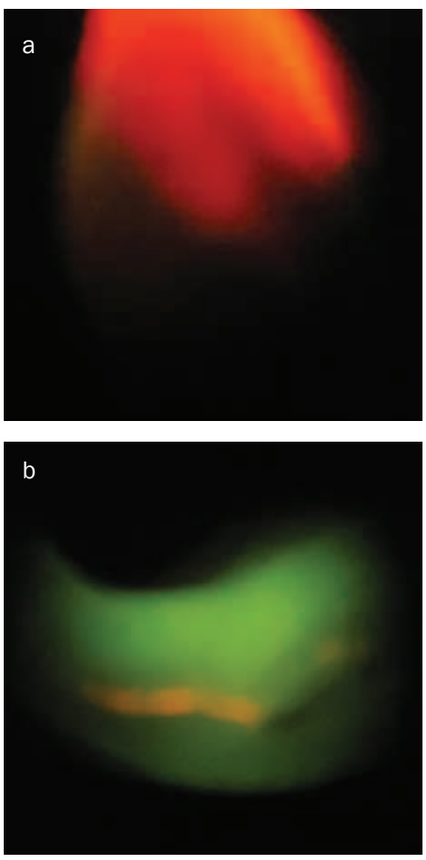

Figure 10: CL images of the cross sections of (a)cross-shaped pearls and (b) elongated bar-shaped pearls.

Depending on the shape of the pearl sac, non-beaded second generation pearls are usually thin and have the shapes of curved flakes or petals *(Figure 6)*. Mostly the surfaces of the pearls are not very smooth. Their colours are mostly white, orange or purple. However, the iridescence of the pearls varies on the surface, commonly being pink, peacock green, golden or purple. Another shape in this non-beaded category is the so-called soufflé pearl which is baroque shaped. Soufflé pearls are large in size but light in weight. They may also show a range of metallic pastel shades and mixed lustres *(Figure 7)*.

Before the grafting process, high-quality harvest mussels in good health and of large size are selected. After opening the shell, the viscera and the abdominal foot are pushed to one side, before cutting a suitable incision into the pearl sac to take out the first grown pearl. After carefully dressing the wound to prevent infection, tiny pieces of mantle or bead are implanted in the already existing pearl sac. If a soufflé pearl is desired, a muddy liquid is injected into the pearl sac using an injector. Finally the grafted mussel is put back into fresh water.

3. The structure of new varieties of freshwater pearls

The following samples were selected for our study: two non-beaded cultured shaped pearls, two new-shaped beaded cultured pearls and two freshwater cultured second generation pearls from a pearl-culturing farm in the Shanxiahu area, Zhuji City, Zhejiang Province, China. Their cross sections were polished and studied using the gemmological microscope, cathodoluminescence (CL) microscopy and Raman spectroscopy to record their structural features.

3.1 The structure of the non-beaded cultured new-shaped pearls

Under the gemmological microscope, the cross sections of non-beaded cultured new-shaped pearls show successive concentric lines parallel to the shape of the outline of the pearl, which is similar to that of already-known non-beaded freshwater pearls (*Figures 8* and *9*). In the centre of the pearl shown in *Figure 9* there is an irregular hole which contains some black organic substance.

Under the CL microscope, almost all samples show yellowish-green fluorescence, except in the centres of the cross-shaped and the elongated bar-shaped pearls where orange fluorescence is found *(Figure 10)*.

All the samples and the powders of the parts showing orange and

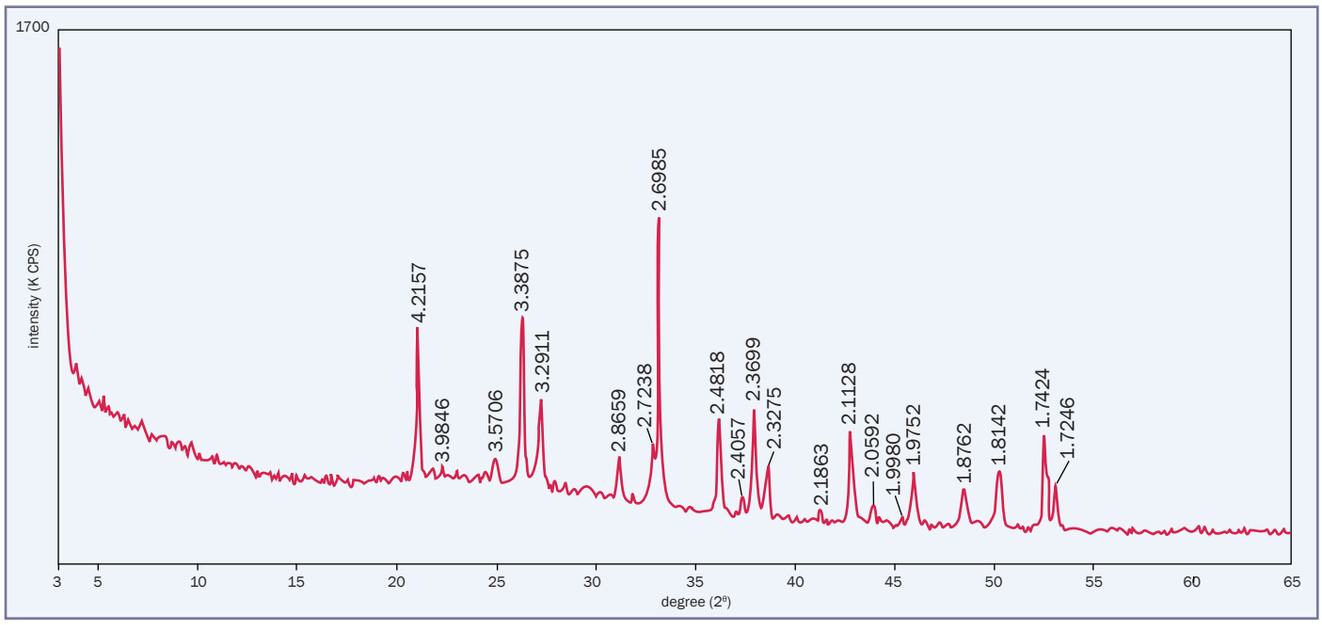

Figure 11: The XRD peaks of the powders of the central part of the cross-shaped pearl which shows orange CL, indicating the additional presence of vaterite.

yellowish-green CL were analyzed using X-ray powder diffraction (XRD) in order to investigate their mineralogical composition. Those samples showing yellowish-green CL contain only aragonite, as determined by comparing the peaks with the standard data of aragonite (diffraction peaks at 3.3875, 3.2911, 2.6985, 2.4818, 2.3699, 2.1863, 1.9752, 1.0876, 1.8142 and 1.7424). However, the powder sample collected from the central part of the cross-shaped pearl showing orange CL, shows peaks at 4.2157, 3.5706, 3.2911, 2.7238, 2.3275, 2.1128, 2.0592, 1.8142 and 1.7424 *(Figure 11)*, which indicates the additional presence of vaterite. Therefore, the freshwater pearls in the new shapes contain both aragonite with yellowish-green CL and vaterite showing orange CL. Such a composition is almost the same as that of freshwater pearls in traditional spherical shapes[4].

3.2 The structure of the new-shaped beaded cultured pearl

Observation of the cross sections of rhombic and coin-shaped beaded cultured pearls under the gemmological microscope shows a sharp boundary *(Figure 12)* and no prismatic layer or other dividing line between the pearl layer and the pearl bead — which features

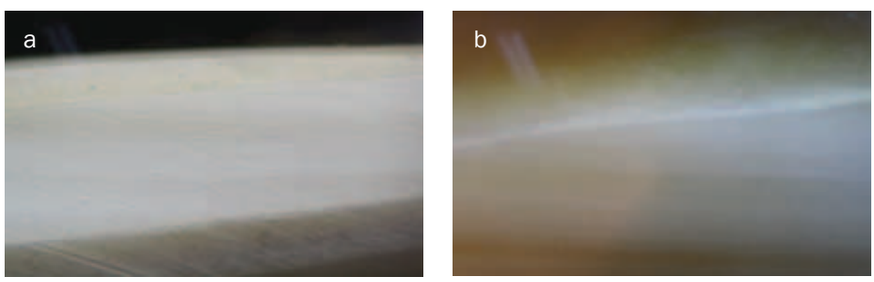

Figure 12: The microstructures of cross sections of (a) rhombic and (b) coin-shaped beaded pearls.

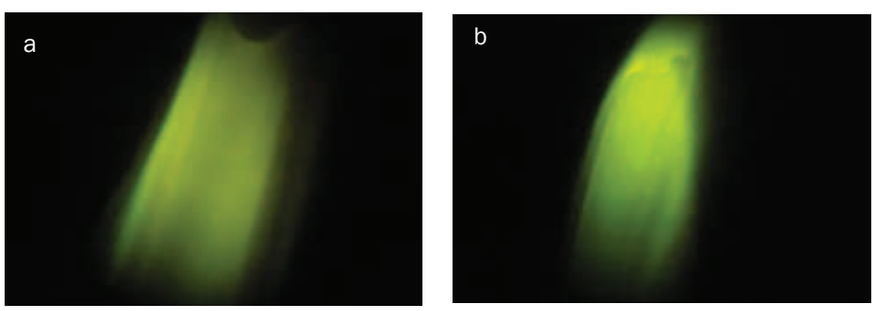

Figure 13: The CL images near the bead boundaries in (a) circular and (b) rectangular flat beaded pearls.

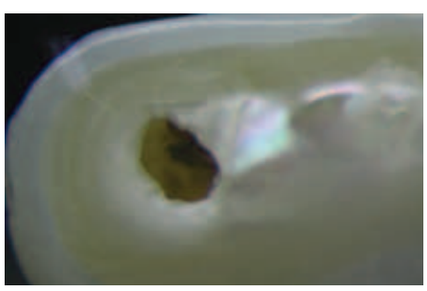

Figure 14: The concentric nacreous layers are visible in this cross-section of a flake-shaped second generation pearl.

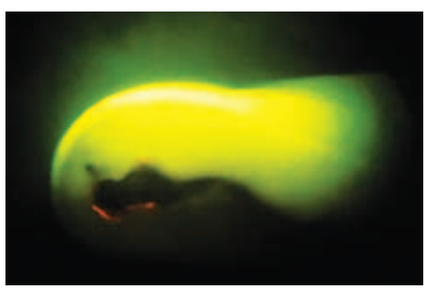

Figure 15: The CL image of a flake-shaped second generation pearl.

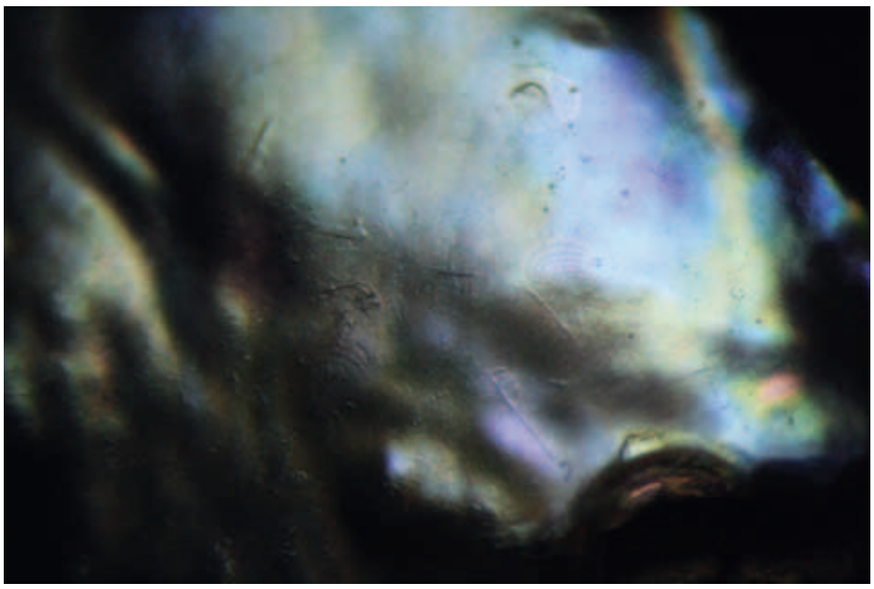

Figure 16: The surface of the soufflé pearl under the microscope.

are always present in beaded saltwater pearls[4].

Under the CL microscope, the bright yellowish-green CL and the clear laminar structure in the shell bead are distinctive, with a dark yellow-green CL at the boundary and in the surrounding pearly layers *(Figure 13)*.

3.3 The structure of second generation pearls

The cross section of a second generation non-beaded pearl *(Figure 14)* displays its concentric structure and a yellowish organic substance in an inner cavity. Overall yellowish-green CL with pinpoint orange CL in the cavity edge is visible under the CL microscope *(Figure 15)*.

The soufflé pearl is hollow and contains a large proportion of space, so it is very light. When it is cut in two, the nacreous layers are revealed to be very thin and there is a small amount of black mud powder in the central hole. However, its surface iridescence is very strong *(Figure 16)*. Under the gemmological microscope it shows thin nacreous layers and a visible laminar structure in the broken surface.

4. Conclusions

The implantation of different shapes of mantle tissue into the mantle of a mussel can produce new shapes of non-beaded cultured pearls. Also shell beads in different shapes can be implanted into the mantle or into the visceral sac or the gonad to produce beaded pearls in different shapes. By implanting a mantle tissue or injecting muddy liquid into the sac from which a pearl has just been harvested one can obtain second generation pearls. The basic structure of the new varieties of freshwater pearls is similar to that of traditional freshwater cultured pearls, which consists of concentric nacreous layers; these are mainly of aragonite with small quantities of vaterite, and some organic residue remaining in the central hole.

References

1. Patent number 200510026149.8, innovation patent, issued date 2005-5-25, inventors: Li Jiale, Zheng Hanfeng, Yuan Weikang. A cross hybrid of *Hyriopsis schlegelii* and *Hyriopsis cumingii*. (In Chinese)
2. Xu Chong, Li Li-ping and Yang Chun, 2010. New varieties of freshwater cultured pearls and new development for techniques in China. *Journal of Gems and Gemmology,* **1**, 50–4 (In Chinese with English abstract)
3. Yu Yongsheng, 2006. Technical essential of non-nucleated cultured pictographic pearls in China. *Famous Special Aquatic Product,* **6**, 26–7. (In Chinese)
4. Li Liping, 2009. Composition of seawater and freshwater cultured pearls in China. *Earth Science — Journal of China University of Geoscience*. **9**, 752–8. (In Chinese with English abstract)

The Authors

Professor Li Liping PhD FGA DGA* and Wang Min
Gemmological Institute,
China University of Geosciences,
Wuhan, P.R. China

* Corresponding author:
liliping12@gmail.com

Titanium-bearing synthetic alexandrite and chrysoberyl

Dr Karl Schmetzer, Dr Heinz-Jürgen Bernhardt and Thomas Hainschwang

Abstract: The inclusions, compositions and spectra of synthetic reddish violet titanium-bearing chrysoberyl and synthetic alexandrites grown by the Czochralski method by Kyocera in Japan are described. These samples are compared with titanium-, chromium- and vanadium-bearing synthetic alexandrite cat's-eyes and six-rayed alexandrite stars. It is concluded that reddish violet chrysoberyl is coloured by trivalent titanium; the alexandrites are predominantly coloured by chromium with minor amounts of vanadium being also present. Both groups of samples contain inclusions typical of Czochralski-grown chrysoberyl. The colour and pleochroism of chatoyant and asteriated alexandrites is caused by a combination of some trivalent titanium and chromium with minor traces of vanadium. Three light bands are produced by three series of needle-like, titanium-bearing crystals, most probably rutile needles, which are orientated at about 60° to each other. The production technique of alexandrite cat's-eyes described in numerous patent documents is discussed.

Keywords: asterism, chatoyancy, Czochralski, electron microprobe analysis, rutile, synthetic chrysoberyl, titanium contents, visible range spectra

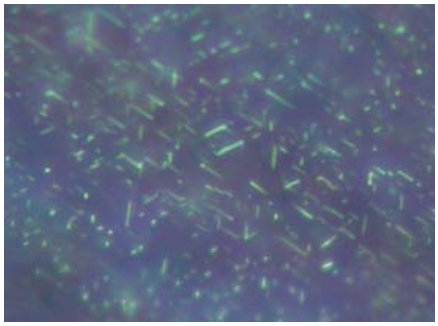

*A thin section of a star synthetic alexandrite from Kyocera oriented almost parallel to the **a** pinacoid shows three series of needles which form angles near 60° to each other. Reflected light, crossed polarizers, field of view 56 x 42 µm. Photo by H.-J. Bernhardt.*

Introduction

Synthetic alexandrite cat's-eyes produced by Kyocera in Japan appeared on the market in the late 1980s with the trade name 'Inamori synthetic alexandrite' or 'Inamori created alexandrite' (Kane, 1987; Scarratt, 1988; Koivula *et al.*, 1988). The material – when cut as cabochon in the proper direction – normally showed a well-centred light band *(Figure 1),* but Kane (1987) mentioned that "when the cabochons were viewed under a strong, single incandescent light source down the long direction, asterism was observed".

When a cabochon is cut with its base perpendicular to that producing a good cat's-eye, a six-rayed asteriated alexandrite can be obtained (*Figure 1;* see also Schmetzer and Hodgkinson, 2011). During the microscopic examinations of the stones mentioned in that paper (*op. cit.*), in immersion it was observed

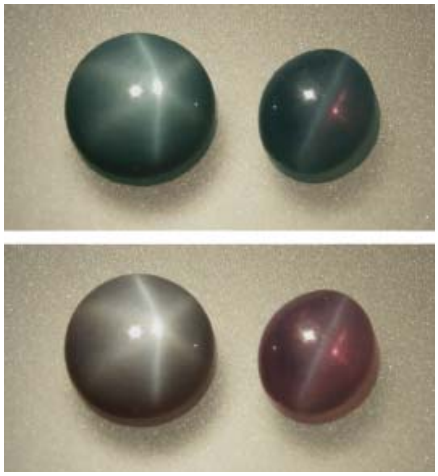

Figure 1: Synthetic asteriated alexandrite (left, 2.62 ct, diameter 8.0 mm) and synthetic alexandrite cat's-eye (1.55 ct, 7.0 x 6.0 mm) produced by Kyocera in Japan in daylight (above) and incandescent light. Photo by K. Schmetzer.

*Table I: Trace element contents, colour and spectroscopic properties of titanium-bearing synthetic chrysoberyl and synthetic alexandrite.**

Reddish violet chrysoberyl

Colour and pleochroism

	X || a	Y || b	Z || c
Daylight	light yellow orange	intense orange red	reddish violet
Incandescent light	light yellow orange	intense orange red	reddish purple

Spectroscopic properties, with polarization, absorption maxima (in nm)

Polarization	X || a	Y || b	Z || c
Maxima	565 shoulder	565 shoulder	565
	490	498	495

Chemical properties (average, wt.%)

Sample	RV1 faceted	RV2 faceted	RV3 faceted	RV4 faceted
Technique	microprobe	microprobe	microprobe	microprobe
No. of analyses	10	10	10	10
TiO_2**	0.210	0.228	0.213	0.373
V_2O_3	0.008	0.006	0.019	0.005
Cr_2O_3	0.005	0.008	0.010	0.006
MnO	0.008	0.006	0.010	0.004
Fe_2O_3	0.009	0.006	0.009	0.014

Alexandrite

Colour and pleochroism

	X || a	Y || b	Z || c
Daylight	blue violet	yellow green	blue green
Incandescent light	red purple	yellow orange	blue green

Chemical properties (average, wt.%)

Sample	A1 faceted	A2 faceted	A3 faceted	A4 faceted
Technique	microprobe	microprobe	microprobe	microprobe
No. of analyses	10	10	10	10
TiO_2**	0.014	0.008	0.007	0.007
V_2O_3	0.149	0.158	0.151	0.164
Cr_2O_3	0.393	0.291	0.254	0.308
MnO	0.007	0.009	0.009	0.009
Fe_2O_3	0.007	0.008	0.008	0.010

*Based on a morphological cell with a 4.42, b 9.39, c 5.47 ** total titanium as TiO_2

that the samples did not show the exact pleochroism which has hitherto been observed for synthetic vanadium- and chromium-bearing alexandrite (see, e.g., Schmetzer and Bosshart, 2010; Schmetzer and Malsy, 2011; Schmetzer *et al.*, 2013). In addition, a preliminary spectroscopic examination indicated some differences to the absorption spectra commonly observed for such chromium- and vanadium-bearing, iron-free synthetic samples (with distinctly higher chromium- than vanadium-contents). It was suspected that another colour-causing trace element might be present, but the analytical data had shown only traces of vanadium, chromium and titanium, with the titanium assumed to be present in the form of rutile precipitates, which in turn were responsible for asterism and/or chatoyancy.

Titanium-bearing chrysoberyl with pink coloration was briefly described by Krzemnicki and Kiefert (1999), but no data for pleochroism or spectroscopic properties were given. Titanium-bearing synthetic sapphires as well as titanium-doped synthetic chrysoberyls are grown for technical use as laser crystals. In some of these laser materials, the aim is to create and retain as much as possible of the titanium in its trivalent form. In gemmology, Ti^{3+} was reported as being responsible for the coloration of specifically doped synthetic corundum (Johnson *et al.,* 1995) and titanium-bearing Kashan synthetic ruby in which titanium is present in its trivalent state (Schmetzer and Schwarz, 2007). In the natural environment however, i.e. in most rocks and minerals, titanium is present as Ti^{4+} and trivalent titanium is unstable.

Thus, to explain the colours mentioned above in paragraph two for the phenomenal synthetic alexandrites grown by Kyocera, in this study we investigate the role of Ti in the Kyocera synthetic chrysoberyls and alexandrites, with or without stars or cat's-eyes.

Samples

Stones examined:

a) Reddish-violet chrysoberyl (see samples RV 1–4 in *Table I*): three rough crystals and nine faceted stones *(Figure 2)*. The rough crystals were of somewhat irregular hexagonal cylindrical shape with six side faces and upper and lower bases. Obviously, these cylinders had been sawn from rough Czochralski-grown crystals and the upper and lower bases as well as the side faces had been roughly polished to clean the crystals and give a better visual impression. The faceted gemstones had been cut without specific orientation. All samples had been donated by Kyocera Germany to the Bavarian State Collection for Mineralogy, Munich, Germany.

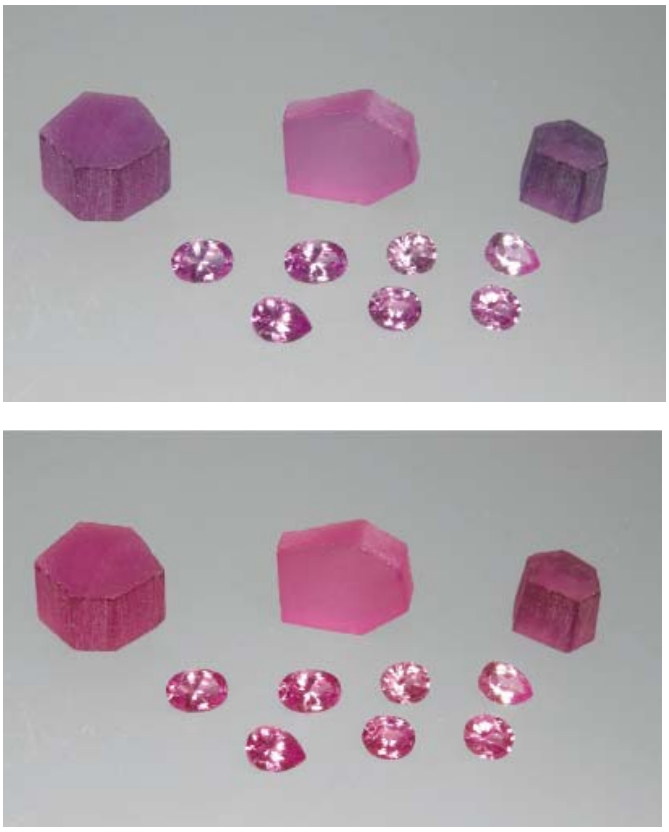

Figure 2: Rough and faceted titanium-bearing synthetic chrysoberyls produced by Kyocera in Japan in daylight (above) and incandescent light; size of the rough crystal above left 16.0 x 15.5 x 10.0 mm, weight 34.12 ct, the faceted sample below left weighs 1.08 ct and measures 7.8 x 5.7 mm. Photo by K. Schmetzer.

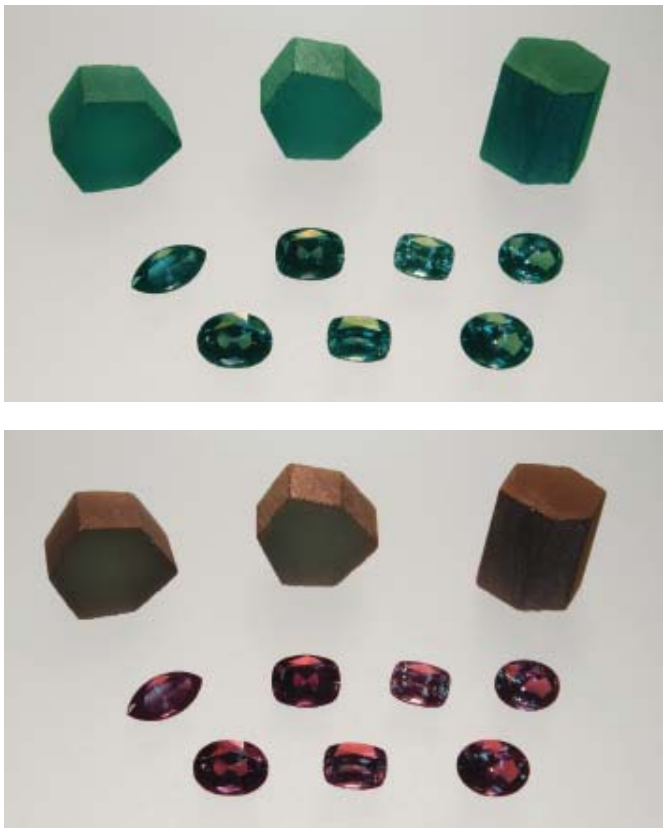

Figure 3: Rough and faceted synthetic alexandrites produced by Kyocera in Japan in daylight (above) and incandescent light; size of the rough crystal above right is 12.2 x 11.2 x 15.6 mm, weight 32.45 ct, the faceted sample below left weighs 1.71 ct and measures 8.0 x 6.0 mm. Photo by K. Schmetzer.

b) Alexandrites from Kyocera (see samples A 1–4 in *Table I*), three pseudohexagonal cylinders and nine faceted samples *(Figure 3)*. The features described in (a) for the rough cylinders of reddish violet chrysoberyl are similar to those shown by these alexandrites.
c) Alexandrite cat's-eyes and stars (*Table II*): three cabochon-cut samples had been prepared by A. Hodgkinson from a rod-shaped synthetic crystal of 18.84 ct that had been originally purchased in 1988. Two samples showed six-rayed asterism, and the other was a cat's-eye *(Figure 1)*. Two additional cat's-eyes (C2 and C3 in *Table II* and *Figure 4*) were available from the private collection of G. Bosshart.

Results

Titanium-bearing chrysoberyls

The orientation of the edges of the somewhat irregular hexagonal cylinders *(Figure 2)* was more or less parallel to the crystallographic a-axis, which indicates that this was the direction of pulling and growth in the Czochralski process. The overall colour of the samples was reddish violet in daylight with a colour variation to reddish purple in incandescent light.

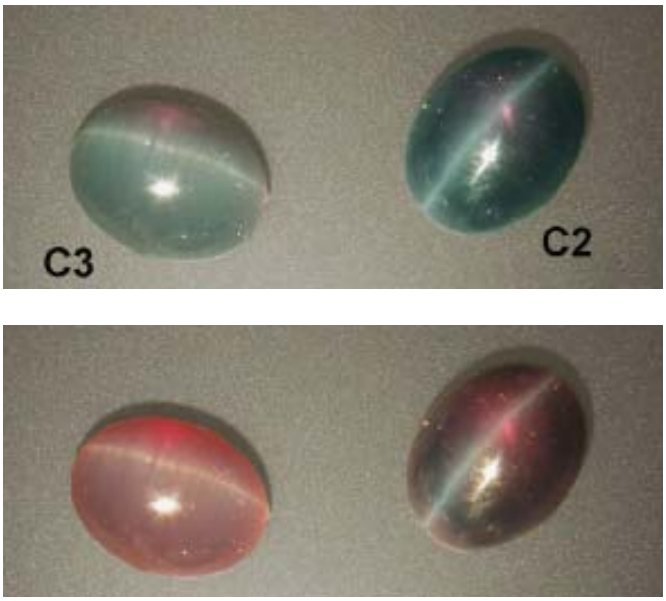

Figure 4: Synthetic alexandrite cat's-eyes produced by Kyocera in Japan in daylight (above) and incandescent light; sample C2 with lower Ti^{3+} contents weighs 3.29 ct and measures 9.2 x 7.2 mm, sample C3 with higher Ti^{3+} contents weighs 3.19 ct and measures 9.2 x 7.1 mm. Bosshart collection. Photo by K. Schmetzer.

*Table II: Trace element contents, colour and spectroscopic properties of synthetic alexandrite cat's-eyes and asteriated alexandrite.**

Colour, pleochroism and spectroscopic properties

Cabochon C1 base approx. || **a** (100) weak asterism		X || a	Y || b	Z || c
Incandescent light	view || a-axis, d = 2.5 mm		orange	orange
	view ⊥ a-axis, d = 8.0 mm	intense red orange	non-transparent	non-transparent
Spectroscopic properties, measurement || a-axis			Cr^{3+} spectrum, strong influence of Ti^{3+}	Cr^{3+} spectrum, strong influence of Ti^{3+}

Cabochon C2 base approx. || **b** (010) distinct cat's-eye		X || a	Y || b	Z || c
Incandescent light	view || b-axis, d = 2.8 mm	light purplish red		light green
	view ⊥ b-axis, d = 6.9 or 8.7 mm	intense purplish red	orange	intense green
Spectroscopic properties, measurement || b-axis		Cr^{3+} spectrum, moderate influence of Ti^{3+}		Cr^{3+} spectrum, moderate influence of Ti^{3+}

Cabochon C3 base approx. || **b** (010) weak cat's-eye		X || a	Y || b	Z || c
Incandescent light	view || b-axis, d = 2.6 mm	light yellowish orange		darker orange
	view ⊥ b-axis, d = 6.3 or 8.2 mm	intense red orange	non-transparent	non-transparent
Spectroscopic properties, measurement || b-axis		Cr^{3+} spectrum, strong influence of Ti^{3+}		Cr^{3+} spectrum, strong influence of Ti^{3+}

* based on a morphological cell with a 4.42, b 9.39, c 5.47 and X || a, Y || b, Z || c
d = diameter, representing the maximum path length of light in this orientation of the sample

Chemical properties (average, wt.%)

Sample	Cabochon C1 asteriated**	Cabochon C2 cat's-eye	Cabochon C3 cat's-eye
Technique	LA-ICP-MS	microprobe	microprobe
No. of analyses	2	10	10
TiO_2***	0.58	0.462	0.485
V_2O_3	0.11	0.123	0.119
Cr_2O_3	0.23	0.256	0.257
MnO	bdl	0.006	0.007
Fe_2O_3	bdl	0.007	0.005

** Schmetzer and Hodgkinson, 2011 *** total titanium as TiO_2
bdl = below detection limit

The pleochroism is variable, with similar colours observed for X and Y (yellow orange and orange red), and a more marked difference in the Z direction. The colour for both X and Y is almost identical in daylight and incandescent light, but in the Z direction a colour change from reddish violet in daylight to reddish purple in incandescent light is visible *(Figure 2)*.

The dominant colour-causing trace element of this group of samples is titanium *(Table I)*, the contents ranging from 0.21 to 0.23 wt.% TiO_2 in three samples, to 0.37 wt.% in a somewhat more intensely coloured stone (sample RV4). Other trace elements were only slightly above their respective detection limits in the electron microprobe.

The absorption spectra of the samples show a strong absorption band in the 495 nm range for X, Y and Z, and an additional band in the Z direction located at 565 nm *(Figure 5a, Table I)*. The absorption bands in the visible are assigned provisionally to Ti^{3+} which replaces Al^{3+} in the chrysoberyl structure, which is consistent with literature data (Segawa *et al.,* 1987; Anzai *et al.,* 1987, 1988; Sugimoto *et al.,* 1989). The spectra from the randomly orientated faceted stones *(Figure 5b)* are consistent with these data.

The microscopic examination showed almost plane, only slightly curved growth striations *(Figures 6, 7)* with a predominant orientation more or less parallel to the **a** (100) face, which represent the successive growth surfaces of the chysoberyl. As shown in *Figures 6* and *7*, the distances between these striations are variable. The centres of the rough crystals and the faceted samples were extremely clean with few, if any, inclusions. But in the outer areas of the rough samples, numerous gas bubbles and their migration traces within the growing crystal are present *(Figure 8)*.

Alexandrites

The synthetic alexandrites *(Figure 3)* contain two colour-causing trace elements, chromium and vanadium, with chromium contents always exceeding

Titanium-bearing synthetic alexandrite and chrysoberyl

those of vanadium. In detail, chromium ranges from 0.25 to 0.39 wt.% Cr_2O_3 and vanadium from 0.15 to 0.16 wt.% V_2O_3 *(Table I)*. Other trace elements were only slightly above their detection limits in the electron microprobe.

The orientation of the edges of the somewhat irregular hexagonal cylinders was more or less parallel to the crystallographic a-axis of chrysoberyl, which again indicates growth in this direction in the Czochralski process. Colour, colour change and absorption spectra (see *Table I*) are consistent with data from other iron-free, chromium- and vanadium-bearing synthetic alexandrites grown from the melt, e.g. Czochralski-grown or HOC-grown Russian alexandrites (for further details see Schmetzer and Bosshart, 2010; Schmetzer *et al.,* 2013).

The microscopic examination showed almost plane, only slightly curved growth striations *(Figure 9)* with an orientation parallel to the **a** (100) face, which again reflects the growth surfaces. Some samples showed extremely strong growth zoning which revealed a characteristic interference pattern under crossed polarizers *(Figure 10 a,b)*. Mostly rounded, occasionally also somewhat elongated gas bubbles were seen in some samples *(Figure 11),* and there are a few

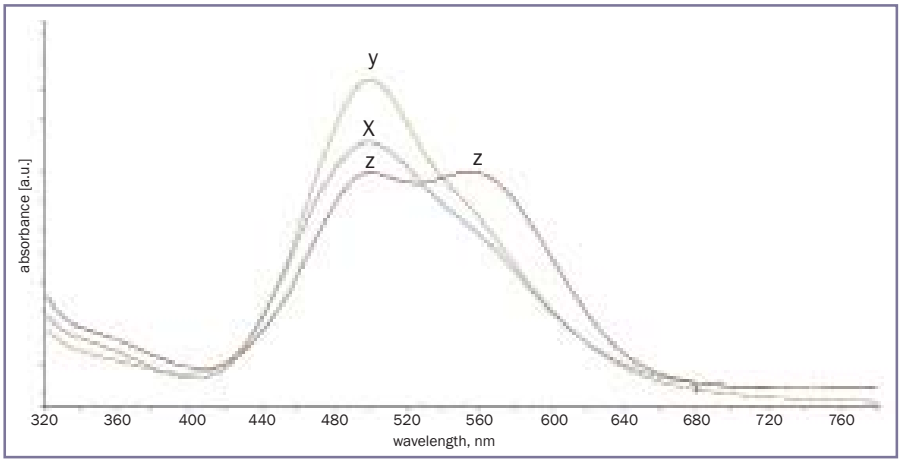

Figure 5a: Absorption spectra of a titanium-bearing synthetic chrysoberyl crystal in polarized light (with X || a, Y || b and Z || c).

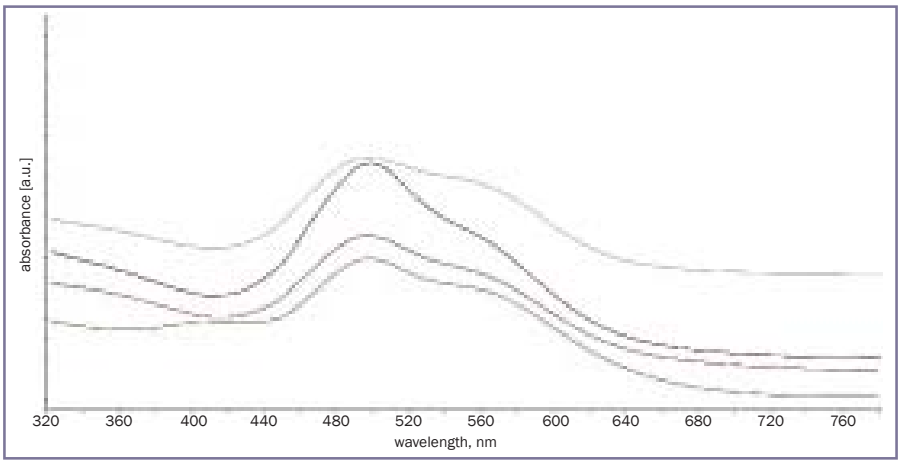

Figure 5b: Absorption spectra of four faceted titanium-bearing synthetic chrysoberyls in random orientation; the spectra of three chrysoberyls are vertically displaced for clarity.

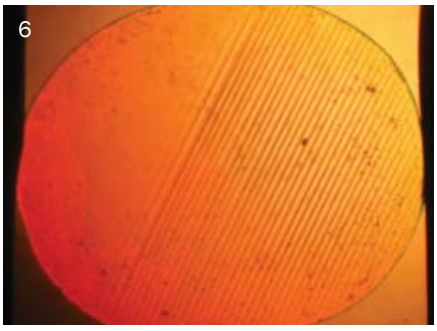

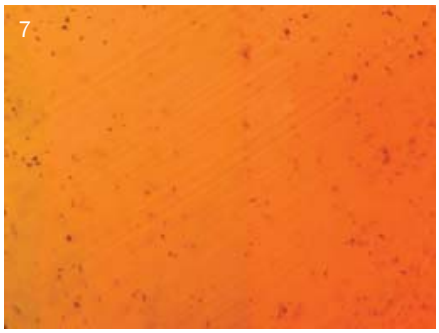

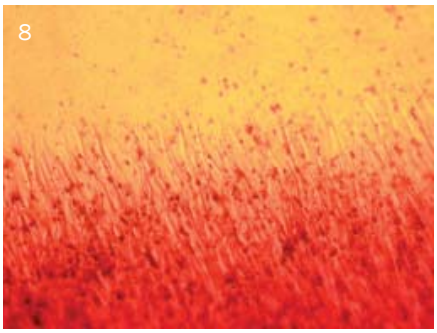

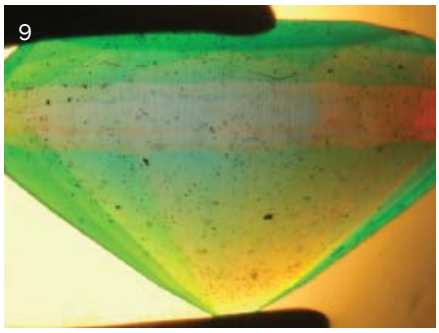

Figure 6: Slightly curved and quite coarse growth striations in reddish violet, titanium-bearing synthetic chrysoberyl produced by Kyocera in Japan. Immersion, field of view 6.9 x 5.2 mm. Photo by K. Schmetzer.

Figure 7: A sample of reddish violet, titanium-bearing synthetic chrysoberyl produced by Kyocera in Japan, is different from that in Figure 6, in which slightly curved growth striations show a much finer structure. Immersion, field of view 3.4 x 2.5 mm. Photo by K. Schmetzer.

Figure 8: Gas bubbles and the traces left as they migrated during growth of the crystal of reddish violet, titanium-bearing synthetic chrysoberyl. Immersion, field of view 2.4 x 1.8 mm. Photo by K. Schmetzer.

Figure 9: Slightly curved growth striations in synthetic alexandrite. Immersion, field of view 6.5 x 4.6 mm. Photo by K. Schmetzer.

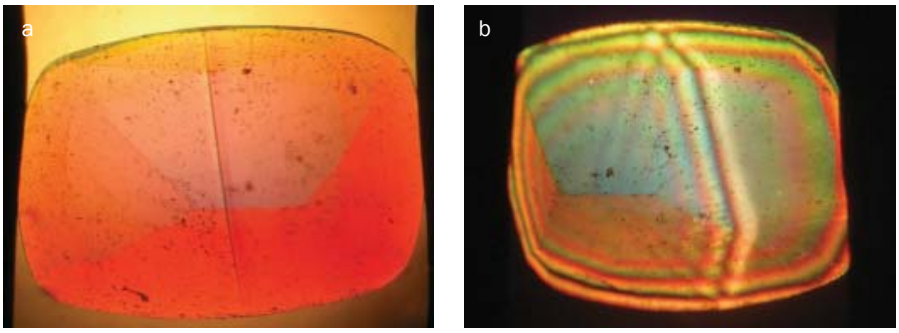

Figure 10: (a) Very distinct growth boundary in Kyocera synthetic alexandrite viewed in plane-polarized light. (b) Under crossed polarizers, a characteristic interference pattern is visible. Immersion, field of view 7.5 x 5.7 mm. Photos by K. Schmetzer.

Figure 11: Mostly rounded, occasionally also somewhat elongated gas bubbles in synthetic alexandrite. Immersion, field of view 3.7 x 2.7 mm. Photo by K. Schmetzer.

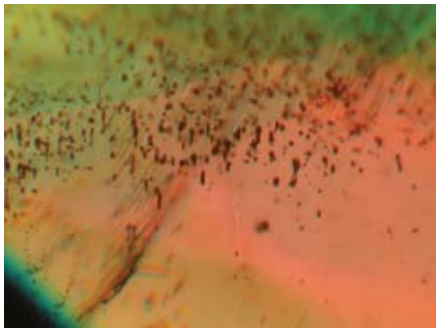

Figure 12: Gas bubbles and their migration traces within the growing crystal in Kyocera synthetic alexandrite. Immersion, field of view 2.1 x 1.6 mm. Photo by K. Schmetzer.

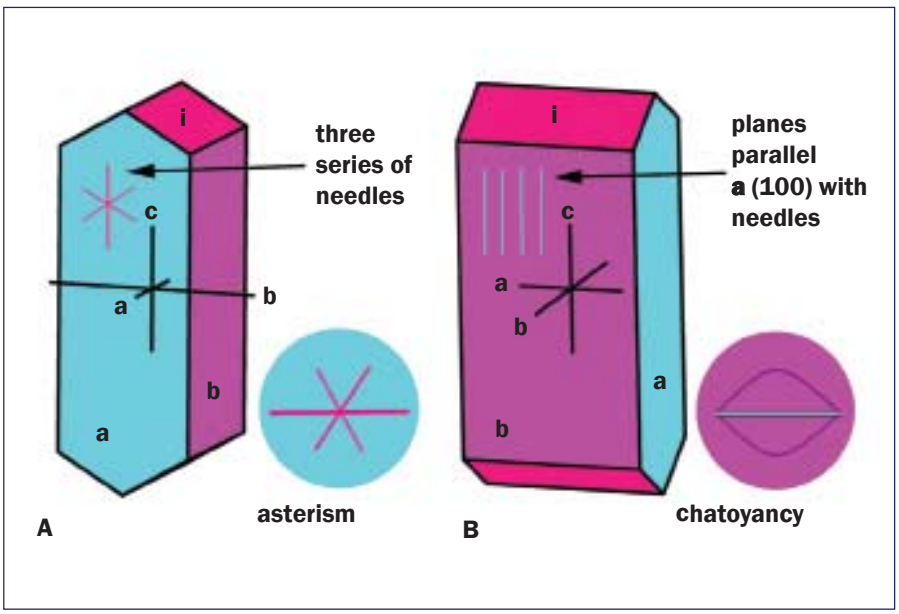

*Figure 13: Schematic drawings of asteriated or chatoyant synthetic alexandrite crystals in views parallel to the a-axis (A) and parallel to the b-axis (B). The light effect is due to three series of needles which are all located in planes parallel to the **a** (100) pinacoid; the orientations of the needles are parallel to the c-axis and the two **i** (011) faces. In a view parallel to the a-axis (A) the orientations of the needles reflect light to form a regular six-rayed star; in a view parallel to the b-axis (B), only one strong light band is seen in the centre of the chatoyant cabochon.*

gas bubbles with migration traces *(Figure 12,* see also *Figure 8).*

In summary, both varieties — the titanium-bearing chrysoberyl and the chromium- and vanadium-bearing, iron-free alexandrite — showed the typical structural features and inclusions which are common in synthetic chrysoberyl grown by the Czochralski technique. Colour, colour change, pleochroism and absorption spectra of the alexandrites are comparable to other synthetic samples with similar trace element contents. The spectra of the pink titanium-bearing samples are consistent with literature data.

Alexandrites showing chatoyancy and/or asterism

All the Kyocera alexandrite cat's-eyes or star stones seen by the authors show three different light bands. With an orientation of the base of the cabochon parallel to the **a** (100) pinacoid, a star will be visible, but with the base of the cabochon parallel to the **b** (010) pinacoid, only one dominant light band will be seen through the centre of the cabochon's dome, and the other two light bands at the girdle are almost invisible *(Figure 13 A,B,* see also *Figures 1, 4).*

From the orientation of these light bands it was concluded that three series of elongated particles are present which cause the reflections. These particles are located in layers parallel to the **a** (100) pinacoid, with one series of particles oriented parallel to the c-axis and the other two forming angles of 60° and -60° with the c-axis (i.e. particles elongated along the **i** and **–i** {011} prism faces of chrysoberyl). These minute particles, however, were too small to be identifiable with the gemmological microscope.

Chemical properties: The samples revealed distinct chromium and vanadium contents, with chromium contents always exceeding the amounts of vanadium measured. In detail, chromium contents were found between 0.23 and 0.26 wt.% Cr_2O_3 with vanadium contents ranging from 0.11 to 0.12 wt.% V_2O_3 *(Table II).* The titanium contents range from 0.46 to 0.58 wt.% TiO_2, distinctly higher than the values found in the

reddish violet titanium-bearing samples (see *Table I*). Also, consistent with these small ranges, the microprobe scans across polished windows at the bases of the two cabochons indicate the absence of any distinct chemical zoning.

Examination of dark layers: The two asteriated alexandrite cabochons and the three cat's-eyes examined contain darker, non-transparent layers within a matrix of transparent alexandrite *(Figure 14)*. Careful optical orientation of the samples (for the method see Schmetzer 2010, 2011) indicate that these layers are oriented parallel to the **a** (100) pinacoid. To evaluate the nature of these dark layers, we cut thin slices parallel to the slightly curved base of two of the chatoyant cabochons and of one asteriated alexandrite and prepared petrographic thin sections approximately 60 µm thick. According to the orientation of these dark layers, the thin section cut from the asteriated alexandrite was parallel to, and the two thin sections prepared from the cat's-eyes were perpendicular to these layers.

The thin section of the asteriated alexandrite, i.e. the section parallel to the **a** (100) pinacoid, showed a dense pattern of small reflecting needles. These needles have three preferred orientations of their long axes and intersect with angles of approximately 60° (*Figure 15,* see also Figure with the Abstract). The other two sections perpendicular to the b-axis, i.e. perpendicular to the dark layers, showed a clear zoning consisting of layers with high concentrations of needles alternating with areas which are more or less free of any needles *(Figure 16 a,b)*. The needles are sometimes visible in the form of parallel strings *(Figure 16a),* but occasionally also thicker layers containing needles were seen *(Figure 16b)*.

The individual needles in the Kyocera samples were too small either for microprobe or for Raman analysis, but visually similar, somewhat larger needles with identical orientation in natural alexandrite crystals were proven by microprobe analysis to be rutile single crystals and twins (Schmetzer and Bernhardt, unpublished research). Thus,

*Figure 14: In a view perpendicular to the a-axis of a cat's-eye or star Kyocera alexandrite, numerous dark planes within a transparent matrix are visible using an immersion microscope; these layers parallel to the **a** (100) pinacoid contain numerous tiny titanium-bearing needles which are the cause of the three light bands observed. The a-axis runs vertically, field of view 3.6 x 2.7 mm. Photo by K. Schmetzer.*

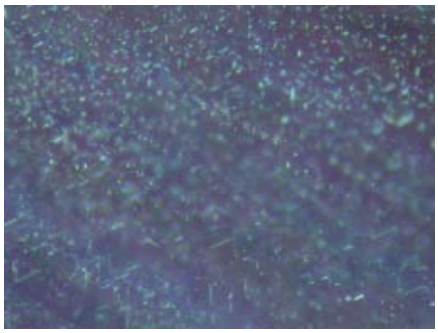

*Figure 15: A thin section of a star synthetic alexandrite from Kyocera oriented almost parallel to the **a** pinacoid shows three series of needles which form angles near 60° to each other. Reflected light, crossed polarizers, field of view 112 x 84 µm. Photo by H.-J. Bernhardt.*

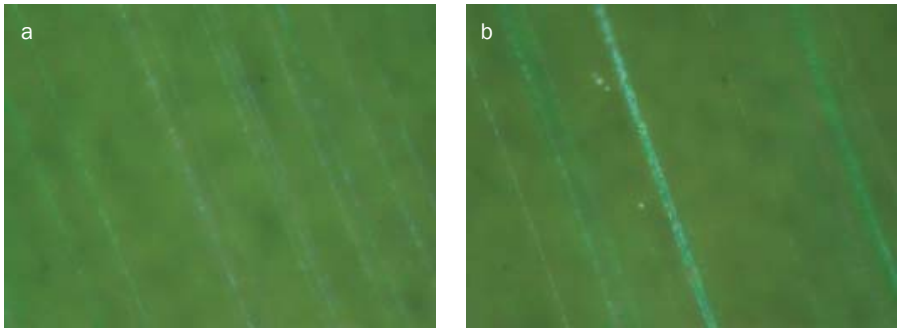

*Figure 16a,b: Thin sections of Kyocera chatoyant synthetic alexandrites oriented almost perpendicular to the **b** pinacoid show layers parallel to the **a** plane with numerous tiny needles alternating with layers of transparent alexandrite. The layers are thicker in b. Reflected light, crossed polarizers, field of view 112 x 84 µm. Photos by H.-J. Bernhardt.*

by analogy, these needles in the Kyocera titanium-doped synthetic alexandrites are most probably rutile. This probability is consistent with the information in various patent documents mentioned in Box A.

Colour and pleochroism: After careful orientation of the available cabochons using optical methods in the immersion microscope it was observed that the pleochroism of these samples was not always consistent with the pleochroism that had been and is commonly observed in natural and synthetic alexandrite. Although the slightly curved bases of the cabochons showed only minor deviations (< 15°) to the **a** (100) and **b** (010) pinacoids of the crystals, we found it difficult to obtain the exact position of all three crystallographic axes if not in immersion. This matters because we observed that only a slight deviation from a precise orientation (say, in a view exactly parallel to one of the three axes) causes quite large differences in the observed colours and pleochroism. We also noted that there are significant differences in colour, in different directions, which relate to the path lengths of the light through the stones.

Consequently, at this stage in the investigation, we confined our observations to the immersed stones in incandescent light. The presence of the dark layers in combination with the position of the optic axes obtained under crossed polarizers enabled an exact orientation of each cabochon in the immersion microscope. However, in assessing colour, one must keep in mind path length differences, and it is evident

Table A. Production of alexandrite cat's-eyes

Author(s)/applicant	Patent documents in Japanese/date*	Patent documents in English/date*	Method for crystal growth	Annealing step/ atmosphere	Dopant for cause of colour	Dopant/cause for asterism
Kawachi (Kochi) Suwa Seikosha KK (Seiko Epson Corporation), Tokyo	JP 54-006900 A (1979)	US 4,218,282 (1980)	Floating zone	Not mentioned	Chromium oxide	Titanium oxide
Kawachi and Kojima Miyasaka Kunugi Saito all assigned to Seiko Epson Corporation, Tokyo	JP 55-062884 A (1980) JP 58-130197 A (1983) JP 59-152291 A (1984) JP 59-152292 A (1984)		Floating zone	oxidising	Chromium oxide, iron oxide	Titanium oxide
Shindo *et al.*, National Institute for Research in Inorganic Materials, Tsukuba	JP 57-191297 A (1982) JP 57-191298 A (1982)		Floating zone	oxidising		Titanium oxide
Oguri and Hirota, Sumitomo Cement Co., Ltd., Tokyo	JP 58-120597 A (1983) WO 85/00392 A1 (1985)	EP 0148946 A1 (1985) US 4,634,492 (1987)	Floating zone	oxidising	Chromium oxide, vanadium oxide, iron oxide	Titanium oxide
Saito, Seiko Epson Corporation, Tokyo	JP 59-162196 (1984)		Floating zone, starting material is aluminium hydroxide	Not mentioned	Chromium oxide, iron oxide	Development of tubular fluid inclusions
Isokami and Nagata (Isogami and Nakata), Kyocera Corporation, Kyoto	JP 60-071598 A (1985)	US 4,621,065 (1986)	Czochralski, flux (lithium molybdate)	Not mentioned	Oxides of iron, cerium, vanadium, cobalt, tungsten, chromium, nickel, manganese	Oxides of titanium, tin, zirconium, germanium
Miyasaka, Seiko Epson Corporation, Tokyo	JP 61-256998 A (1986)			Diffusion treatment		Titanium oxide powder

* abbreviations: JP Japan; WO World Intellectual Property Organization; EP Europe; US United States of America
patent family members in other languages, e.g. German, were omitted

annealing at high temperatures not mentioned

annealing at high temperatures in oxidising atmospheres

growth from aluminium hydroxide, no annealing step

diffusion treatment

Box A

Production of synthetic alexandrite cat's-eyes in the patent literature

The production of synthetic chrysoberyl and alexandrite cat's-eyes is described in numerous Japanese and international patent applications, most of them published in the 1980s *(Table A)*. A first short note is found in two patent documents published in 1979 and 1980, assigned to Seiko Epson Corporation (Suwa Seikosha KK, see *Table A*). Later, two different processes were described in more detail, the first one published in various applications by Seiko Epson Corporation, by the National Institute for Research in Inorganic Materials and by Sumitomo Cement Co. The second process is assigned to Kyocera Corporation.

The first method for the production of alexandrite cat's-eyes involves a two-step growth and annealing process (see, e.g., the patent documents by Oguri and Hirota, 1983, 1985 a,b, 1987, assigned to Sumitomo Cement Co.). The first step includes the production of homogeneous single crystals containing titanium oxide as dopant. It is claimed that such specifically-doped crystals can be grown by any known technique suitable for the crystal growth of chrysoberyl, but the floating zone method is described in detail (the floating zone technique was described in a gemmological journal by Schmetzer, 2012). Crystal growth is performed under neutral (e.g. argon or nitrogen) or reducing atmospheres and most titanium is present in its trivalent state. In the second step, the crystal is annealed at elevated temperatures in an oxidizing atmosphere when the titanium is oxidized and elongated particles, most probably rutile needles, are precipitated. These exsolved particles are responsible for the chatoyant effect of the material when cut as a cabochon.

A process assigned to Kyocera Corporation describes the production of chrysoberyl cat's-eyes with a similar first step growth process using a specific dopant. But, there is no mention of a subsequent heat treatment step (Isogami and Nakata, 1985, 1986). Unfortunately, the authors were unable to obtain any conclusive information from the Kyocera Company to throw light on this omission. The following substances are listed by Kyocera as possible dopants: titanium oxide (TiO_2), germanium oxide (GeO_2), zirconium oxide (ZrO_2), and tin oxide (SnO_2). In addition to introducing a dopant to cause chatoyancy, the oxides of vanadium and/or chromium and/or nickel and/or cobalt and/or iron are added for colour. As examples, crystal growth by the Czochralski technique and the flux method are described, but there is no information about the orientation of the precipitates which are responsible for the cat's-eye.

Two further ways of producing cat's-eyes should be mentioned briefly. In a patent document assigned to Seiko Epson Corporation (Saito, 1984b), the production of alexandrite cat's-eyes by the floating zone technique is described. Due to the use of aluminium hydroxide as starting material and a special growth atmosphere, tubular fluid inclusions were developed, which are responsible for chatoyancy. Secondly, the production of alexandrite cat's-eyes by diffusion treatment of synthetic alexandrite crystals in titanium oxide powder was described by Miyasaka (1986).

that observations perpendicular to the bases of the cabochons (viewing only two of the three pleochroic colours X, Y or Z) are along much shorter path lengths than the two directions of view parallel to the bases of the cabochons. These latter paths of light range from 6.3 to 8.7 mm, while across the cabochons, the paths are 2.5 to 2.8 mm long. A summary of observations is given in *Table II*.

In detail, we observed that in one of the cabochons examined, the pleochroism shows only minor deviations from the pleochroism of chromium- and vanadium-bearing alexandrite (cabochon C2 in *Table II*). In contrast, the other cabochons (samples C1 and C3 in *Table II*) showed a yellowish orange or orange coloration for smaller paths of light. For observations in directions parallel to the bases of the cabochons (i.e. with longer paths of light) X was intense red orange, and Y and Z were dark (not transparent, see *Figure 17 A,B*).

Absorption spectra were recorded perpendicular to the bases of the cabochons. Cabochon C2 has a pleochroism almost identical to that of normal alexandrite but showed a chromium spectrum with somewhat less transparency around 500 nm, i.e. in the area between the two strong chromium absorption bands (*Figure 18,* sample C2). In contrast, the transparency in the same area was very much reduced within the spectra of cabochons C1 and C3 *(Figure 18)*. This means that, in addition to the chromium-vanadium absorption bands, there is also a stronger absorption in the 500 nm range.

From the pure spectra of chromium (Cr^{3+}) and titanium (Ti^{3+}) in chrysoberyl shown in *Figure 19,* it is evident that the maximum titanium absorption around 500 nm is more or less at the position of the absorption minimum between the two strong chromium bands. Consequently the absorption spectra of the asteriated and chatoyant Kyocera alexandrites can be understood if we postulate the presence of Ti^{3+} in the structure in addition to the Ti within the rutile needles. Sample C2 shows a smaller influence of Ti in the spectrum. This indicates that a higher percentage of the titanium is present in the form of rutile needles causing a stronger cat's-eye in this sample (see

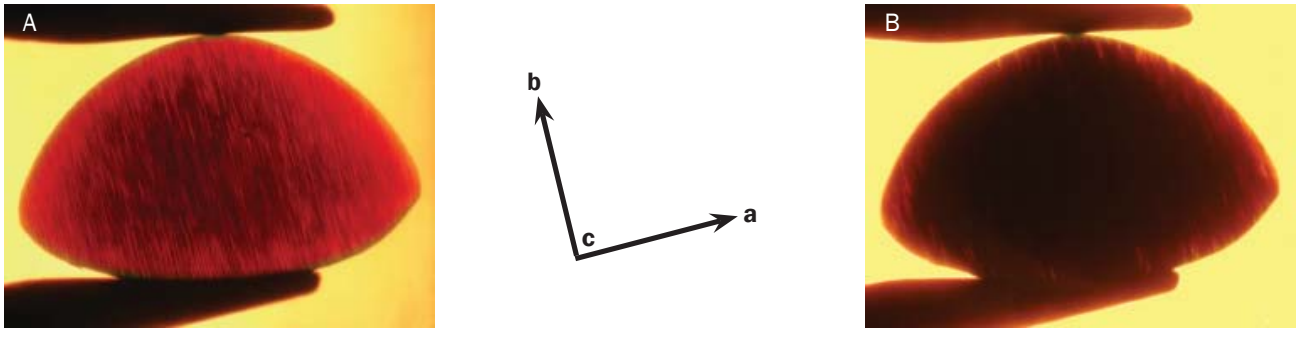

*Figure 17A,B: A view parallel to the c-axis of a Kyocera chatoyant synthetic alexandrite; the orientations of the three axes are indicated. The base of the cabochon is almost perpendicular to the b-axis (parallel to the **b** plane); dark layers with titanium-bearing needles are oriented perpendicular to the a-axis (parallel to the **a** plane). In this orientation in immersion and plane polarized light, with rotation of the polarizer (Figures A and B, respectively) the two pleochroic colours X and Y can be observed; X || a is intense red orange (A) and Y || b is non-transparent (B). Field of view 9.1 x 6.8 mm. Photos by K. Schmetzer.*

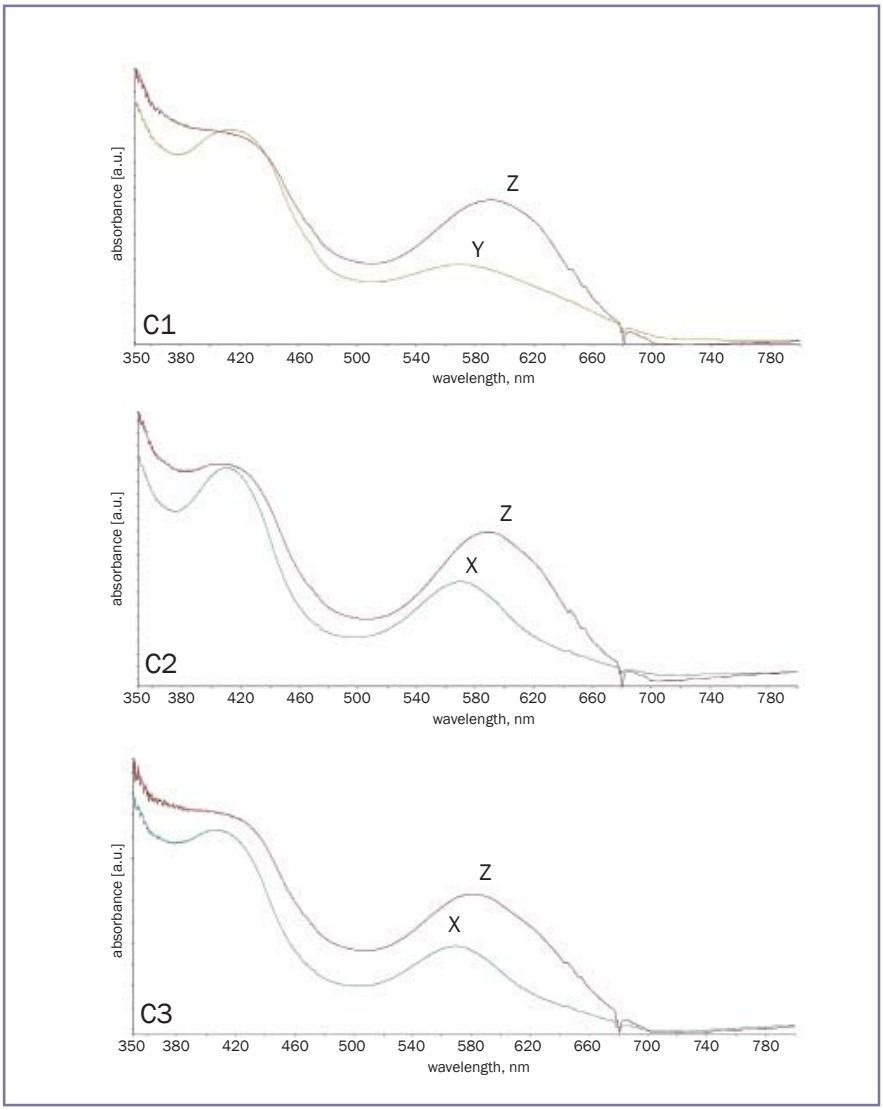

Figure 18: Absorption spectra for star synthetic alexandrite cabochon C1 (see Table II*) and cat's-eye cabochons C2 and C3 for polarized light with X || a, Y || b and Z || c; the spectra were recorded perpendicular to the bases of the cabochons with maximum sample thickness from 2.5 to 2.8 mm; for each sample, only two polarized spectra were taken, i.e. Y,Z for sample C1 (beam parallel to the a-axis) and X,Z for samples C2 and C3 (beam parallel to the b-axis).*

Figure 4). The two other cabochons C1 and C3 show a distinctly higher absorption in the 500 nm range probably caused by an elevated percentage of titanium in the trivalent state. Thus, the main light bands in these samples are somewhat weaker due to fewer rutile needles being present *(Figures 1,4)*.

Discussion

The average chromium and vanadium contents of Kyocera synthetic alexandrites showing asterism or chatoyancy are slightly lower than those measured in the 'normal' synthetic alexandrites from that producer. But their total titanium contents are higher and at least twice those of the reddish-violet chrysoberyls which are coloured by trivalent titanium.

The spectra indicate that titanium in asteriated or chatoyant alexandrites is present in the structure in its trivalent state on aluminium lattice sites (and so contributes to the colour). The titanium is present in its tetravalent state in the needle inclusions, probably as rutile, and is responsible for the light bands in the cabochons. Three series of needles are oriented parallel to the c-axis, to the **i** and to the **–i** {011} prism faces in layers parallel to the **a** (100) pinacoid. Although various amounts of titanium might also be present as Ti^{4+} within the chrysoberyl structure, Ti^{4+} does not cause absorption in the visible range. Therefore, most probably, the absorption spectra in our stones are due to a superimposition of the absorption bands of trivalent chromium,

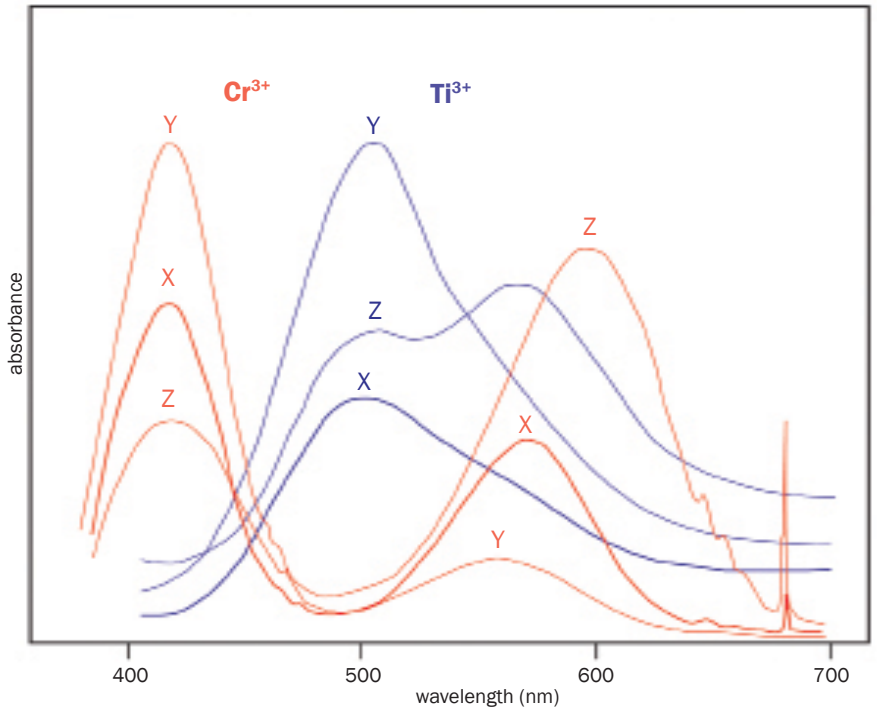

Figure 19: Plot of the polarized absorption spectra of chromium (Cr^{3+}, taken from Heller et al., *1999) and titanium (Ti^{3+}, taken from Anzai* et al., *1987) in chrysoberyl; for all three directions (X, Y and Z) the absorption maxima for titanium are located between the two strong chromium absorption bands; for samples which contain distinct amounts of chromium together with titanium in its trivalent state, only X is intense red orange, and Y and Z become very dark, almost non-transparent.*

vanadium and titanium — with variable intensity of the titanium absorption bands. This situation is similar to the presence of trivalent chromium and trivalent titanium in some Kashan synthetic rubies as described by Schmetzer and Schwarz (2007).

The formation of needle-like titanium-bearing precipitates in synthetic chrysoberyl by annealing the grown crystal is described in numerous patent documents (see Box A, *Table A*), but the mechanism of this process is not explained in them. It is not known whether titanium in its tetravalent state is first produced from Ti^{3+} before the exsolution of titanium oxide and formation of titanium-bearing precipitates. Neither do they contain the reason why there are bands or zones of needle-like inclusions in the stones. In synthetic titanium-bearing star corundum, a similar zoning of needle-like precipitates has been described. This zoning is present in crystals which were grown under fluctuating thermal conditions (Burdick and Jones, 1954) with zones with varying concentrations of needle-like precipitates only becoming visible after a subsequent annealing step. So it is possible that similar fluctuating temperatures during crystal growth might be responsible for the zoning of rutile precipitates in the Kyocera synthetic alexandrites, zones which are invisible until highlighted by the treatment.

Acknowledgements

The authors are grateful to Dr R. Hochleitner, Bavarian State Collection for Mineralogy, Munich, Germany, for the loan of faceted and rough samples of titanium-bearing chrysoberyl and synthetic alexandrite produced by Kyocera in Japan. The cabochons of asteriated and chatoyant synthetic alexandrite were kindly provided by the late George Bosshart, Horgen, Switzerland, and by Alan Hodgkinson, Portencross, Scotland, for which the authors express their thanks. The authors also appreciate the clarifications provided by an anonymous referee.

References

Anzai, Y., Yamagishi, K., Yamaguchi, Y., and Moriya, K., 1987. Solid state laser hosts. EP 0 238 142 A2, assigned to Mitsui Mining & Smelting Co. Ltd, 23.9.1987

Anzai, Y., Yamagishi, K., Yamaguchi, Y., and Moriya, K., 1988. Solid state laser hosts. US 4,765,925, assigned to Mitsui Mining and Smelting Co. Ltd, 23.8.1988

Burdick, J.N., and Jones, R.A., 1954. Synthetic corundum crystals and process for making same. US 2,690,062, assigned to Union Carbide and Carbon Corporation, 28.9.1954

Heller, D.F., Chin, T.C.-K., and Krasinski, J.S., 1999. Method and apparatus for pumping of transition metal ion containing solid state lasers using diode laser sources. US 6,009,114, assigned to Light Age Inc., 28.12.1999

Isokami, M., and Nagata, R., 1985. Synthetic chrysoberyl cat's-eye single crystal. JP 60-071598 A, assigned to Kyocera Corporation, 23.4.1985 [in Japanese]

Isogami, M., and Nakata, R., 1986. Chrysoberyl cat's-eye synthetic single crystal. US 4,621,065, assigned to Kyocera Corporation, 4.11.1986

Johnson, M.L., Mercer, M.E., Fritsch, E., Maddison, P., and Shigley, J.E., 1995. "Ti-sapphire": Czochralski-pulled synthetic pink sapphire from Union Carbide. *Gems & Gemology,* **31**(3), 188–95

Kane, R.E., 1987. Inamori synthetic cat's-eye alexandrite. *Gems & Gemology,* **23**(3), 158–62

Kawachi, A., 1979. Production of clean chrysoberyl single crystal. JP 54-006900 A, assigned to Suwa Seikosha KK (Seiko Epson Corporation), 19.1.1979 [in Japanese]

Kawachi, A., and Kojima, H., 1980. Chrysoberyl single crystal showing cat's-eye effect and production thereof. JP 55-062884 A, assigned to Seiko Epson Corporation, 12.5.1980 [in Japanese]

Koivula, J.I., Fritsch, E., and Fryer, C., 1988. The gemmological characteristics

of Inamori synthetic cat's-eye alexandrite chrysoberyl. *Journal of Gemmology,* **21**(4), 232–6

Kochi, A., 1980. Method of preparation of chrysoberyl and beryl single crystals. US 4,218,282, assigned to Suwa Seikoska KK (Seiko Epson Corporation), 19.8.1980

Krzemnicki, M.S., and Kiefert, L., 1999. Bluish green, light green and pink synthetic chrysoberyl. *Gems & Gemology,* **35**(3), 175

Kunugi, M., 1984. Synthesis of chrysoberyl cat's-eye. JP 59-152291, assigned to Seiko Epson Corporation, 30.8.1984 [in Japanese]

Miyasaka, H., 1983. Manufacture of artificial alexandrite cat's-eye. JP 58-130197 A, assigned to Seiko Epson Corporation, 3.8.1983 [in Japanese]

Miyasaka, H., 1986. Production of alexandrite cat's-eye. JP 61-256998 A, assigned to Seiko Epson Corporation, 14.11.1986 [in Japanese]

Oguri, H., and Hirota, M., 1983. Chrysoberyl single crystal showing luster effect and its production. JP 58-120597 A, assigned to Sumitomo Cement Co. Ltd., 18.7.1983 [in Japanese]

Oguri, H., and Hirota, M., 1985a. Chrysoberyl single crystal showing iridescent effect and process for its preparation. WO 85/00392 A1, assigned to Sumitomo Cement Co. Ltd., 31.1.1985 [in Japanese]

Oguri, H., and Hirota, M., 1985b. Chrysoberyl single crystal showing iridescent effect and process for its preparation. EP 0 148 946 A1, assigned to Sumitomo Cement Co. Ltd., 24.7.1985

Oguri, H., and Hirota, M., 1987. Chrysoberyl single crystal and method for producing the same. US 4,634,492, assigned to Sumitomo Cement Co. Ltd., 6.1.1987

Saito, M., 1984a. Synthesis of alexandrite cat's eye crystal by floating zone method. JP 59-152292 A, assigned to Seiko Epson Corporation, 30.8.1984 [in Japanese]

Saito, M., 1984b. Production of artificial crystal of alexandrite cat's-eye by floating zone process. JP 59-162196 A, assigned to Seiko Epson Corporation, 13.9.1984 [in Japanese]

Scarratt, K., 1988. Kyocera synthetics. *Journal of Gemmology,* **21**(3), 136–9

Schmetzer, K., 2010. *Russian alexandrites.* Schweizerbart Science Publishers, Stuttgart, 141 pp.

Schmetzer, K., 2011. Measurement and interpretation of growth patterns in chrysoberyl, including alexandrite. *Journal of Gemmology,* **32**(5–8), 129-44

Schmetzer, K., 2012. Natural alexandrites and chrysoberyls from Madagascar with irregular and regular growth patterns. *Australian Gemmologist,* **24**(10), 243–8

Schmetzer, K., Bernhardt, H.-J., Balmer, W.A., and Hainschwang, T., 2013. Synthetic alexandrites grown by the HOC method in Russia: internal features related to the growth technique and colorimetric investigation. *Journal of Gemmology,* **33**(5/6), 113-29

Schmetzer, K., and Bosshart, G., 2010. Colorimetric data of Russian alexandrite and yellowish green to green chrysoberyl. In: Schmetzer, K. *Russian alexandrites.* Schweizerbart Science Publishers, Stuttgart, 107–20

Schmetzer, K., and Hodgkinson, A., 2011. Synthetic star alexandrite. *Gems & Jewellery,* **20**(3), 9–11

Schmetzer, K., and Malsy, A.-K., 2011. Alexandrite and colour-change chrysoberyl from the Lake Manyara alexandrite-emerald deposit in northern Tanzania. *Journal of Gemmology,* **32**(5–8), 179–209

Schmetzer, K., and Schwarz, D., 2007. The causes of colour variation in Kashan synthetic rubies and pink sapphires. *Journal of Gemmology,* **30**(5/6), 331–7

Segawa, Y., Sugimoto, A., Kim, P.H., Namba, S., Yamagishi, K., Anzai, Y., and Yamaguchi, Y., 1987. Optical properties and lasing of Ti^{3+} doped $BeAl_2O_4$. *Japanese Journal of Applied Physics,* **26**(4), L291–2

Shindo, I., Sakauchi, H., and Takegawa, S., 1982a. Preparation of single crystal of chrysoberyl shedding luster. JP 57-191297 A, assigned to National Institute for Research in Inorganic Materials, 25.11.1982 [in Japanese]

Shindo, I., Sakauchi, H., and Takegawa, S., 1982b. Preparation of single crystal of chrysoberyl shedding luster. JP 57-191298 A, assigned to National Institute for Research in Inorganic Materials, 25.11.1982 [in Japanese]

Sugimoto, A., Segawa, Y., Kim, P.H., Namba, S., Yamagishi, K., Anzai, Y., and Yamaguchi, Y., 1989. Spectroscopic properties of Ti^{3+}-doped $BeAl_2O_4$. *Journal of the Optical Society of America B,* **6**(12), 2334–7

The Authors

Dr Karl Schmetzer
D 85238 Petershausen, Germany
email: SchmetzerKarl@hotmail.com

Dr Heinz-Jürgen Bernhardt
ZEM, Institut für Geologie, Mineralogie und Geophysik, Ruhr-Universität, D 44780 Bochum, Germany
email: Heinz-Juergen.Bernhardt@rub.de

Thomas Hainschwang
GGTL Laboratories, Gemlab (Liechtenstein)/GemTechLab, FL 9496 Balzers, Liechtenstein/CH 1227 Geneva, Switzerland
email: thomas.hainschwang@ggtl-lab.org

The Journal of Gemmology / 2013 / Volume 33 / No. 5–6

Liquid hydrogen sulphide (H_2S) fluid inclusions in unheated tanzanites (zoisite) from Merelani, Tanzania: Part 1. Recognition, characterization and gemmological importance

Dan Taylor*, Professor Andrew H. Rankin and Professor Peter J. Treloar

This is the first of two papers dedicated to the memory of Dan Taylor.

Abstract: Microscopic (*c.* 5 to 150 µm), multiphase liquid-filled inclusions have been identified in several samples of unheated blue-brown tanzanite (zoisite) rough stones from the D mine area, of Merelani, NE Tanzania. Raman and microthermometric analysis confirm that the liquid and vapour phase comprise 'pure' hydrogen sulphide (H_2S), with only very minor traces of methane and nitrogen in the vapour phase. Various solids are also present. The dominant phases, confirmed using Raman spectroscopy, are native sulphur (S_8), a disordered form of graphite (C) and a magnesium-rich calcite ($CaCO_3$ with *c.* 7% Mg). The inclusions typically occur in clusters and in planar to curvi-planar groupings, but larger, isolated inclusions can also occur. This shows that H_2S-dominant fluids were present during primary growth and subsequent fracture-healing of the zoisites during their natural cooling history. The highly unusual nature of this fluid, of presumed metamorphic origin, is hitherto unreported as a liquid phase in inclusions in the gemmological literature. The liquefied and compressed nature of this entrapped fluid means that it is very unlikely to withstand the high internal pressures generated on heating above 100 °C (the critical temperature of H_2S). Positive identification of liquid H_2S (strong Raman peak at 2583 cm^{-1}) in such inclusions therefore provides a valuable criterion for identifying natural, un-treated tanzanites and distinguishing them from any crystals that may be laboratory-grown. A simple laboratory scratch-chip test is outlined. This is based on the characteristic 'rotten egg' odour of H_2S when near-surface inclusions are opened, and the extreme sensitivity of the human nose to this gas (threshold value of *c.* 11 µg in 1 m^3 of air).

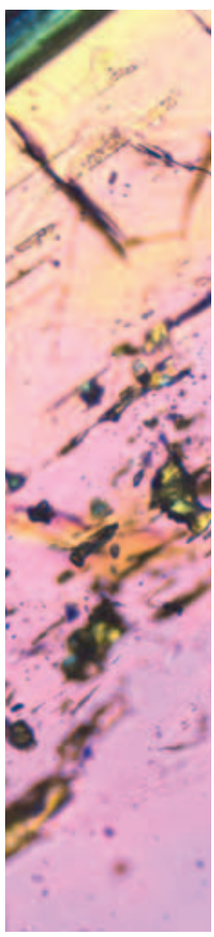

Keywords: fluid inclusions, gemmology, hydrogen sulphide liquid, metamorphic fluid, microthermometry, native sulphur, odour, Raman spectra, tanzanite, zoisite

* Sadly Dan Taylor died on 29 October 2009.

Liquid hydrogen sulphide fluid inclusions in unheated tanzanites (zoisite): Part 1.

Introduction

Liquid inclusions containing varying proportions of liquid, vapour and solids are common microscopic features of many types of gemstones. Their importance in gemmology has long been recognized, and they often add interest and uniqueness to individual gems (Gübelin and Koivula, 2005; Roedder, 1982). Recognition of different types of inclusions in gemstones, and identification of phases present, even at low (×10) magnifications, is a particularly valuable guide to likely provenance. This is best illustrated by the characteristic three phase liquid (L) + vapour (V) + salt (halite) brine inclusions so typical of Colombian emeralds. Liquid inclusions also provide valuable insights into whether a gemstone has been subjected to heat treatment. For example, two-phase liquid plus vapour carbon dioxide inclusions, which become single phase on gentle warming up to 31°C, are a common feature in unheated sapphires and rubies but are usually destroyed during heating to much higher temperatures (Koivula, 1986; Hughes 1997; Rankin, 2002).

In view of the gemmological value of fluid inclusions, published reports of their nature and occurrence in tanzanite are notably lacking. Only very small (*c.* 5–10 µm (microns)) liquid-vapour inclusion trails have been reported in tanzanite (Malisa *et al.,* 1986) and associated quartz (Olivier, 2006), and their occurrence has only been briefly mentioned in a recent geological review of tsavorite occurrences in East Africa (Feneyrol *et al.,* 2013). Here we report on the common occurrence of well developed (up to *c.* 150 µm) multiphase (L+V+S) inclusions of exceptional distinctiveness and highly unusual compositions in unheated tanzanites (zoisites) from the Merelani mining area, Tanzania. Optical microscopy, laser-Raman microspectrometry and microscope cooling-heating studies have been used to identify the phases present. Most notable is the persistent and dominant presence of an extremely rare liquid phase in nature (Roedder, 1984) — liquid hydrogen sulphide (H_2S). The properties and origin of this unusual liquid, hitherto unreported in inclusions in the gemmological literature, are discussed. We also suggest a simple diagnostic 'chip and scratch' test, for gemmological purposes which is based on the distinctive 'rotten egg' odour of H_2S when inclusions are opened. We believe that recognition of inclusions containing liquid H_2S provides a characteristic feature of *unheated,* natural tanzanites (zoisites) compared to simulants or their manufactured counterparts.

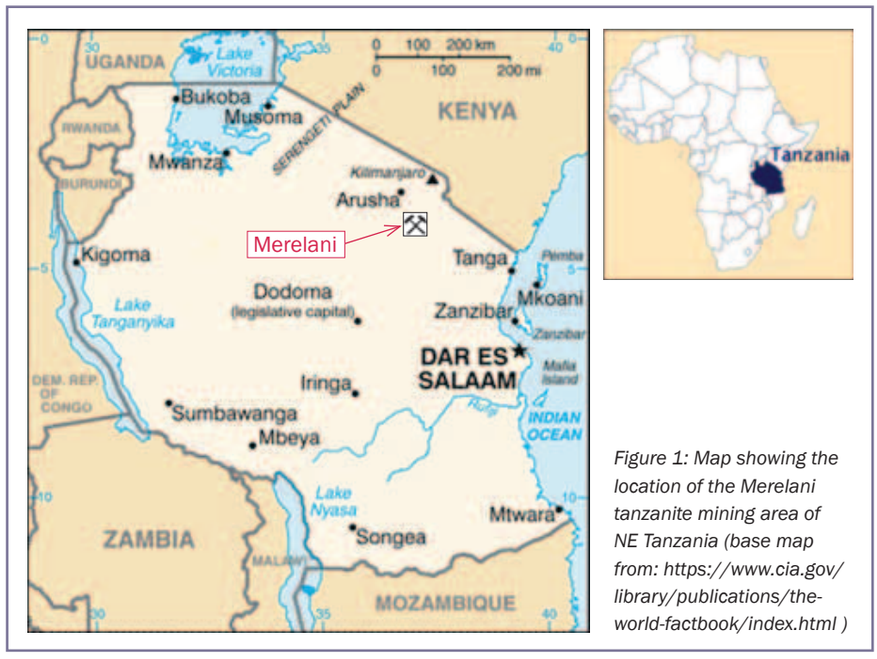

Figure 1: Map showing the location of the Merelani tanzanite mining area of NE Tanzania (base map from: https://www.cia.gov/library/publications/the-world-factbook/index.html)

In an accompanying paper (Rankin *et al.,* 2013, this volume) we discuss the likely effect of these inclusions on the thermal stability of natural and heat-treated tanzanites by modelling the internal pressures and stresses within the inclusions at different temperatures, to 800°C.

Samples description and preparation

The Merelani tanzanite mines are located in NE Tanzania due south of Mount Killimanjaro close to the town of Arusha *(Figure 1).* The deposits are centred on a latitude of 3° 33" and a longitude of 37° 01", occupying a zone some 7–8 km in length and 1 km wide. These are divided into separate mining blocks (A to D), with blocks C and D dedicated to artisanal mining operations. On a regional scale, the deposits form part of the important East African gem belt that continues through Mozambique, Kenya and Tanzania (Hughes, 1997). High-grade metamorphic rocks are a characteristic feature of this belt, but the geology of individual deposits is complex. Recent reviews of the geological setting, occurrence and mineral paragenesis of the Merelani tanzanite deposits are provided by Olivier (2006) and Walton and Marshall (2007).

For the purposes of the present study five samples of uncut, unheated blue-brown zoisite (tanzanite) were obtained by Dan Taylor from artisanal workings in the Block-D mine area of Merelani, during a visit to the Tanzanite mining district in 2008. The samples studied comprised stubby, single crystals ranging in size from about 1 × 1 × 0.5 cm to 0.2 × 0.2 × 0.4 cm, some with sharp terminations, showing colour variations from brown at the base to blue at the tip *(Figure 2).* For optical, microthermometric and Raman analysis of the fluid inclusion population, a series of optical quality polished wafers, *c.* 300 µm thick, were prepared. These

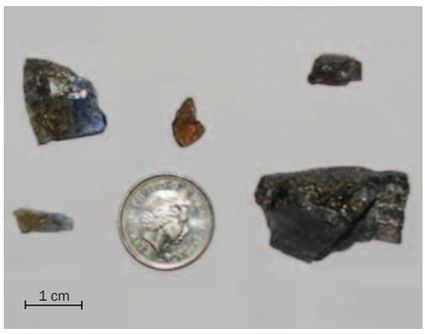

Figure 2: Uncut and unheated rough tanzanites (zoisites) from the D Block mine area used in the present study.

were obtained from slices cut parallel to the prism faces of the specimens where possible. To ensure the integrity of the inclusions care was taken to avoid heating the sample above 50°C during sample preparation by following established fluid inclusion wafer preparation techniques (Shepherd *et al.,* 1985).

Initial microscopic examination revealed a lack of suitable fluid inclusions in one sample (Tanz2), poorly developed inclusions in another (Tanz3) but abundant inclusions suitable for further study in the other three (Tanz1, Tanz6, Tanz8).

Analytical methods

The initial optical examination and characterization of inclusion populations was carried out on the polished wafers using a standard Olympus petrological microscope, in plane polarized light and under crossed polars, at magnifications up to ×1000.

Raman microanalysis was carried out on individual phases in selected inclusions, in confocal mode, using a Renishaw RM1000 Raman spectrometer attached to an Olympus BH-2 microscope. A neon ion laser (633 nm), with a source power of 500 mW and a focused spot size of ~2 µm, was used. The Raman equipment was calibrated regularly to check for instrument drift using a pure silicon standard at 520 cm^{-1} and the methane (CH_4) and carbon dioxide (CO_2) Raman peak positions at 2914, and at 1285 and 1387 cm^{-1}, respectively, in the KUFLINC fluid inclusion standard (Beeskow *et al.,* 2005). Peak positions above background were recorded and compared with published Raman data for phases likely to be present in fluid inclusions (Burke, 2001; Van der Kerkhof and Sousa, 2012: Frezzotti *et al.,* 2012).

Heating and cooling stage studies (microthermometry) provide information on fluid inclusion compositions based on diagnostic phase changes observed in inclusions during controlled heating and cooling runs (Shepherd *et al.,* 1985, Van der Kerkhof and Sousa, 2012). Studies were carried out over the temperature range -196°C and +80°C, on chips (a few mm^2) broken from selected wafers, using a Linkam THM600 heating-freezing stage with temperature controller, attached to a Nikon Optiphot microscope, with liquid nitrogen coolant. Details are shown in *Figure 3*. The microscope was equipped with long work distance (× 20 and × 40) objective lenses which allowed the various phase changes to be observed on heating and cooling the inclusions. The important changes reported here are the melting temperature of the frozen liquid phases on heating (Tm), and homogenization temperature of the liquid and vapour components into a single liquid phase (Th). These phase changes could be observed even in inclusions as small as 10 µm. The stage was regularly calibrated using synthetic fluid inclusion standards containing pure CO_2 (triple point at -56.6°C) and H_2O (critical temperature at 372.4°C; melting temperature at -0.2°C). Heating rates of 1–10°C/min were employed for measurements of phase changes after the inclusion contents had been frozen following rapid cooling down to *c.* -150°C. All microthermometric measurements reported here are believed to be accurate to within ± 0.2°C. Because of super-cooling effects the temperatures at which the contents of liquid inclusions freeze (Tf) is not a reliable indicator of the true freezing temperature. Under equilibrium conditions Tf is the same as Tm (the melting temperature). This is why Tm, rather than Tf, is used in conventional fluid inclusion studies (Shepherd *et al.,* 1985).

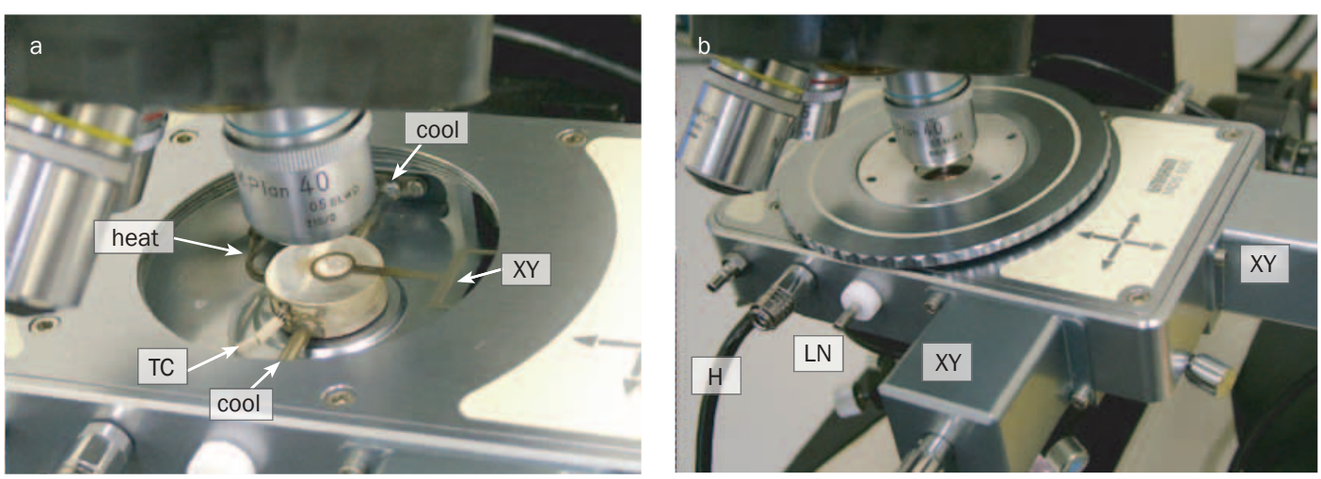

Figure 3: The Linkam THM600 combined microscope heating-cooling stage used in this study. (a) Close up of the inner heating-cooling block showing the inlet and outlet tubes for the liquid nitrogen coolant (cool), the platinum resistance heater (heat), thermocouple (TC) and sample carrier with X-Y movement controller (XY). (b) Outer stage with lid in place showing XY controls (XY), inlet valve for liquid nitrogen coolant (LN) and leads for the heat controller (H).

Liquid hydrogen sulphide fluid inclusions in unheated tanzanites (zoisite): Part 1.

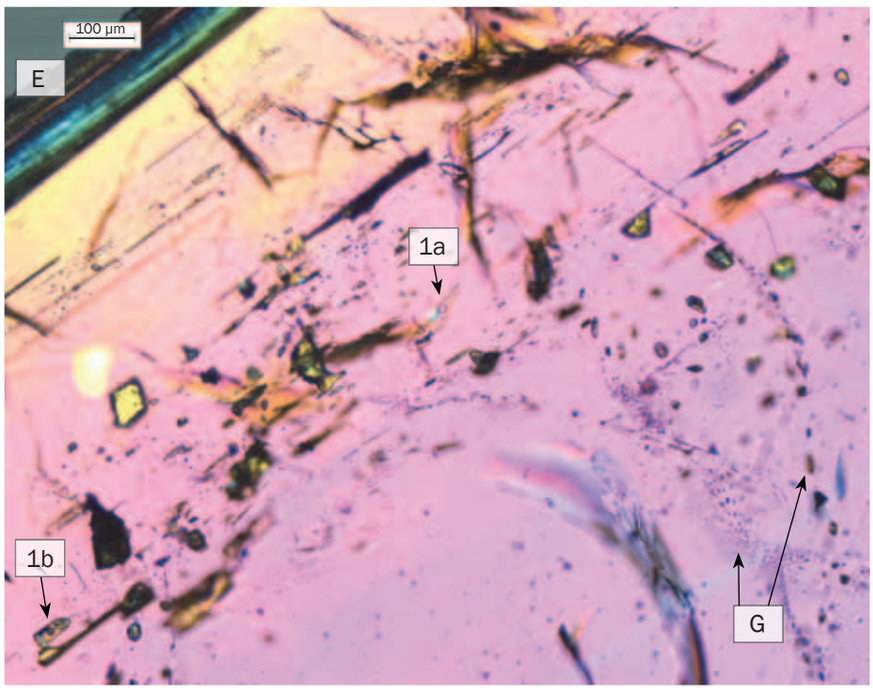

Figure 4: Photomicrograph of a thick polished section of unheated inclusion-rich tanzanite (zoisite) viewed under crossed polars. Note the variations in size and distribution of the fluid inclusions. Larger, elongate type I inclusions (e.g. 1a and 1b) tend to align parallel to crystal growth zones. These are picked out by variations in birefringence colour, parallel to the external crystal face (E). Smaller type II and III inclusions occur in curvi-planar groups and irregular clusters (G).

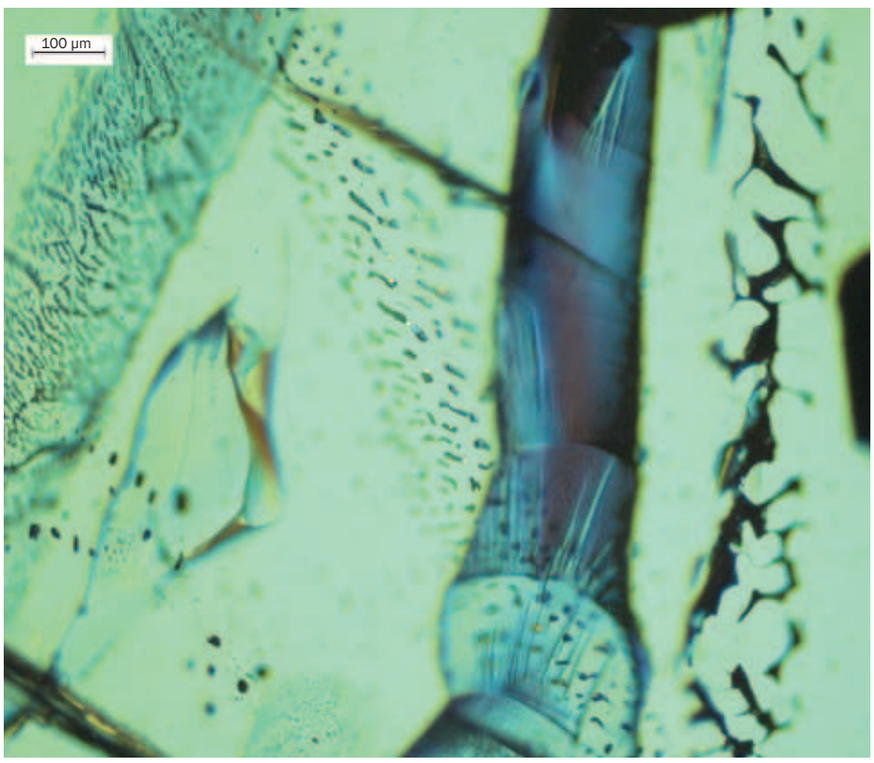

Figure 5: Planes of irregularly-shaped and branching (necked) type III inclusions decorating healed and partially healed fractures.

Fluid inclusion characteristics

Classification and distribution

Under the microscope the fluid inclusions are typically observed to be between 5 and 100 µm in size. However a few larger inclusions, reaching up to 150 µm in length are present. The inclusions occur in clusters and as isolated cavities (type I), as well as regularly-shaped inclusions in trails as linear and curvi-planar groupings (type II) as shown in *Figure 4*. Less commonly, they occur as indistinct and irregular-shaped planes that traverse the crystal (type III), as shown in *Figure 5*. Each type can be described as multiphase L+V+S inclusions at ambient temperatures (20–25°C) in which the liquid phase occupies *c*.75–45 volume percent of the inclusion. All type I, II and those III inclusions not showing any obvious signs of leakage, contain a small mobile vapour bubble within a colourless liquid. The bubble occupies *c*. 5 % of the inclusion volume, and several solid phases occupying up to 50% of the inclusion volume, are also present *(Figures 6, 7)*.

Fluid inclusions in minerals generally result either from entrapment of mineral-forming fluid during primary crystal growth as primary (P) inclusions, or during later recystallization or resealing of micro-fractures in the presence of a fluid phase to form secondary (S) inclusions, or pseudosecondary (PS) inclusions (Roedder, 1984). Primary inclusions tend to occur as isolated cavities or in clusters along growth zones. In contrast, S and PS inclusions typically occur in trails that traverse the crystals. In the case of PS inclusions, the fracturing and resealing took place during crystal growth, and the trails terminate inside the crystal. On this basis Type I correspond to P inclusions, Type II to PS and/or S inclusions and Type III to S inclusions.

Identification of phases present

The results of Laser Raman microanalysis of individual phases in the inclusions are illustrated in *Figure 8a,b* which shows typical Raman spectra for

the various phases present in inclusions. Identification of each phase was based on literature values for their characteristic major Raman peak positions (Burke, 2001; Van der Kerkhof and Sousa, 2012; Frezzotti *et al.,* 2012) and also their morphology and optical properties.

The Raman spectra of the liquid showed a strong diagnostic peak for liquid H_2S at ~2583 cm^{-1} in all inclusions analysed. Similarly, in every inclusion analysed the Raman spectra for the vapour phase showed a dominant peak at 2610 cm^{-1}, which is characteristic of H_2S vapour. Typical Raman bands and peaks for carbon dioxide and water (liquid or vapour) were not present, but traces of methane and nitrogen were detected in a few inclusions based on very small Raman peaks at the typical wave numbers of 2917 and 2331 cm^{-1} respectively. Native sulphur (S_8), characterized by its pale yellow colour and stubby crystal or globular habit, was also positively identified from its two strong diagnostic peaks at 473 and 218 cm^{-1}. Sometimes, this phase nucleated and reassembled as a globule inside the inclusion upon laser excitation during analysis. Similar behaviour has also been reported in S-rich fluid inclusions by Giuliani *et al.* (2003). A strong Raman peak at 1583 cm^{-1} and a lesser peak at 1625 cm^{-1} were recorded for a commonly observed opaque solid mass within the inclusion; these confirmed its identity as a disordered form of graphite. Well formed faceted colourless crystals which are commonly present inside the inclusion were identified as calcite based on Raman bands at ~1088 cm^{-1} and ~714 cm^{-1}; these Raman positions also suggest around 7% Mg in the calcium carbonate structure.

Gypsum was tentatively identified in some inclusions, but other solid phases could not be identified due to a lack of Raman signals. A summary of the phases identified in the inclusions based on their diagnostic Raman peaks and main optical/morphological characteristics is shown in *Table I*.

Microthermometric characteristics

Microthermometric data were obtained on type I and II inclusions

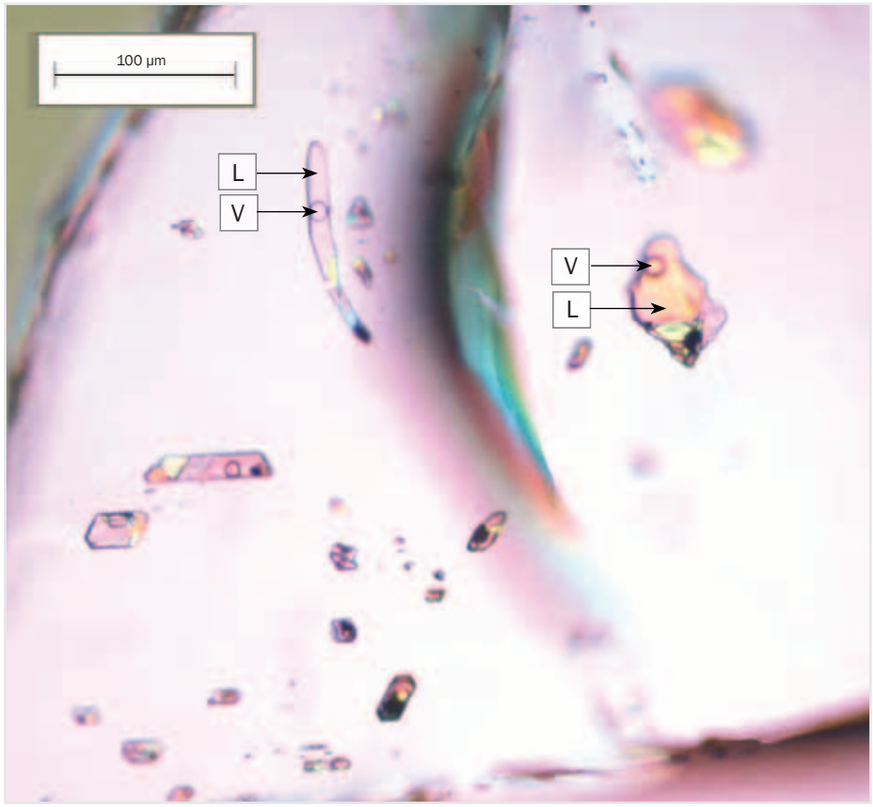

Figure 6: Clusters of multiphase (L+V+S) type I inclusions in an inclusion-rich area viewed under crossed polars. Note the rounded and oblate vapour bubbles (V) which can be made to move within the liquid (L) on gentle cooling and warming between 10 and 30°C, and various opaque, transparent and birefringent solid phases.

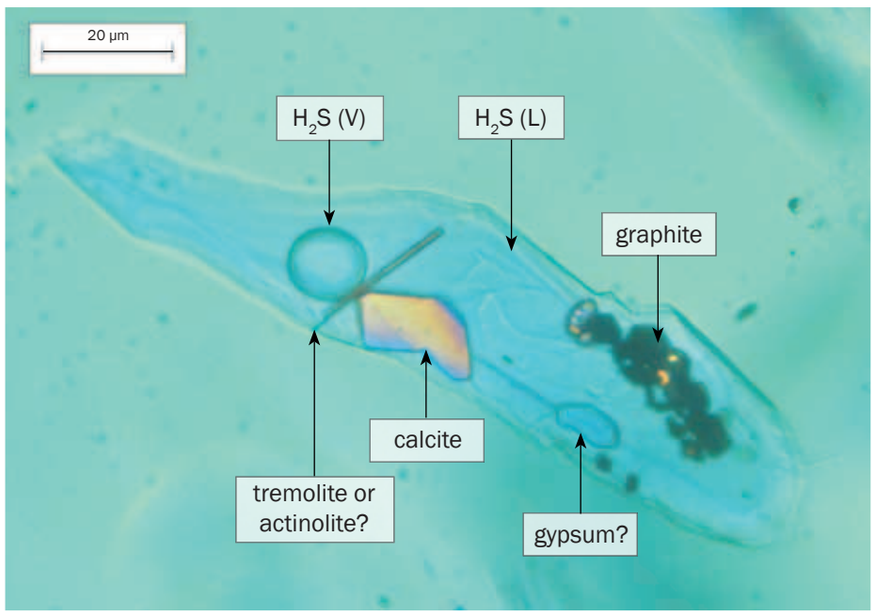

Figure 7: Close up of inclusion 1a shown in Figure 4 showing typical characteristics of phases identified in multiphase vapour-liquid-solid inclusions in unheated tanzanite observed under crossed polars. During Raman analysis a new mineral, sulphur, nucleated. This was pale yellow, of high relief and initially formed a perfect prismatic shape but later changed to a more amorphous blob. The high relief birefringent phases within the graphite cluster are tentatively identified as sphene, xenotime or rutile.

Liquid hydrogen sulphide fluid inclusions in unheated tanzanites (zoisite): Part 1.

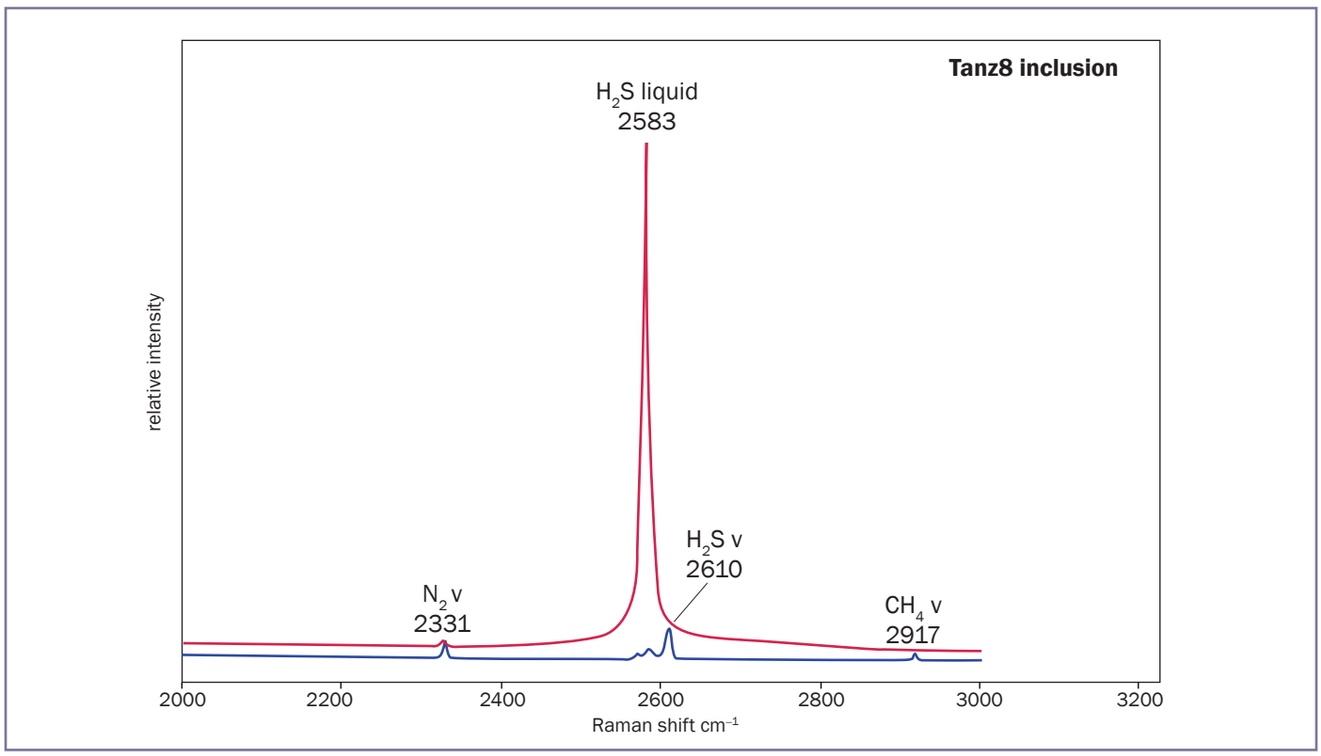

Figure 8a: Typical Raman spectra for fluid phases present in H_2S-bearing inclusions. Spectra vertically displaced for clarity.

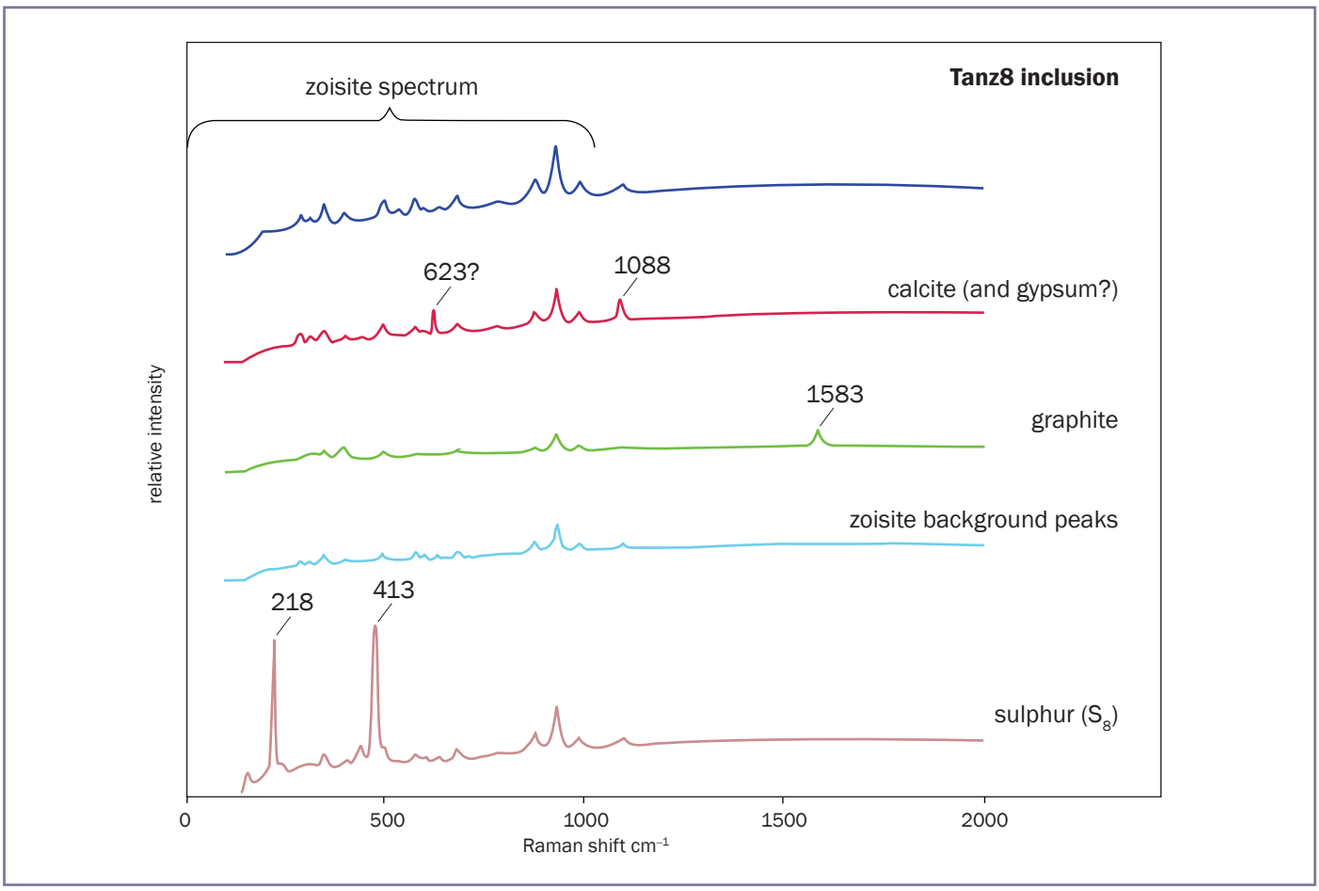

Figure 8b: Typical Raman spectra for solid phases present in H_2S - bearing inclusions. Spectra vertically displaced for clarity.

Table I: Summary of the major phases identified in the inclusions, their characteristic features and diagnostic Raman peaks.

Phase	Formula	Occurrence	Morphological and optical properties	Raman peaks cm^{-1}	Comment
Hydrogen sulphide (L)	H_2S	ubiquitous	colourless liquid	2583	
Hydrogen sulphide (V)	H_2S	ubiquitous	round or distorted bubble	2610	
Methane (V)	CH_4	traces	in bubble	2917	X <0.025
Nitrogen (V)	N_2	traces	in bubble	2330	X <0.025
Disordered graphite (S)	C	v. common	opaque, irregular mass	1583	
Sulphur (S)	S_8	common	transparent, high relief globules or stubby crystals	473 218	may nucleate under laser
Magnesian calcite (S)	$CaCO_3$	common	transparent, rhombic crystals high birefringence	1088 714	
Unidentified (S)		occasional	transparent, tabular crystals low birefringence	623?	gypsum?
			thin, acicular needles	n.d.	tremolite?
			yellow-brown transparent crystals in graphite clusters	n.d.	possibly sphene, xenotime or rutIle?

X means mole fraction in the inclusion

in three of the four samples. Sample Tanz6 was unsuitable because of the poor optical quality of the predominant type III inclusions present. The melting temperature of the liquid (Tm) was determined by rapidly cooling the inclusions until the liquid contents froze suddenly at between -90 and -120°C. The inclusions were then heated at a rate of 10°C/minute up to ~ -88°C, then at a rate of 1–2°C/minute until the onset of rapid melting of the frozen liquid occurred at the temperature of melting (Tm). The Tm values, based on measurements of some 47 inclusions, are shown in *Table II*. These ranged from -84.7 to -86.6°C, with the majority forming a very narrow range between -85 and -85.9°C. The freezing or melting point of pure liquid H_2S is at -85.5°C (NIST, 2011), which suggests that the main fluid present is H_2S of very high purity. This is in agreement with the Raman data on the main fluid and vapour phases, which only showed peaks for hydrogen-sulphide (H_2S). The occasional lower Tm values, at around -86 to -86.5°C can be ascribed to very minor amounts of methane and nitrogen (<0.025 of the total mole fraction) which are known to lower the melting temperature of pure H_2S (Van der Kerkhof and Sousa, 2012).

Table II: Summary of microthermometric data (T°C) for rough tanzanites (zoisites).

Sample no.	Inclusion type	Occurrence	Number	$T_{min.}$	$T_{max.}$	T_{mean}
a) Melting temperatures of frozen liquid (Tm) °C						
Tanz6	I and II	Cl	9	-86.3	-84.0	-84.7
Tanz1	I and II	Iso, Cl, Pl	24	-86.6	-84.7	-85.5
Tanz8	I and II	Iso, Cl, Pl	15	-86.0	-84.8	-85.5
b) Homogenization of liquid and vapour phases (Th) °C						
Tanz6	I and II	Cl	47	47.8	67.3	54.4
Tanz1	I	Iso	36	39.1	84.1	54.6
Tanz1	II	Iso, Cl, Pl	13	39.6	60.5	45.4
Tanz8 brown	I and II	Iso, Cl, Pl	15	28.1	73.9	43.0
Tanz8 blue	I and II	Iso, Cl, Pl	9	39.3	51.8	47.4

Iso = isolated, Cl = clusters, Pl = planes

This is confirmed by their detection in trace amounts by Raman analysis in a few inclusions.

The temperatures at which the liquid and vapour H_2S homogenized to a single liquid phase on heating (Th) were recorded for 120 inclusions. As shown in *Table II* these ranged from 28 to 84°C with mean values between 43 and 55°C for all samples. It is noteworthy that there is no significant variation in Th or Tm values between Type I and II inclusions, or between blue and brown colour zones in the samples.

The 'rotten egg' odour from opened inclusions

When small chips were broken off the polished wafers prior to microthermometric analysis a distinctive 'rotten egg' odour was commonly noted. This can now be attributed to the release and volatilization of liquid H_2S from opened inclusions, despite their very small size. The nose is extremely sensitive to H_2S. According to published data (Amoore *et al.,* 1983) the mean threshold for detecting this odour in air is around 8.1 parts per billion, although this varies

Table III: Estimates of the size and number of inclusions from which H_2S(V) needs to be released from inclusions into (10 cm)^3 and (20 cm)^3 of air in order to exceed the mean threshold value of 11µg/m^3 (indicated in red) to detect its odour.

Inclusion dimensions µm	H_2S (V) concentration (µg) in (10 cm)^3 of air	H_2S (V) concentration (µg) in (20 cm)^3 of air	No. of inclusions needed for (10 cm)^3 of air	No. of inclusions needed for (20 cm)^3 of air
10 × 10 × 10	0.6	0.08	200	>1000
10 × 10 × 20	1.2	0.15	10	80
20 × 20 × 20	4.8	0.6	3	24
30 × 30 × 30	16.2	2.25	1	5
50 × 50 × 50	125	15.4	1	2
100 × 100 × 100	600	75	1	1

somewhat depending on the health and age of individuals and other factors. This threshold corresponds to a detection limit of 11 µg in 1 m^3 of air. Estimates of the amount of gas released from inclusions of different sizes are shown in *Table III*. These are based on estimates of the mean density of the combined L+V H_2S components of the inclusions of between 0.5 and 0.7 g/cm^3 based on the Th values and published thermo-physical data as detailed in the accompanying paper (Rankin *et al.,* 2013). The estimates demonstrate that the fortuitous opening of just one large equidimensional inclusion, 50 µm across, is enough to release detectable levels of H_2S within 20 cm of the nose, or one equidimensional inclusion 30 µm across some 10 cm from the nose. Preferential breakage is more likely to occur along planes of weakness occupied by linear arrays of type II and III inclusions, in which case opening of just 24 smaller inclusions, 20 µm in size, is still detectable at a distance of just 10 cm.

Discussion

Occurrence and origin of H_2S in fluid inclusions

Hydrogen sulphide is a relatively common volatile in natural gas fields (usually referred to as 'sour gas' fields) in sedimentary basins. It can occur in inclusions in minerals from low temperature mineral deposits associated with these basins (e.g. Rankin and Shepherd, 1978; Beny *et al.,* 1982), in which the source of sulphur is generally believed to be from reduction of sulphate minerals (gypsum or anhydrite) from sedimentary evaporite sequences.

Gaseous H_2S often occurs in volcanic fumaroles and associated geothermal systems contributing to the distinctive sulphurous odour around these systems. Trace amounts have also been detected in fluid inclusions in associated epithermal (<300°C) minerals, and in both instances a magmatic source for H_2S-sulphur is generally accepted (Henley and Ellis, 1983).

A metamorphic source for H_2S may also be envisaged, resulting from the release of volatiles from de-sulphidation metamorphic reactions of rocks under moderate to high temperatures and pressures. For example, Giuliani *et al.* (2003) report a metamorphic origin for gaseous H_2S in well characterized inclusions in ruby from some gem-bearing high-temperature skarn deposits of Vietnam. Feneyrol *et al.* (2013) noted the occurrence of H_2S in inclusions in gem tsavorites (and tanzanite) from the Pan-African metamorphic belt of East Africa, and Olivier (2006) reported on H_2S-rich inclusions in quartz associated with the Merelani tanzanite mineralization within this belt. Both sets of authors suggest a metamorphic origin for the H_2S in the belt. Thus, a metamorphic origin is also envisaged for the high density H_2S fluids reported here.

Optical, thermal and olfactory characteristics of liquid H_2S inclusions compared to other common liquid phases in gem minerals; gemmological implications

Liquid-filled cavities with vapour bubbles are a common feature of many minerals and gemstones at ambient temperatures. The most commonly reported liquids (Gübelin and Koivula, 2005; Roedder, 1982) in untreated gem

Where might the sulphur come from?

Metamorphism is a process of devolatilization which essentially means that volatile species such as CO_2, H_2O, CH_4, SO_4 and H_2S will be released into the metamorphic fluids as a range of hydrous, carbonate sulphate and sulphide minerals break down during metamorphic reactions. Both Cr and V, normally insoluble and immobile, will go into solution under the right redox conditions. At low pH, as indicated by the presence of H_2S in the fluid phase, Cr^{3+} is soluble. The presence of tanzanite in quartz rich veins (Olivier, 2006) means that Cr and V must have been leached, likely from black shales, during metamorphism and then transported in solution to the site of crystal growth. Feyrerol *et al.* (2013) suggest on the basis of stable sulphur isotope data that the source of the S in the metamorphic fluids that are trapped in tsavorite crystals were a series of sedimentary sulphate phases (baryte and anhydrite) that formed during evaporation and were then later metamorphosed. A combination of reduced, organic rich black shales that fix Cr and V from sea water during sedimentation, and interbedded sulphate rich evaporate horizons will provide an appropriate chemical factory that will release reduced, H_2S rich fluids that will carry Cr and V to the site of growth of minerals such as tanzanite and tsavorite.

minerals in order of increasing rarity are water (aqueous brines), liquid carbon dioxide, silicate glass (supercooled silicate melts) and liquid petroleum (oil). Simple optical tests can be used to distinguish between them (Roedder, 1982). Liquid petroleum which is common in Herkimer 'diamonds' (quartz) is readily distinguished from other liquids because of its yellow to brown colour and UV fluorescence. The refractive indices of common inclusion liquids vary (Van der Kerkhof and Sousa, 2012) with typical values as follows: silicate glasses *c.* 1.50 to 1.65; water and brines *c.* 1.34; liquid CO_2 1.12. This can aid identification by means of the visible differences in relative relief between the host mineral and contained fluid. However, the refractive index of pure H_2S (1.374) is quite close to that for water and brines. So, both H_2S and aqueous liquids will show similar relative reliefs and would be difficult to distinguish optically.

An important property useful for recognizing CO_2 (V+L) inclusions is based upon gentle warming or cooling of the sample under the microscope. Liquid CO_2 cannot exist in the liquid state above its critical point temperature of 31.1°C. Thus, inclusions containing both CO_2 (V) and CO_2 (L) at room temperatures will show homogenization to a single phase on gentle warming up to this critical temperature. The test is so sensitive that even the heat from a microscope light source is sometimes sufficient to cause homogenization of liquid and vapour CO_2, unless infrared filters are used (Roedder, 1982). The critical point temperature for H_2S at 100.4°C is markedly higher. Therefore, liquid and vapour H_2S cannot co-exist above this temperature. This is reflected in the low homogenization temperature ranges for the inclusions reported here (28 to 84°C) compared to the Th ranges generally recorded in the literature for water and brine inclusions in minerals from a variety of geological environments from 70 to 550°C (Wilkinson, 2001). Thus, a simple heating test up to 100°C might seem appropriate for distinguishing between liquid H_2S, liquid CO_2 and liquid H_2O in L+V fluid inclusions. But this is inadvisable, due to potential irreversible damage to tanzanite even at these lower temperatures, as discussed in the accompanying paper (Rankin *et al.* 2013).

Diagnostic gemmological tests for liquid H_2S inclusions in tanzanites (zoisites)

We suggest that the H_2S inclusions reported here provide a valuable means of identifying natural, un-treated tanzanites (zoisites) and distinguishing them from any crystals that might be laboratory-grown. Identification of liquid H_2S is best achieved by Raman microanalysis based on its strong characteristic Raman peak at 2583 cm^{-1}. Positive results can be obtained on individual inclusions down to 10 µm in size in inclusion trails and clusters with signal count times of about 60 seconds.

A simple laboratory scratch-chip odour test is also suggested. This is based on the characteristic 'rotten egg' odour of H_2S when near-surface inclusions are opened by scratching or breaking off a very small chip from the underside of a rough stone (where inclusions are often most abundant). Zoisite (tanzanite) with a hardness of 6.5 on the Mohs scale is easily scratched. But care should be taken when taking a small chip because zoisite is easily cleaved and may break in an uncontrolled way if too much force is used. The human nose is extremely sensitive to this gas, provided the amount released exceeds the threshold value for H_2S at *c.*11 µg in 1 m^3 of air. Our current experience, and a previous study of inclusions in barytes (Rankin and Shepherd, 1978), has shown that it should be readily detected by immediately placing the nose close to (within 10 to 20 cm) the scratch or chipped area. *Table III* illustrates the sensitivity of the method by presenting the calculated amounts of H_2S released from inclusions of different size into different volumes of air. Even a single inclusion 30–50 µm in size, which is less than the width of a human hair *(Figure 9)* will release detectable amounts in volumes of air between (10 to 20 $cm)^3$.

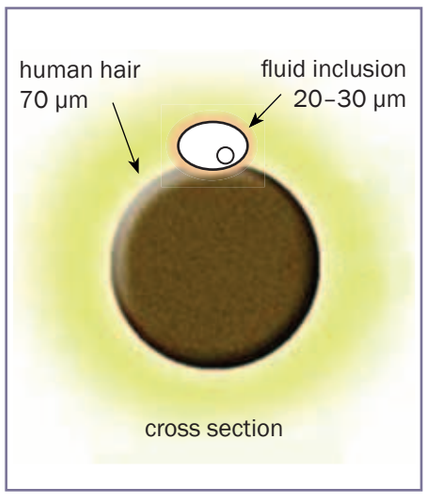

Figure 9: Typical size of type I and type II H_2S fluid inclusions in tanzanite in comparison to the width of a human hair.

Alternatively, detectable amounts can be released in similar volumes of air from a plane of some 20 inclusions averaging 20 µm in size.

One of the main limitations of the method is whether inclusions of relevant size and abundance are present. Most unheated gem-quality tanzanites are selected for their clarity and tend to be relatively inclusion-free. Therefore, a negative test would not rule out an unheated natural tanzanite from the Merelani district.

Summary of conclusions

Multiphase H_2S-bearing fluid inclusions, up to *c.* 150 µm in size, occur as both primary and secondary inclusions in some uncut, unheated blue-brown rough tanzanites from the Merelani deposits of Tanzania. All generations of inclusions are characterized by the presence of high density H_2S that represents trapped portions of metamorphic fluids present during primary growth and subsequent recrystallization of the host zoisite.

Inclusions containing liquid H_2S are rare in minerals and hitherto have barely been reported in the gemmological literature. Recognition of these unusual inclusions with such distinctive features provides a valuable criterion for identifying natural, un-treated rough

tanzanites from its type locality and for distinguishing them from laboratory-grown crystals or substitutes should these be produced in the future. Positive identification of cut stones, for which any fracturing is not an option, is based on the characteristic Raman peak for H_2S (liquid) at 2583 cm^{-1}.

A simple scratch-chip test on rough stones is proposed for gemmological purposes based on the distinctive 'rotten egg' odour of H_2S (gas), when the inclusion contents are released causing the liquid H_2S to spontaneously evaporate. The human nose is highly sensitive to this odour. Calculations show that it is possible to detect H_2S released from a single inclusion some 30–50 µm in size, or from an opened trail of some 20 inclusions, averaging 20–30 µm in size. Further studies are recommended on a wider range of material to more fully evaluate the potential of this olfactory test.

Acknowledgements

This paper is based on data collected by Dan Taylor as part of his Masters Research thesis on inclusions in tanzanites at Kingston University. Tragically, Dan died following a road traffic accident before he completed his research. The present paper is based primarily on the comprehensive optical, Raman and microthermetric data set and images that Dan methodically kept in his laboratory notebook and computer files. We gratefully acknowledge the kind permission from Dan's family to use these data to write up the present paper as a contribution to his beloved subject of gemmology, which we dedicate to his memory, Most of the data and ideas presented here have arisen out of numerous discussions with us (PJT and AHR) as his co-supervisors prior to his untimely death. We have meticulously checked their validity against his notebook entries and by re-plotting the data. As such, we take full responsibility for any errors, omissions, misrepresentation or misinterpretation of the scientific data.

References

Amoore, J.E., and Hautala, E., 1983. Odor as an aid to chemical safety: Odor thresholds compared with threshold limit values and volatilities for 214 chemicals in air and water dilution. *J. Applied Toxicology,* **3**, 272–90

Beeskow, B., Rankin, A.H., Murphy, P.J., and Treloar, P.J., 2005. Mixed CH_4–CO_2 fluid inclusions in quartz from the South Wales Coalfield as suitable natural calibration standards for microthermometry and Raman spectroscopy. *Chemical Geology,* **223**, 3–15

Bény, C., Guilhaumou, N., and Touray, J.C., 1982. Native-sulphur-bearing fluid inclusions in the CO_2-H_2S-H_2O-S system — microthermometry and Raman microprobe (MOLE) analysis — thermochemical interpretations. *Chemical Geology*, **37**, 113–27

Burke, E.A.J., 2001. Raman microspectrometry of fluid inclusions. *Lithos*, **55**, 139–58

Feneyrol, J., Giuliani, G., Ohnenstetter, D., Fallick, A.E., Martelat, J.E., Monié, P., Dubessy, J., Rollionard, C., LeGoff, E., Malisa, E., Rakotondrazafy, A.F.M., Pardieu, V., Kahn, T., Ichang'i, D., Venance, E., Voarintsoa, N.R., Ranatsenho, M.M., Simonet, C., Omito, E., Nyamai, C., and Saul, M., 2013. New aspects and perspectives on tsavorite deposits. *Ore Geology Revs.,* **15**, 1–25

Frezzotti , M.L., Tecce, F., and Casagli, A., 2012. Raman spectroscopy for fluid inclusion analysis. *Journal of Geochemical Exploration,* **112**, 1–20

Giuliani, G., Dubessy, J., Banks, D., Vinh, H.Q., Lhomme, T., Pironon, J., Garnier, V., Trinh, P.T., Van Long, P., Ohnenstetter, D., and Schwarz, D., 2003. CO_2-H_2S-COS-S_8-AlO(OH)-bearing fluid inclusions in ruby from marble-hosted deposits in Luc Yen area, North Vietnam. *Chemical Geology,* **194**, 167–85

Gübelin, E.J., and Koivula J.I., 2005. *Photoatlas of inclusions in gemstones, Vol. 2.* Opinio, Basel

Henley, R.W., and Ellis, A.J., 1983. Geothermal systems ancient and modern: a geochemical review. *Earth Science Reviews,* **19**, 1–50

Hughes, R.W., 1997. *Ruby and Sapphire.* RWH Publishing, Colorado. 511 pp

Koivula, J. I., 1986. Carbon dioxide fluid inclusions as proof of natural-colored corundum *Gems & Gemology,* **22**, 152–5

Malisa , E., Kinnunen, K., and Koljonen, T., 1986. Notes on fluid inclusions in vanadiferous zoisite (tanzanite) of the Merelani area, Tanzania. *Bull. Geol. Soc. Finland,* **58**, 53–8

NIST 2011. NIST Chemistry WebBook. *US National Institute of Standards and Technology (NIST)*, Standard Reference Database No. 69. http://webbook.nist.gov/chemistry/. Accessed April 2013

Olivier, B., 2006. *The Geology and Petrology of the Merelani Tanzanite deposit, NE Tanzania.* Unpublished Ph.D. Thesis, University of Stellenbosch, RSA. 434 pp

Rankin, A.H., 2002. Natural and heat-treated corundum from Chimwadzulu Hill, Malawi: genetic significance of zircon clusters and diaspore-bearing inclusions. *J. Gemmology,* **28**(2), 65–75

Rankin, A.H., and Shepherd, T.J., 1978. H_2S-bearing fluid inclusions in barytes from the North Pole deposit, Western Australia. *Mineral. Mag.,* **42**, 408–10

Rankin, A.H., Taylor, D., and Treloar, P.J., 2013. Liquid hydrogen sulphide (H_2S) fluid inclusions in unheated tanzanites (zoisite) from Merelani, Tanzania: Part 2. *J. Gemmol.,* **33**(5/6), 161–9

Roedder, E., 1982. Fluid inclusions in gemstones — valuable defects. *International Geological Symposium, Proceedings, 1982*, Dianne M. Eash (Ed.): Santa Monica, Gemological Institute of America, 479–503

Roedder, E., 1984. *Fluid inclusions. Reviews in Mineralogy, Vol. 12.* Mineralogical Society of America, Washington DC, 644 pp

Shepherd, T.J., Rankin, A.H., and Alderton, D.H.M., 1985. *A practical guide to fluid inclusion studies.* Blackie and Sons, Glasgow. 254 pp

Van der Kerkhof, A., and Sousa, G. M., 2012. Fluid inclusions – Petrography and genetic interpretation of fluid inclusions. *Short course notes. University of Goettingen,* 57 pp Available online: www.uni-goettingen.de/de/document/.../Fluidhandout_2012_BsAs.pdf. Accessed May 2013

Walton, L., and Marshall, D., 2007. Tanzanite and Tsavorite. Chapter 6, p. 153–60 In: Groat, L.A. (Ed.). Geology of Gem Deposits. *Mineralog. Assoc. Canada, Short Course Series*, **37**, 288 pp

Wilkinson, J.J., 2001. Fluid inclusions in hydrothermal ore deposits. *Lithos,* **55**, 229–72

The Authors

Dan Taylor, Professor Andrew H. Rankin[1]* and Professor Peter J. Treloar[1]

1. Centre for Earth and Environmental Science Research, Faculty of Science, Engineering and Computing, Kingston University, Kingston upon Thames, Surrey KT1 2EE

* Corresponding author

The Journal of Gemmology / 2013 / Volume 33 / No. 5–6

Liquid hydrogen sulphide (H_2S) fluid inclusions in unheated tanzanites (zoisite) from Merelani, Tanzania: Part 2. Influence on gem integrity during and after heat treatment

Professor Andrew H. Rankin, Dan Taylor* and Professor Peter J. Treloar

This is the second of two papers dedicated to the memory of Dan Taylor.

Abstract: The estimated densities of the H_2S phase (0.58 to 0.77g/cm^3) in isolated and fracture-bound multiphase inclusions in tanzanite have been used to model internal fluid pressures during progressive heat treatment to 600°C. When internal fluid pressures exceed the confining strength of the host, the inclusions will re-equilibrate and the contents will be lost through leakage and/or decrepitation. The internal pressures beyond which 'typical' microscopic inclusions in zoisite will leak (P_d) under an external atmospheric pressure of 1bar, is estimated at 90 MPa (901 bars), but for larger inclusions (>100 µm) this value will be much lower. Thermophysical modelling of internal fluid pressures shows that virtually all except the smallest (<2–10 µm) inclusions in zoisite would not survive the heating process to temperatures above 600°C. Some inclusions larger than 20 µm may survive heating to 450°C, but the largest (*c.* 100 µm) will decrepitate or leak at even lower temperatures. Alignment of planar groupings of re-equilibrated inclusions will produce zones of internal weakness or internal stress which may be exposed and could be 'unzipped' along these planes, after heat treatment, during cutting and polishing. This explains why tanzanites can be difficult to cut unless free of inclusions and may also explain, at least in part, why some cut tanzanites may be more susceptible to fracturing than others. The results, overall, support the view expressed in Part 1 of this preliminary investigation (Taylor *et al.*, 2013) that microscopic H_2S inclusions (*c.* 20 to 100 µm) are generally a distinguishing feature of tanzanite/zoisite from Merelani which has not been heat treated.

Keywords: decrepitation, fluid inclusions, gemmology, heat-treatment, hydrogen sulphide liquid, microthermometry, PVTX modelling, tanzanite, zoisite

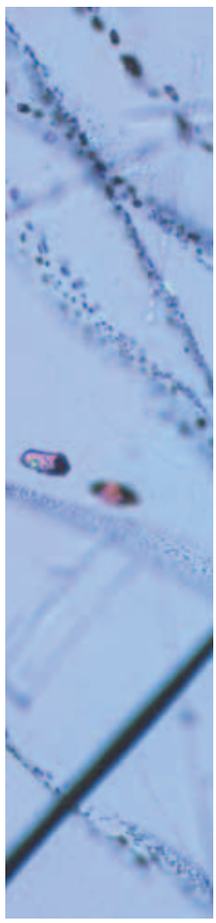

* Sadly Dan Taylor died on 29 October 2009.

Liquid hydrogen sulphide fluid inclusions in unheated tanzanites (zoisite): Part 2.

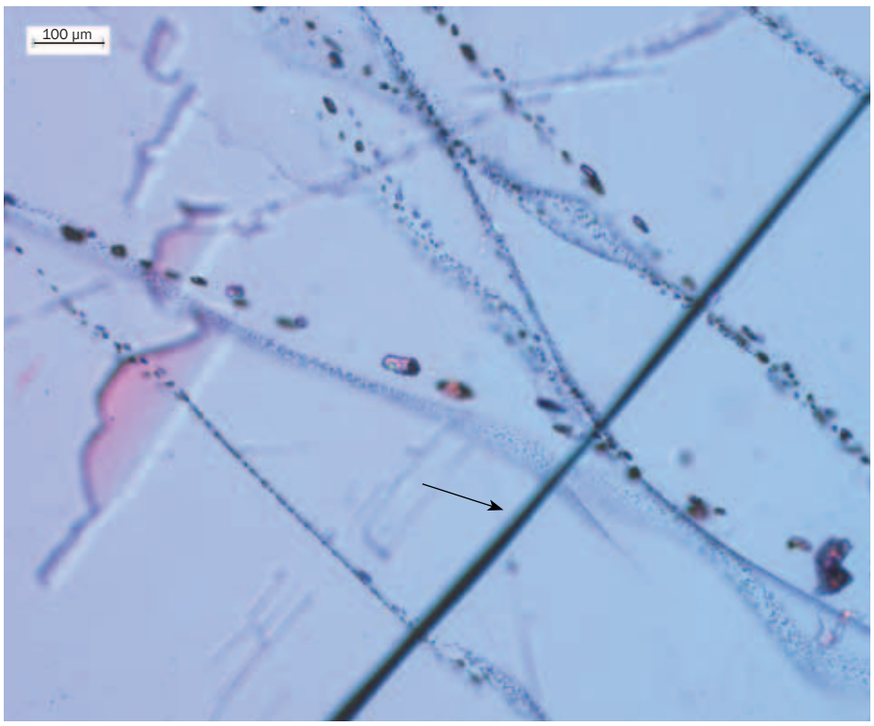

Figure 1: Planar and curviplanar criss-crossing trails of type II inclusions in unheated zoisite/tanzanite. Note relationship of inclusions to the linear cleavage direction (arrowed).

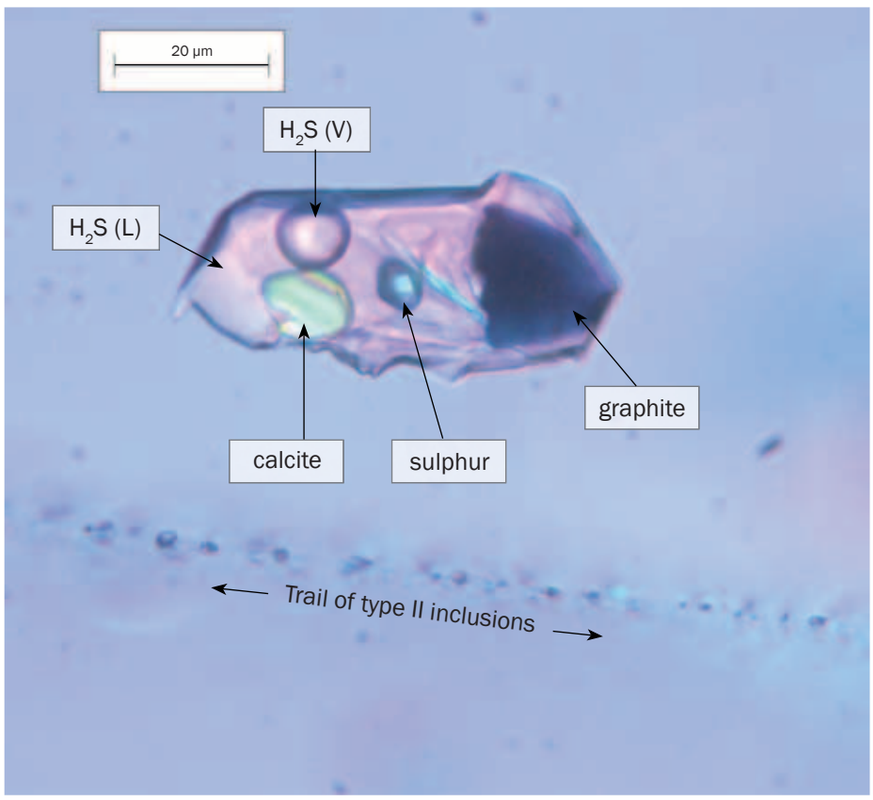

Figure 2: Typical phase proportions present in multiphase vapour-liquid-solid inclusions in unheated zoisite/tanzanite. Those illustrated in this isolated type I inclusion are similar to those present in very small type II inclusions in the trail below.

Introduction

In an accompanying paper (Taylor *et al.,* 2013) we reported on the occurrence and distribution of multiphase microscopic fluid inclusions of unusual and distinctive compositions characterized by the presence of unusually large amounts of liquid H_2S. We discussed their origin and highlighted their potential as gemmological indicators of provenance for unheated tanzanite (zoisite). Here we evaluate the likelihood of their survival after heat treatment; we also explore the effect that these inclusions will have on the integrity and mechanical stability of natural and heat treated tanzanites/zoisites i) during and after heat treatment, and ii) on cutting and polishing .

Nearly all trade tanzanites of gem quality are known to have been heat-treated to improve their colour (Bocchio *et al.,* 2012: GIA, 2013). Flawed rough stones, including those with inclusions visible with a 10× loupe, are avoided as far as possible because they are generally known not to survive the heating process up to 500–700°C causing the crystal to fracture and break apart (Roskin, 2005). Lower temperatures of 450°C are sometimes employed to minimize the risk of inclusion-induced fracturing, and it is conceivable that microscopic inclusions could survive the heating process to these lower temperatures as relict indicators of the original provenance of the stone. Where microscopic fluid inclusions have been destroyed, or partially opened, they could give rise to inherent weaknesses that may only be relieved or exposed during and after cutting. Tanzanite is known to be sensitive to thermal shock, which can increase its potential to fracture (GIA, 2013). Therefore, it is interesting to explore the likely influence that partly destroyed, or intact, inclusions might have on the thermal stability of cut tanzanites.

Approach and methodology

Information on the size and distribution of the H_2S inclusions in three rough zoisite/tanzanite crystals and their liquid-vapour homogenization temperatures (Th), have been previously

reported (Taylor *et al.,* 2013). These data form the basis of the present study. The homogenization temperatures of the liquid and vapour phases in fluid inclusions are widely used in mineralogical and petrological studies to determine the bulk density of the trapped inclusion fluid (Shepherd *et al.,* 1985). Here we use the Th data (28 to 84°C) for the three studied samples of rough tanzanite (zoisite) previously described (Taylor *et al.,* 2013) to estimate the bulk fluid densities of the homogeneous H_2S phase. The density estimates are then used to model internal pressures within these constant-density fluids, at different temperatures up to 800°C, using thermophysical data for pure H_2S. The temperatures at which the internal fluid pressures are likely to cause the inclusion in zoisite to leak or rupture are then estimated. The estimates are based on the established relationship between the Mohs hardness and the internal fluid pressures needed to initiate re-equilibration of fluid inclusions of varying size, in different minerals (Bodnar, 2003).

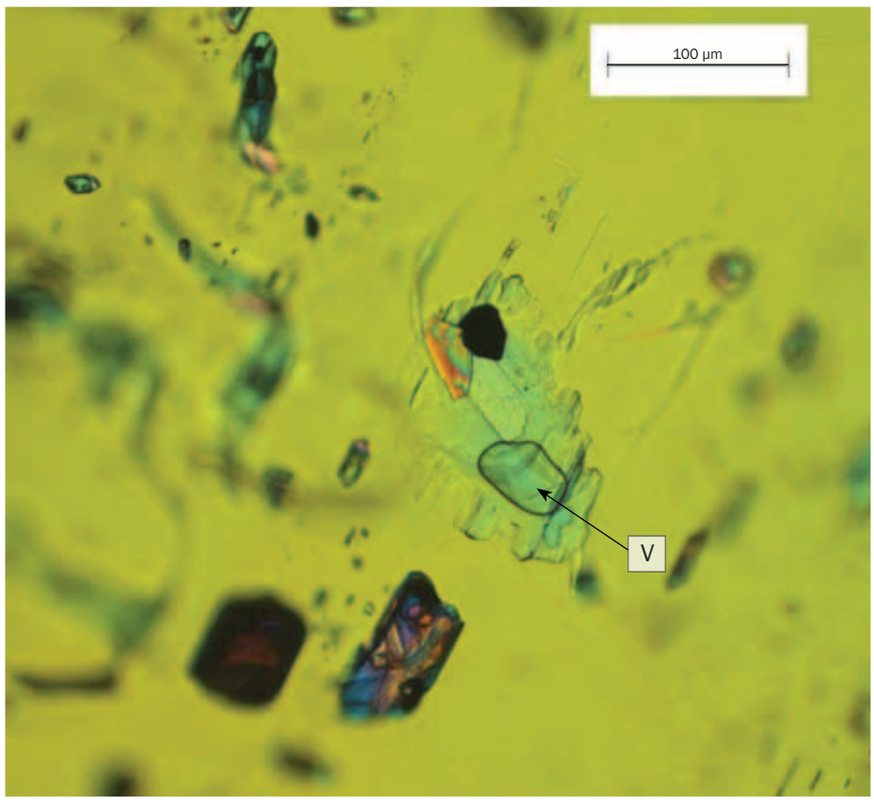

Figure 3: Large, highly irregular and flattened type I inclusions (c. 120 µm across) in a thick polished section of unheated zoisite/tanzanite viewed under crossed polars. Note the squashed and distorted vapour bubble (V) and elongated internal facets of the inclusion wall.

Fluid inclusion characteristics

As previously reported, three distinct groups of multiphase H_2S-dominant fluid inclusions, typically between 10 and 100 µm in size, are recognized (*Figures 1* to *4*). Type I inclusions are present in clusters and as larger isolated cavities which can be regular or highly irregular in shape (*Figures 2* and *3*). Type II inclusions occur as regularly-shaped inclusions in linear and curvi-planar groupings. Type III inclusions are less common and occur as indistinct and irregular-shaped planes that traverse the crystal *(Figure 4)*. In type I and II inclusions, at room temperature, the approximate volumetric proportions of the different phases identified are: liquid H_2S (75–45%), vapour H_2S (*c.* 5%) various solid phases (10–50%, see *Figures 2* and *3*). In type III inclusions H_2S liquid and vapour have been identified, but their small size and irregular shape precluded further identification of phases or

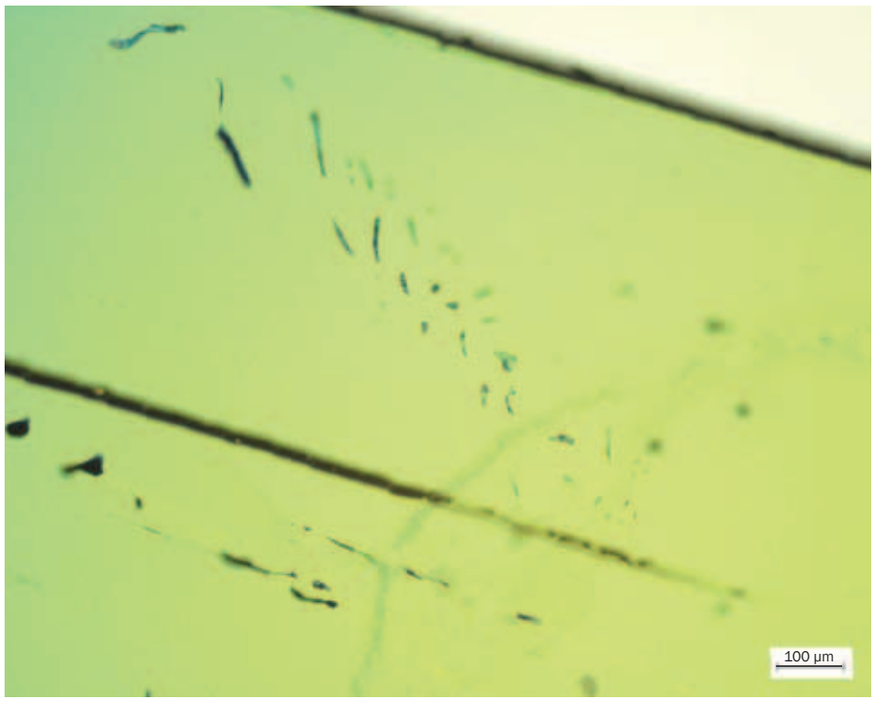

Figure 4: Elongate, irregular-shaped type II and III inclusions viewed under crossed polars. Note their small size and occurrence in trails in relation to the strong cleavage along the dark top of the section and the discontinuous straight line towards the centre of the image.

microthermometric measurements. The purity of the H_2S phase in all inclusions is greater than 95%.

Estimates of H_2S fluid densities from Th data

The distribution of homogenization temperatures for all 118 inclusions previously reported (Taylor *et al.,* 2013) together with separate data for isolated (type I) and fracture bound (type I and II) inclusions are presented in *Figure 5*. Some 95% of all inclusions homogenized over the temperature range from 45 to 75°C. The modal values for fracture bound inclusions (45°C) are slightly lower than for isolated inclusions (50°C) which also show a wider, skewed distribution of data up to 85°C.

The temperature at which the H_2S liquid (L) and vapour (V) phase in the inclusions homogenize to liquid will plot on the V+L ↔ L equilibrium curve as illustrated in *Figure 6*. Estimates of the densities based on this temperature-density diagram are also shown in *Figure 6*. These range from 0.58 to 0.77 g/cm^3 but most values are between 0.72 and 0.67 g/cm^3.

Internal fluid pressures within the inclusions

Estimates of changes in internal fluid pressure as a function of temperature are based on fundamental 'equations of state' that express the interdependence of pressure (P), temperature (T), and density (ρ) for fluids of fixed composition (see Bakker, 2009, for details). If two of these variables are known, or fixed, the other can be calculated, as evident from *Figure 6*. The use of bulk fluid density data to determine the internal P-T conditions, at any given temperature, is illustrated in *Figure 7* which shows the vapour-liquid equilibrium curve for H_2S based on available pressure-density-temperature (PρT) data (Lemmon *et al.,* 2011). On heating, an inclusion containing both liquid and vapour H_2S will follow the vapour-liquid equilibrium curve as the liquid expands and the vapour bubble shrinks. The point at which homogenization occurs (Th V+L → L) defines a unique position on this curve at which point all three variables (PρT) are fixed or can be calculated. Continued heating beyond Th will cause the inclusion to enter the single phase region. Provided the volume and mass, and therefore density, remain unchanged the inclusion will move along a PT path defined by a line of equal density (an isochore). It will continue to follow this isochoric path, maintaining its integrity, until the build up of internal fluid pressure exceeds the confining strength of the host mineral at atmospheric pressure (1 bar = 0.1 MPa). Beyond this point, relief of internal stresses will induce fractures or flexures in the host and the inclusions will either leak or decrepitate.

In the context of the previous paper (Taylor *et al.,* 2013) it will be apparent from *Figure 7* why a simple heat test for H_2S inclusions in natural tanzanites (zoisites) is inadvisable. For a typical inclusion homogenizing at 50°C

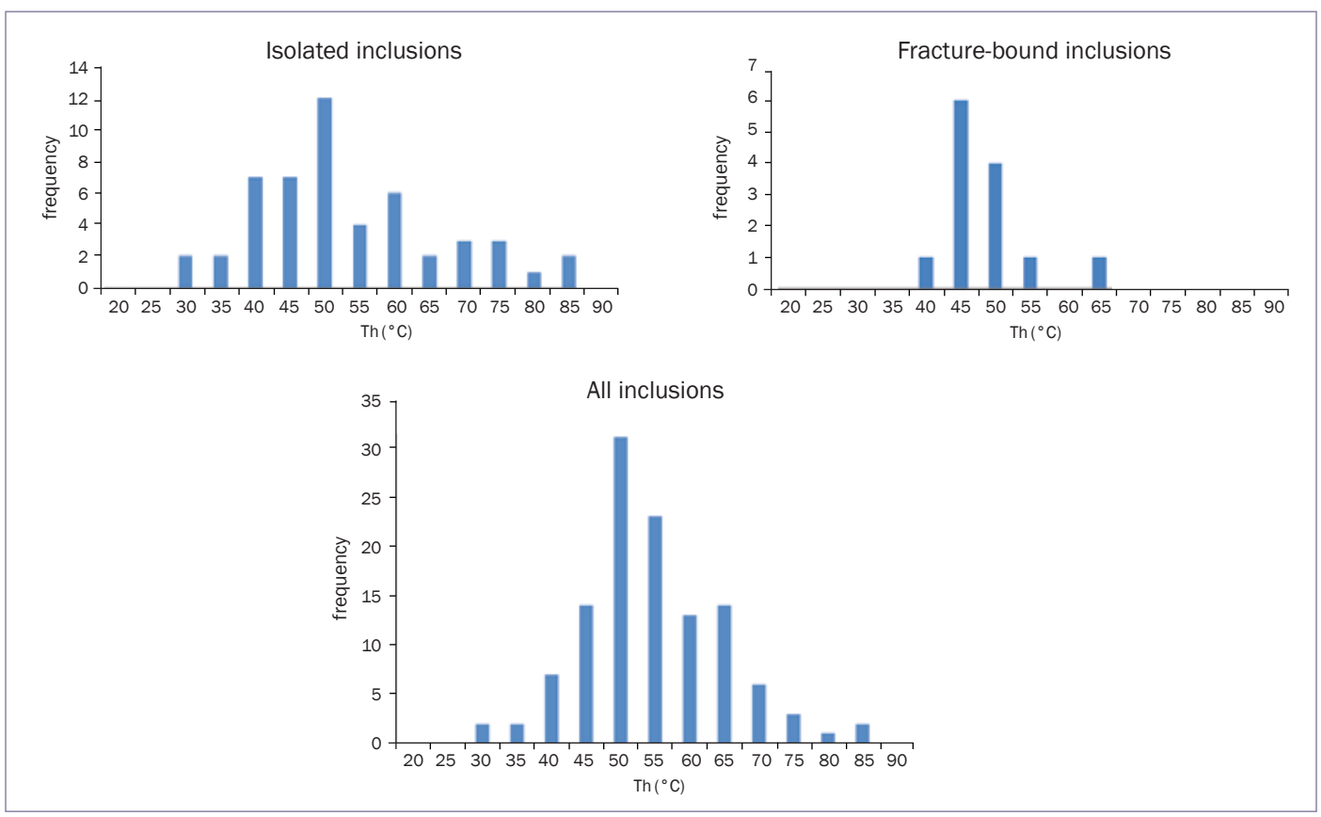

Figure 5: Histograms for vapour-liquid homogenization temperatures (Th) for isolated (type I) fracture-bound (type II) inclusions, and all inclusions in all three samples.

(ρ = 0.7) the pressure at the point of homogenization will be 35 bars (3.5 MPa), but if heated to just 75°C the internal fluid pressure would increase to 20 MPa which is 200 times greater than atmospheric pressure — significantly increasing the risk of fracture.

Experimental PρT data for pure H_2S is limited so for the present paper it is necessary to calculate the isochoric PT paths using 'equations of state'. Several are available but the Peng-Robinson equation (Peng and Robinson, 1976) is one of the most widely used, though uncertainties increase at temperatures > *c.* 500°C. However, the use is justified because ranges, rather than precise estimates of pressures, are adequate for evaluating the overall potential for leakage/decrepitation of inclusions on heating treatment to between 450 and 600°C. Calculations were carried out using the Loner PW computer programs developed by Bakker (2009). The results are shown in *Figure 8*. The minimum and maximum internal fluid pressures (P_i) for all inclusions, over the temperature range 450 to 600°C are 130 and 320 MPa respectively. For most inclusions (Th from 40 to 70°C) the P_i values are between 160 and 300 MPa.

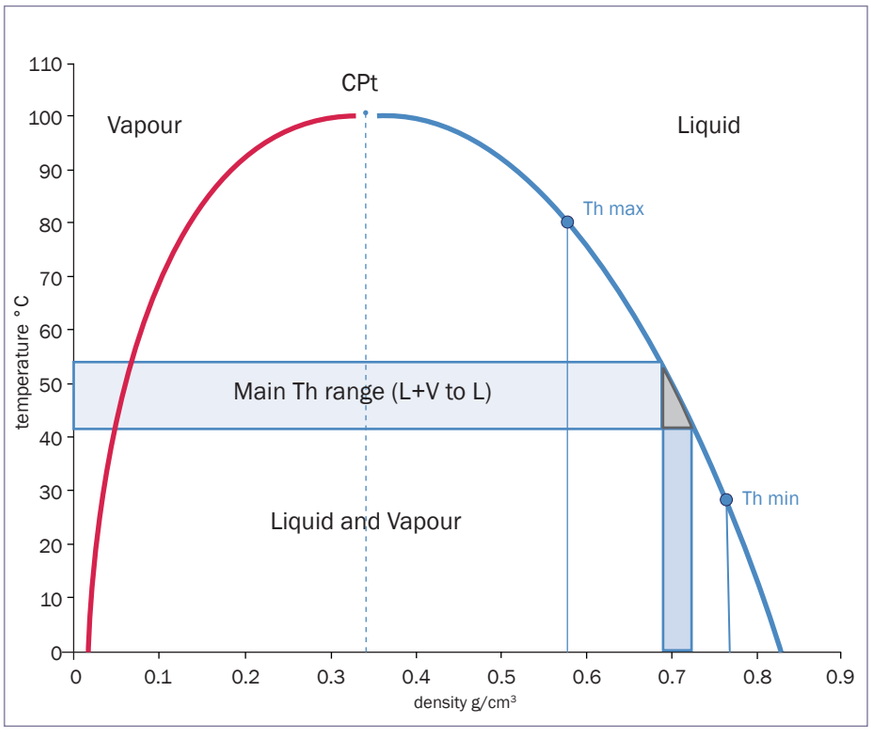

Figure 6: Temperature–density diagram for pure H_2S, constructed from NIST data (Lemmon et al.*, 2011) showing the equilibrium curve separating the two phase (liquid+vapour) and single phase (liquid or vapour) stability fields up to the critical point (CPt at 100°C). Homogenization temperatures (Th) for inclusions containing pure H_2S that homogenize to liquid (L+V → L) will plot on this right-hand side of the curve (in blue). The maximum, minimum and main Th ranges for inclusions in zoisites are shown in the shaded band together with their corresponding densities (g/cm³).*

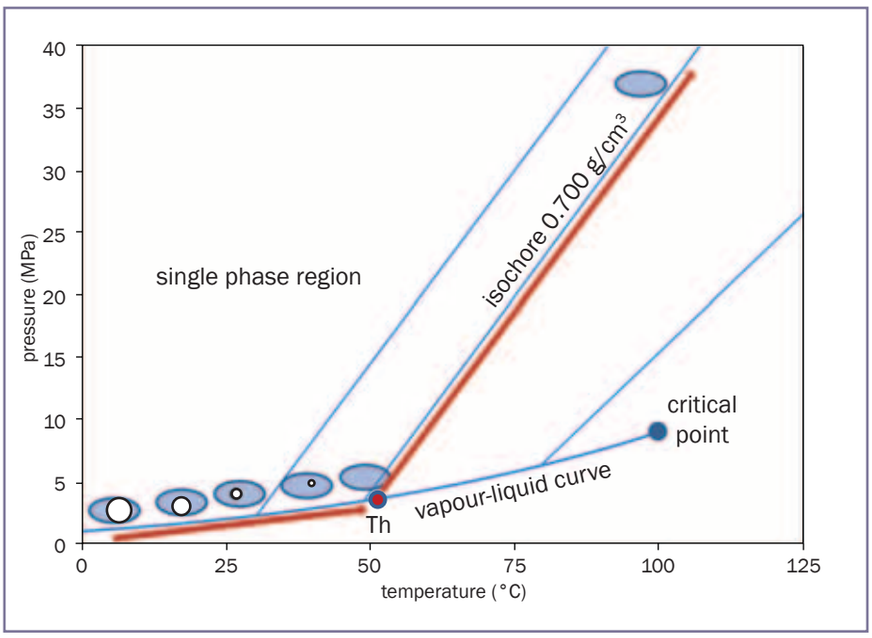

Figure 7: P-T plot for H_2S, constructed from NIST data (Lemmon et al.*, 2011) for pure H_2S illustrating the pathway (red) followed by an inclusion a) on heating along the vapour-liquid co-existence curve up to the point of homogenization (Th) which uniquely defines the bulk fluid density, then b) beyond along a PT isochoric path defined by this density. Note that the vapour bubble size in the inclusion schematically reduces on heating.*

Influence of internal fluid pressures on stress relief and inclusion integrity

Background

It has long been recognized that the build up of pressures in fluid inclusions during heating can cause the inclusion contents of minerals to leak. This is often accompanied by the sudden, and audible, explosive release of fluid and shattering of the crystal (decrepitation). Decrepitation may occur spontaneously in soft cleavable minerals such as baryte and halite containing compressed gas inclusions where heat from the hand may be sufficient to cause shattering, accompanied by audible 'pops' (popping salt) and 'jumping' of fragments out of the hand (Dons, 1956; Roedder, 1984). Even in more resistate minerals, such as quartz, spontaneous stress release

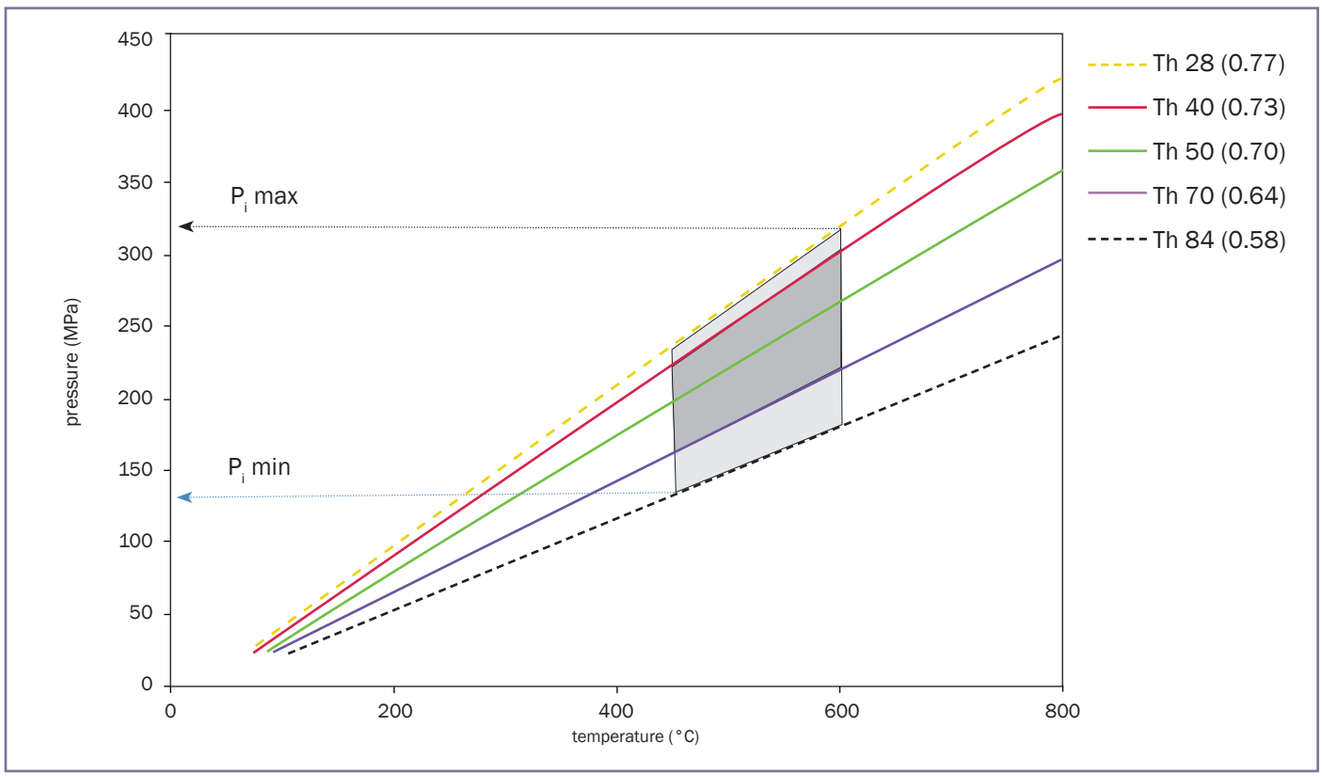

Figure 8: P-T plot for H_2S showing isochores for inclusions that homogenized over the determined temperature range of 28 to 84 °C. The light shaded area defines the internal pressures for all determined inclusion densities between 450 and 600 °C. The darker shaded area defines the PT region corresponding to the main range of fluid densities. The arrows define maximum and minimum P_i values.

may occur from compressed CO_2-gas inclusions, if they are sufficiently large (>*c.* 100 µm) and abundant. For example, Roedder (1982) records an instance where a museum specimen of Brazilian quartz containing planar groups of such inclusions spontaneously decrepitated breaking the glass display case.

Internal fluid pressure needed to initiate re-equilibration of fluid inclusions in zoisite

Published quantitative decrepitation data and estimated internal fluid pressures for individual inclusions in different minerals under a confining pressure of 1 atmosphere (0.1 MPa) have been compiled by Bodnar (2003). There is a linear relationship between internal fluid pressure needed to initiate re-equilibration (decrepitation) of fluid inclusions (P_d), and the Mohs hardness of the mineral host *(Figure 9)*. The relationship is expressed by the equation:

Pressure (bars) = 69 + (128 × Mohs hardness)

Based on this equation and Mohs hardness for zoisite between 6 and 7, the estimated mean internal pressure (P_d) is 901 bars (90.1 MPa). Fluid inclusion size is also an important factor. This is illustrated in *Figure 9* which shows the influence of both hardness and inclusion size on P_d values for several minerals. Quartz is only slightly harder than zoisite. It is therefore reasonable to suppose that the established P_d range for inclusions in quartz in the 1 to 100 µm size range also approximates to that for zoisite. *Figure 9* presents both the calculated and indicative P_d values for zoisite for inclusion sizes between 1 and 100 µm. Also shown are the internal fluid inclusion pressure estimates (P_i) for 95% of inclusions (160 to 300 MPa) from the present study based on isochore projections to between 450 and 600°C. These are significantly higher than the pressures at which all but the smallest inclusions would be expected to leak or decrepitate.

The influence of inclusion size on the P_d values for quartz, based on published experimental data, is shown in more detail in *Figure 10*. Superimposition of the P_i estimates for 95% of the inclusions from the present study are also shown. These are separated into P_i values at 450 and 600°C (160 to 230 MPa, and 220 to 300 MPa respectively). The lower and upper P_i values cross the 'best fit' P_d line at 7 and 2 µm respectively, further demonstrating the general inability of larger inclusions to maintain their integrity under these pressures.

Discussion

Validity of isochore projections

We have previously argued that extrapolating isochore projections above 500 °C is valid for the purpose of this paper. Another question to consider is the influence of variations in inclusion composition on the isochores. The determined isochores relate only to pure H_2S. They will differ if other components are present. The only other volatiles previously detected (Taylor *et al.* 2013) are very small amounts of methane

and nitrogen in a few vapour bubbles. Calculations based on PT estimates using the Loner PR computer program (Bakker, 2009) show that at such low levels (<0.025 mole fraction) there is little effect on the shape and position of the determined isochores. Water was not recognized optically or detected by Raman analysis as previously reported (Taylor *et al.,* 2013). This is somewhat unexpected in view of recent studies on mineralization at Merelani that suggest a significant hydrothermal component to the zoisite/tanzanite mineralization in the area (Olivier, 2006). However, this does not necessarily preclude its absence especially as liquid water has a similar refractive index to liquid H_2S and interfaces between these two, partially-miscible liquids will be indistinct. The hydrated mineral, gypsum, tentatively identified in some inclusions also suggests that the inclusion contents are not anhydrous. Further studies are needed to establish the extent to which water is present, but for reasons outlined in the Acknowledgements this has not been possible in the present study. However, the effect of water on pure H_2S isochores has also been modelled in data for the H_2S–H_2O system for fluids of similar or slightly higher densities (0.90 to 0.60 g/cm^3) using the Loner PR program of Bakker (2009). The results show that pure H_2S isochores steepen with increasing H_2O contents meaning that the inclusions will become more susceptible to decrepitation and leakage at even lower temperatures.

Major solid phases identified within the inclusions (graphite, calcite and native sulphur) may also have a significant effect on the isochore calculations. But this depends on whether or not they i) crystallized *in situ* within the inclusions after trapping (daughter minerals) or ii) were accidentally incorporated as captive daughter minerals, in which case they are unlikely to have a significant effect. Graphite and calcite are major components of the host rocks associated with the zoisite (Olivier, 2006) and are quite likely to be captive phases, whereas native sulphur is not. This is based on

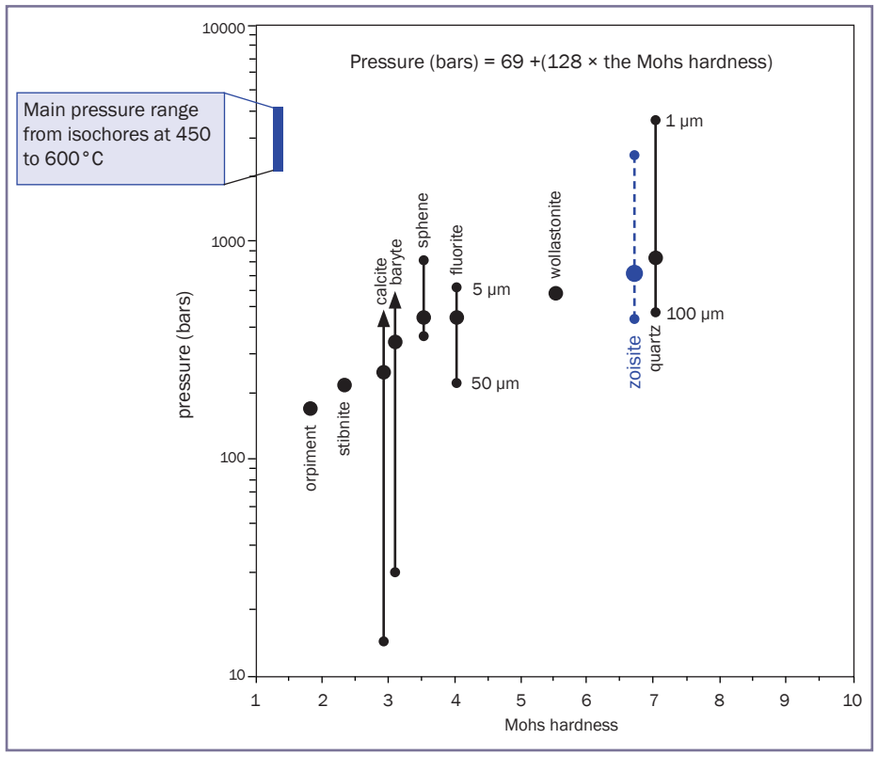

Figure 9: Relationship between internal pressure needed to initiate re-equilibration of fluid inclusions and the Mohs hardness, based on the compilation of Bodnar (2003). Note the effect of inclusion size in quartz and fluorite. The estimated range for zoisite (this work) and the internal fluid pressure estimates at 450 to 600°C are shown in blue.

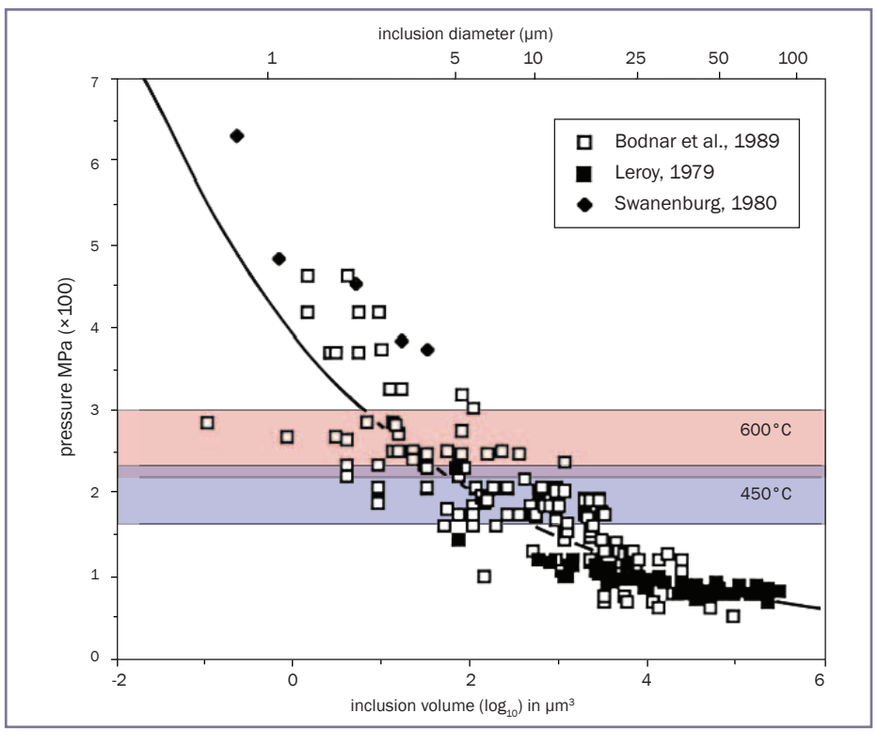

Figure 10: Relationship between inclusion size (and volume) and the pressure required to re-equilibrate fluid inclusions in quartz, based on three sources of published data, represented by different symbols (modified from Bodnar, 2003). The main internal pressure ranges determined for H_2S inclusions in the zoisite at 450 and 600°C are also shown.

the observed precipitation from the H_2S fluid under the laser beam (Taylor *et al.,* 2013) and also its known solubility in high density H_2S fluids at moderate temperatures and pressures (Migdisov *et al.,* 1998). However, as the volumetric proportion of native sulphur within the inclusions is less than about 5% (see *Figure 2*), the effects will be small.

Implications for the production, polishing and care of heat-treated tanzanites

Data on internal fluid pressures from calculated isochores *(Figure 8)*, combined with published P_i data for quartz (at 1 bar external pressure) are shown in *Figure 10*. The data demonstrate that all but the smallest (<2–10 µm), microscopic inclusions are unlikely to survive heat treatment to 600°C due to the high internal fluid pressures generated (to 300 MPa) and will leak or decrepitate above this temperature. On heating up to 450°C some larger inclusions (up 20 µm) may survive heating to this lower temperature, but the majority of inclusions in the size range 20 to 100 µm would not. This is apparent in *Figure 10* from the clustering of data points around the estimated P_d value for zoisite of 90 MPa. Larger inclusions (>100 µm) would be the first to leak or decrepitate at much lower internal pressures and are very unlikely to survive heating even to temperatures below 100°C. This is apparent from the steepness of the isochores for minimum and mean Th values shown *Figure 7*, and also direct observation of leakage from some large and irregularly shaped inclusions during microthermometric analysis to up 100°C (Taylor *et al.,* 2013).

Producers are acutely aware of the influence that 'flaws' or 'inclusions' have on the integrity of zoisites/tanzanites prior to, or during, heat treatment. Stones with inclusions visible with a 10× loupe can be avoided, but microscopic (*c.* 5–20 µm) inclusions can all too easily be overlooked. Leakage or decrepitation of H_2S inclusions may not necessarily lead to immediate fragmentation of the crystal. Instead, relief of internal fluid pressure may be accommodated by flexure of the crystal and creation of zones of stress or weakness in the vicinity of the ruptured inclusions which may be evident from microscopic 'veils' or wisps sometimes observed in heat treated tanzanites (Adamo *et al.,* 2010). Exposure of these internal microfractures or stress zones during cutting and polishing, especially if leaked inclusions occurred in discontinuous planar groupings (type II inclusions), means that stones may be 'unzipped' along planar or curvilinear fractures, not necessarily along cleavage directions as indicated in *Figures 1* and *4*. This suggestion also helps explain why heat-treated tanzanites may be susceptible to fracturing, not just because of good cleavage, when subjected to sudden changes from warm to cold ambient temperatures.

Implications for recognition of unheated, naturally-coloured tanzanites

In the accompanying paper (Taylor *et al.,* 2013) we suggested that the presence of an H_2S-liquid inclusion is a diagnostic feature of natural unheated tanzanites/zoisites. This is supported by the results of the present study which demonstrate that all but the smallest of the H_2S inclusions in heat treated tanzanites should not survive the heat treatment process to 600°C or more with their contents intact. Furthermore, any smaller inclusions that do survive would supply insufficient volumes of gaseous H_2S to the atmosphere to be detectable by the suggested scratch-chip odour test *(op.cit.)*. Some larger inclusions (*c.* 20 µm) could survive internal fluid pressures on heating up to 450°C, but the fortuitous opening of many such inclusions, unaffected by heat treatment, would be required to detect the odour of H_2S in $(20\ cm)^3$ of air (Taylor *et al.,* 2013). Therefore, the probability of this happening is considered to be very low.

Most tanzanites in the market are heat-treated, and currently there is little demand for unheated stones. For the specialist collector the simple scratch-chip odour test would be a useful criterion for helping to identify unheated crystals. However, the method is not entirely reliable as some small inclusions may survive less destructive heat treatment up to the lower temperature of 450°C sometimes employed in heat treatment. It is also suggested that a strong odour of this gas from rough or cut stones prior to heating might indicate those stones more likely to be susceptible to breakage during heat treatment, due to the presence of significant numbers of microscopic inclusions.

Summary of conclusions

The internal fluid pressures in H_2S fluid inclusions in natural zoisite (tanzanite) will increase systematically on heating, until a point where the pressure will exceed the confining strength of the zoisite host and the inclusions will leak or decrepitate. The mean pressure (P_d) at which this will occur is estimated at 901 bars (90.1 MPa), but will vary according to the size and shape of the inclusions.

The calculated densities (ρ) of the H_2S phase for both type I and II inclusions range from 0.77 to 0.58 g/cm^3. On heating, inclusions in zoisite will follow linear pressure-temperature pathways above their determined vapour-liquid homogenization temperatures of between 28 and 84°C. These pathways are defined by the fluid densities (isochores), and are based on PρT modelling of pure H_2S. The determined isochores are useful for estimating internal fluid pressures (P_i) within inclusions at any point during the heat-treatment of zoisite (tanzanite). The effects of minor volatiles (methane and nitrogen) on the isochores are negligible, and water, if present, is shown to increase rather than decrease the internal fluid pressures on heating.

The internal fluid pressure estimates, based on data for three Merelani zoisites, show that only very small microscopic and submicroscopic inclusions (<2–10µm) are likely to survive temperatures to 600°C employed during heat treatment of probably most of the zoisite/tanzanite. The chances of survival of inclusions up to 20 µm in size would be greater if heat treatment were to be carried out to a lower temperature of 450°C. The

destruction or leakage of larger inclusions, especially in planes (type II inclusion), may leave linear zones of weakness or stresses in heat-treated tanzanites which can contribute to the fracture potential of the treated stone.

The resulting loss of H_2S from any sizeable inclusions in heat-treated tanzanite confirms that the scratch-chip odour test is an effective discriminator between natural (unheated) tanzanites and those heated to 600°C. For samples heat treated to lower temperatures (450°C) some larger inclusions (>20 µm) may survive but in most cases are unlikely to provide enough H_2S to be detected by odour alone.

This exploratory study is confined to just a few samples from the D block area of Merelani. Further studies are needed on a wider range of both heated and unheated samples to more generally assess the principles and ideas outlined in this paper.

Acknowledgements

This paper is based on the microthermometric data and microscopic observations collected by Dan Taylor as part of his Masters Research thesis on inclusions in tanzanites at Kingston University. Tragically, Dan died following a road traffic accident before he completed his research. We gratefully acknowledge the kind permission from Dan's family to use these data to write up the present paper as a contribution to his beloved subject of gemmology, which we dedicate to his memory. Many of the ideas presented here have arisen out of numerous discussions with us (AHR and PJT), his co-supervisors, prior to his untimely death. However, responsibility for any errors, omissions, misrepresentation or misinterpretation of the scientific data is ours alone.

References

Adamo, I., and Bocchio, R., 2010. Tanzanite and other zoisites from Merelani (NE Tanzania): new gemmological and chemical data. *Plinius,* **36**, 495

Bakker, R. J., 2009. Package Fluids. Part 3: correlations between equations of state, thermodynamics and fluid inclusions. *Geofluids,* **9**, 3–7

Bocchio, R., Adamo, I., Bordoni, V., Caucia, F., and Diella, V., 2012. Gem-quality zoisite from Merelani (Northeastern Tanzania): review and new data. *Periodico di Mineralogia,* **81**(3), 379–91

Bodnar, R.J., Binns, P.R., and Hall, D.L., 1989. Synthetic fluid inclusions VI. Quantitative evaluation of the decrepitation behaviour of fluid inclusions in quartz at one atmosphere confining pressure. *J. Metamorphic Geol.,* **7**(2), 229–42

Bodnar, R. J., 2003. Reequilibration of fluid inclusions. In: I. Samson, A. Anderson and D. Marshall (Eds). *Fluid Inclusions: Analysis and Interpretation*. Short course series, Mineralogical Association of Canada, **32**, 213–30

Dons, J.A., 1956. Barite which decrepitates at room temperatures. *Norsk Geol. Tidsskr,* **36**, 241–8

GIA Anon, 2013. Tanzanite care and cleaning guide. Gemological Institute of America Web article: http://www.gia.edu/tanzanite-care-cleaning (retrieved 20 May 2013)

Lemmon, E.W., McLinden, M.O., and Friend, D.G., 2011. Thermophysical Properties of Fluid Systems. In: P.J. Linstrom and W.G. Mallard (Eds), NIST Chemistry WebBook, NIST Standard Reference Database Number 69. National Institute of Standards and Technology, Gaithersburg MD, 20899, http://webbook.nist.gov (retrieved 26 May 2013)

Leroy, J., 1979. Contribution à l'étalonnage de la pression interne des inclusions fluides lors de leur décrépitation. *Bull. Mineral.,* 102, 584–93

Migdisov, Art A., Suleimenov O. M., and Alekhin Yu. V., 1998. Experimental study of polysulfane stability in gaseous hydrogen sulfide. *Geochim. Cosmochim. Acta,* **62**, 2627–35

Olivier , B., 2006. *The Geology and Petrology of the Merelani Tanzanite deposit, NE Tanzania*. Unpublished Ph.D. Thesis, University of Stellenbosch, RSA. 434 pp

Peng, D.Y., and Robinson, D.B., 1976. A new two-constant equation of state. *Indust. and Engr. Chemistry: Fundamentals,* **15**, 59–64

Roedder, E., 1982. Fluid inclusions in gemstones — valuable defects. *International Gemological Symposium, Proceedings,* D.M. Eash (Ed.), Gemological Institute of America, 479–503

Roedder, E., 1984. The fluids in salt. *American Mineralogist,* **69**, 413–39

Roskin, G., 2005. Jewel of the month: Natural-Color Tanzanite. *JCK Magazine,* Feb 2005. http://www.jckonline.com/article/286740-Natural_Color_Tanzanite.php#disqus_thread (retrieved 20 May 2013)

Shepherd, T. J., Rankin, A.H., and Alderton, D.H.M., 1985. *A practical guide to fluid inclusion studies*. Blackie and Sons, Glasgow, 254 pp

Swanenburg, H.E.C., 1980. Fluid inclusions in high-grade metamorphic rocks from S.W. Norway. Unpub. Ph.D. Thesis, Geologica Ultraiectina, University of Utrecht, The Netherlands

Taylor, D., Rankin, A.H., and Treloar, P.J., 2013. Liquid hydrogen sulphide (H_2S) fluid inclusions in unheated tanzanites (zoisite) from Merelani, Tanzania : Part 1. Recognition, characterization and gemmological importance. *Journal of Gemmology,* **33**(5/6), 149–59

The Authors

Professor Andrew H. Rankin[1]*, Dan Taylor and Professor Peter J. Treloar[1]

1. Centre for Earth and Environmental Science Research, Faculty of Science, Engineering and Computing, Kingston University, Kingston Upon Thames, Surrey KT1 2EE

* Corresponding author

Abstracts

Diamonds

Gemmologie Aktuell. Notes from the DSEF German Gem Lab.
C.C. Milisenda and K. Schollenbruch. *Gemmologie. Z. Dt. Gemmol. Ges.,* **61**(3/4), 2012, 63–70. 12 photographs. German and English.

The lab received a faceted opaque black stone weighing more than 30 ct with an RI higher than the limits of the standard refractometer. It was said to be a diamond with a broken culet. Chemical analysis showed it to be an ilmenite. E.S.

Gems and Minerals

Bottled up.
G. Choudhary. *Gems&Jewellery,* **22**(2), 2013, 12–13.

An unusual report on the growth and identification of sulphur crystals within bottles of standard RI fluid. A.S.F.

John Kessler donation.
L. Gleave. *Gems&Jewellery,* **22**(4), 2013, 8

The importance of donations to the Gem-A gemstone collection and the significance of John Kessler's recently donated collection to the future of teaching and research. A.S.F.

Die Verwendung von Schmucksteinen aus der Gruppe mikro- bis krypto-kristalliner Quarze bei Tabatieren aus dem Nachlass des preußischen Königs Friedrich II(1712–1786).
G. Holzhey. *Gemmologie. Z. Dt. Gemmol. Ges.,* **61**(3/4), 2012, 71–90. 30 photographs, bibl. German with English abstract.

The author refers to the 300th anniversary in 2012 of the birth of Frederick II. An increase in prosperity during his reign resulted in an increase in the manufacture of gold and jewellery in Berlin. The king was a great collector of snuff boxes, often very ornate, carved and encrusted with diamonds. He was particularly fond of Silesian chrysoprase.

Nine chrysoprase snuff boxes are described, as well as some jasper/agate boxes. The agates might have come from Oberkirchen, south of Idar-Oberstein. E.S.

Saphirblauer Disthen (Kyanit) aus Nepal.
U. Henn and K. Schollenbruch. *Gemmologie. Z. Dt. Gemmol. Ges.,* **61**(3/4), 2012, 91–8. 8 photographs, 1 table, 1 diagram, bibl. German with English abstract.

Intense blue, relatively homogeneous, transparent kyanites have been found in Nepal since 1995. They can be faceted and resemble blue sapphires. Stones up to 10 ct have been on the market. The blue colour is due to iron and titanium. There are traces of chromium which might be the cause of a possible red fluorescence. The stones from Nepal are biaxial positive. There are some cleavage cracks and growth tubes which may cause iridescence. Colour zones, film-like fluid inclusions and a few dark mineral inclusions have been observed. E.S.

Gemmologie Aktuell. Notes from the DSEF German Gem Lab.
C.C. Milisenda and K. Schollenbruch. *Gemmologie. Z. Dt. Gemmol. Ges.,* **61**(3/4), 2012, 63–70. 12 photographs. German and English.

A translucent oval red cabochon weighing 40 ct was submitted to the lab as a ruby. However, the RI was 1.74 (a little low for a ruby) and it also had a slightly lower density; an infrared reflectance spectrum confirmed the stone to be a rhodonite; inclusions resembled those in Tanzanian rubies so reliance cannot be placed on this feature.

Other stones difficult to identify were some small transparent faceted yellow stones which the infrared spectrometer identified as sapphire; however under the microscope flux feathers and dark mineral grains with a blue halo were detected. The sapphires had been beryllium treated, but definite proof can only be obtained with mass spectrometric methods.

The lab received a cabochon-cut dark brown 12-rayed sapphire — a distinct six-rayed star with a weaker six-ray, with arms at nearly 30 degrees to the main star. The stone was double refractive, average RI 1.77. Further investigation showed the stone to be a composite of two pieces of star sapphire, the lower part being turned 30 degrees to produce a 12-rayed star. E.S.

The three feathers.
G. Millington. *Gems&Jewellery,* **22**(1), 2013, 8–11.

A report on three stones — a colour-change stone light yellowish-green in daylight changing to brownish-pink in incandescent light, and a yellow stone and purple stone — submitted for investigation. All displayed very similar feather-like inclusions. The stones were identified as a diaspore, a yellow sapphire and a purple synthetic corundum, respectively. The article concluded with a precautionary reminder for all gemmologists not to take things at face value. A.S.F.

Abstracts (continued)

A tale of two rubies.
G. Millington. *Gems&Jewellery,* **22**(3), 2013, 14–16.

A description of the internal features and the testing process for two red stones. Both were found to be natural ruby, one glass filled. Some of the problems that gemmologists face when trying to identify natural from synthetic are discussed, and the various forms of treatments that abound for corundum. A.S.F.

Is it an emerald?
G. Millington. *Gems&Jewellery,* **22**(4), 2013, 8.

An interesting and precautionary report on the identification of a large green faceted stone, which at first appeared to be emerald but was identified as fluorite. A.S.F.

Red flag: are glass-filled rubies legal?
J. Ogden. *Gems&Jewellery,* **22**(1), 2013, 12–13.

An investigation into the implications of the EU's legislation on lead content in products and its possible impact on the jewellery sector; glass-filled rubies may no longer comply. A.S.F.

Holy chic: a very special man's ring.
J. Ogden. *Gems&Jewellery,* **22**(1), 2013, 14.

The research carried out by Joanna Angelett before designing a modern-day ecclesiastical ring. Named the Holy Kingdom Ring, the ring was set with an ametrine. A.S.F.

Exams.
J. Ogden. *Gems&Jewellery,* **22**(2), 2013, 18–19.

Jack Ogden looks back at the very first FGA examinations in 1913 and poses the question: "Can you answer the same questions successfully today?" A.S.F.

An old attraction: magnetic gems.
J. Ogden. *Gems&Jewellery,* **22**(3), 2013, 9.

The magnetic susceptibility of gemstones has been widely reported on in recent years in *The Journal of Gemmology* by various authors including Don Hoover, but in this article a history dating back as far as 1779 is revealed. A.S.F.

The Scottish Conference.
J. Ogden. *Gems&Jewellery,* **22**(4), 2013, 13–16.

An in-depth look at the annual Scottish conference, focusing on the range of presentations. Notable speakers included Clare Blatherwick (pearls of varying types), Ron Ringsrud (the emeralds of Colombia) and Dr Claudio Milisenda (Ethiopian opals). Humour and historical fact were provided by Jack Ogden, with his unusually titled 'Lap dancers and drill masters' which focused on the history of gem fashioning. A.S.F.

A new kyanite.
C. Williams. *Gems&Jewellery,* **22**(5), 2013, 13.

A look at the recent discoveries of kyanite in various colours (and chromophores), focusing mainly on the blue-green gem variety from Nepal. A.S.F.

Tucson Gem Shows 2013.
H. Seras-Herman. *The Jeweller,* Jan/Feb 2013, 44-7.

A guide for those planning a trip to the Tucson Gemshows. Whether they be seasoned veterans, or first-timers, 20 tips outline the best thoughts for buying strategies. A.S.F.

Instruments and Techniques

A point for pointers: lasers in gemmology.
J. Ogden. *Gems&Jewellery,* **22**(3), 2013, 20–1.

The use of laser pointers — red, green and blue — as a tool in gem identification. A.S.F.

Synthetics and Simulants

Beschichtete Steine und ihre Erkennung.
U. Henn and K. Schollenbruch. *Gemmologie. Z. Dt. Gemmol. Ges.,* **61**(3/4), 2012, 99–114. 15 photographs, 3 diagrams, 1 table, bibl. German with English abstract.

Surface-coated gems are mainly colourless, but there are also some coloured stones like quartz, topaz, glass or synthetic spinel which are colour- or lustre-improved by a thin coating of a metal or metal compound. The coating can be removed mechanically by grinding. Identification is partly possible using only the naked eye or by loupe and microscope. Coatings on synthetic diamond such as diamond-like carbon (DLC) are highly resistant and difficult to identify. CZs can be coated by a CVD process to make them more diamond-like, but can be distinguished from diamond by the different characteristics of the coated stone; however, coated diamonds can be difficult to determine. E.S.

Gemmologie Aktuell. Notes from the DSEF German Gem Lab.
C.C. Milisenda and K. Schollenbruch. *Gemmologie. Z. Dt. Gemmol. Ges.,* **61**(3/4), 2012, 63–70. 12 photographs. German and English.

The cat's-eye effect was imitated in stones in two rings, one green and the other pink. They were shown to be glass fibre imitations which can be identified by a 'window' when viewed parallel to the fibres; also the cat's-eye effect was too good to be expected in natural stones.

A rough green stone weighing approximately 100 g, RI 1.738, density 3.58, had perfect cleavage showing as rectangular cleavage planes visible to the naked eye. The stone was found to be a synthetic periclase which is produced in an electric arc furnace. E.S.

A rainbow... like unto an emerald.
G. Millington. *Gems&Jewellery,* **22**(5), 2013, 14–17.

A highly illustrated examination of a synthetic emerald that showed all the inclusions and features that any gemmologist should look for, as well as interesting interference colour patterns. A.S.F.

Abstractors

A.S. Fellows – A.S.F.
E. Stern – E.S.

Book reviews

Dictionary of Gemstones & Jewelry
1st English edition
A. Chikayama. Translated by S. H. Gill; E. A. Jobbins, editor, 2013. IMACBC Co. Ltd, Tokyo, Japan. 652 pp. ISBN 978-4-9906841-0-5. £85.00 ($100 US)

To some, 'Dictionary' might well portend a dry, utilitarian tome; this book is anything but that. A mirror of the author's own passion for the subject — or in his own words "my personal World Heritage" — it is a delightfully written, wholly interesting and valuable reference text for all those interested in or working within the world of gems and jewellery. As translator Stephen H. Gill writes in his foreword, "We feel that this book reflects something of his far-reaching curiosity and familiarity with so many aspects of this wonderful trade in natural beauty, a trade that has been with us since the Stone Age."

Akira Chikayama (1921-2007) first published his Japanese language dictionary *Hōseki Hōshoku Daijiten* in 1995. The present English version is based on his revised 2004 3rd edition. A monumental effort was put to bear on translating and editing its 900 pages in order to produce a volume whose scope would serve not just the Japanese gemmological community, but a world-wide audience. It accomplishes this while still retaining its cultural roots, thereby honouring its esteemed author, and in the process edifying the reader with a smattering of uniquely Japanese gem and jewellery terms. In his foreword, supervising editor Alan Jobbins writes of Chikayama's "whimsical sense of humour" and "wide scientific knowledge and experience". This is no less evident than when the reader seeks out a specific definition and, after finding it, is drawn by the diversity contained in surrounding pages, exploring hither and delighting in each interesting nugget of lore, scientific wisdom, gemmological concepts, historical trivia and more.

In order to get the most out of the Dictionary, the readers should be encouraged to read the forewords in order to understand the project's mission and also to familiarize themselves with the explanatory notes. The latter explain the organization and defines abbreviations used throughout, some of which might be unfamiliar. Appendices at the back of the book include some data which might diverge from what is expected, but thus is interesting and informative (e.g. Greek & Latin Prefixes Appearing in Mineralogical & Gemological Terminology). Noticeably absent, though not really missed, is a chart of gem properties; such data is instead included under individual entries in the body of text.

One might fault some entries, but certainly most quibbles have more to do with 'point of view' or the limitations imposed by brevity. For example, the definition for chameleon diamond indicates its 'base colour' is green. If one interprets 'base' to mean the diamond is at groundstate (which is in the dark), then the entry is misleading. If it is interpreted to mean the colour one observes in the light (the only time one can observe it), then it could be deemed perfectly correct. Similarly, when defining cerasite, it is given as a "mineralogical term for columnar trillings of cordierite (iolite)" when in fact these so-called cherry blossom stones (sakura ischi) are more properly described as mica pseudomorphs of complex cordierite-indialite intergrowths. Examples such as these are not in any way negatives unless the reader does not know to dig deeper (hardly the fault of the author); in fact they point to the diversity of the contents. Consider such entries as pikal, selenita, kandoro, kalanchu — just a very few of the terms which hale from gem localities around the world, but which might not be familiar to many readers.

Some minor typos aside, this reviewer would argue a few points, such as that early credit might better go to H.L. Chhibber (1934) rather than E. Gübelin (1965) as having described maw-sit-sit and that most references cited state hematite over lepidocrocite as the inclusion responsible for bloodshot iolite.

Another entry which gives pause due to its wording and punctuation, is that of 'FGA'. After correctly spelling out the abbreviation, it proceeds to identify this as a 'diploma' which is "generally regarded as the world's premium gemmological qualification". Punctuation and brevity of words ironically reflects a commonly held concept of the letters 'FGA' (no periods) as a kind of noun — that 'FGA' is synonymous with having successfully passed the coursework (itself often similarly referred to as 'The FGA'). A dozen more words would have made clear that course completion only makes one eligible for election to FGA status, along with yearly dues to retain the title.

The English translation of this Japanese modern classic is arguably the most important gemmology reference text to come off the press in recent years. It joins Robert Webster's *Gemmologist's Compendium* (revised by E.A. Jobbins) as one of the few gemmological dictionaries currently available in-print and competes neatly with the now out-of print GIA hardcover standards, *The Diamond Dictionary and Dictionary of Gems & Gemology*. While no such book can be considered a stand-alone and should rather be used as a companion to other sources, this exceptional and beautifully produced volume will certainly become a

Book reviews (continued)

standard for gemmologists in a wide range of fields the world over. The completion of this project will forever remain a very fine tribute to the legacy of gemmologist Akira Chikayama FGA CG.

E.A. Skalwold

Ivory Identification, A Photographic Reference Guide

William R. (Bobby) Mann and Charles M. Marts, 2012. Published by Ivorymann Publishing. 20 pp, large format, approx. 200 photographs. Price $20 plus shipping from HP Mag Cloud Publications at http://magcloud.com/browse/issue/458047.

For many years we have relied on just one or two books for the identification of ivories, but now there is another book to aid us in this task. Its main author, Bobby Mann, is a Graduate Gemologist (Gemological Institute of America) and Professional Gemologist, Columbia School of Gemology, USA. He is also a co-founder of the International Ivory Society, and runs workshops on ivory identification in Washington DC.

The book is the first of three planned publications on ivory (books 2 and 3 will go into more detail on the subject of ivory identification); meanwhile this is an excellent reference to help with identifying a material that can be tricky.

Each page is devoted to a different ivory or ivory substitute, from elephant tusk to hornbill ivory, and each contains about 20 photographs – mostly in colour, but in black and white too where this better shows the structure, as is often the case with photographs of ivory. A brief description of each material accompanies the photographs, divided into clear sections: 'Natural Teeth', 'As seen in cross section' and 'LWUV'. Each section is again divided: 'Dentine layer', 'Grain pattern', and so forth.

The book is aimed at the gemmologists, collectors, hobbyists and students who have taken Bobby's ivory workshops. It is a very useful reference for anyone interested in the subject, or who comes into contact with ivory through their work. The facts are delivered by good quality photographs and there is no hunting for details – everything is clearly set out on each page. All in all it is an excellent little publication.

M. Campbell Pedersen

Amazing Amber

Andrew Ross and Alison Sheridan, 2013. 48pp, 150 colour photographs, paperback. £7.99. ISBN 978 1 905267 79 8.

The book *Amazing Amber* has been produced as a catalogue for the exhibition of the same name at the National Museum of Scotland in Edinburgh, which has run during the summer of 2013.

It is not aimed at gemmologists, but is an informative little publication in layman's language, and gives an overview of amber as a material, describing many of the most common types in chronological order. Following a Foreword and Introduction, there are eight chapters, starting with 'What is Amber?', 'Where is Amber from?' and continuing through its various uses, fakes, insect inclusions and ending with a brief mention of whether it is possible to obtain DNA from the insects embedded in the resin.

In spite of being an exhibition catalogue the publication is a good stand-alone book. It would make an ideal introduction to amber for someone who knows little about the material. The inclusion of a chapter entitled 'Amber in Scotland's Past' is the only indication that it was written specifically to accompany the Scottish exhibition. (Amber has been used there for over 5500 years.)

The authors, Drs Ross and Sheridan, are experts in their field, so the information given in the book is reliable. The publication is of a high quality, with plentiful, excellent photographs. A single, small criticism is that in some of the photos the resin looks green. As gemmologists know, this phenomenon often occurs when photographing golden amber, but unfortunately it can encourage the mistaken belief in those with less understanding of the subject that green amber occurs naturally. (It can be overcome by manipulating the photographs slightly to bring them back to the correct colour, but this practice is often frowned upon as 'altering' the pictures.)

This minor detail aside, it is a very pleasing book: a truly excellent 'starter' for anyone with less knowledge of amber, and an informative and pleasing addition to the bookshelf for those with more.

The book is available in bookshops, or from www.nms.ac.uk/books.

M. Campbell Pedersen

Gem-A

THE GEMMOLOGICAL ASSOCIATION
OF GREAT BRITAIN

Gem-A Conference 2013

Friday 1 November — Tuesday 5 November

Understanding Gems™

Visit www.gem-a.com

FRIDAY 1 NOVEMBER

Seminar day

A series of practical half-day workshops will be taking place at Gem-A headquarters.

Guest speakers:

- **Richard Drucker** FGA GG
  Coloured stone grading and pricing workshop II
  (Update on grading coloured gems with new grading methods and information)
- **Arthur Groom**
  Exploring emerald clarity enhancements
- **Craig A Lynch** GG, ACCREDITED SENIOR GEMOLOGIST, AGA
  Is the porridge too hot, too cool, or just right? That is the answer!
  (The Somewhere In The Rainbow™ collection of green grossularite garnet and zoisite from East Africa, with hands-on study)

SATURDAY 2 – SUNDAY 3 NOVEMBER

GOLDSMITHS' HALL, LONDON

Gem-A Conference

Guest speakers:

- **John Bradshaw** GG
  Non-traditional gemstones: The rare, medium-rare and well done
- **David Callaghan** FGA
  In the beginning...
  (The history of the London gem lab)
- **Dr John Emmett**
  The colours of corundum: A search for the soul of a padparadscha
- **Dr Emmanuel Fritsch** GG
  Luminescence — what's in a word?
  (Luminescence in gemmology from basic UV to photoluminescence in HPHT treated diamonds)
- **Arthur Groom**
  Emerald clarity enhancement
- **Brian Jackson** FGA DGA
  Scottish gemstones
- **Dr Jack Ogden** FGA
  Treasure, traders and trickery:
  The Cheapside gems in context
- **Sonny Pope**
  The future in coloured diamonds:
  An introduction to the HPHT multistep process
- **Martin Rapaport**
  The state of the diamond industry
- **Gary Roskin** FGA GG
  Mastering the challenges in diamond grading
- **Chris Sellors**
  English gemstones, Blue John and Whitby jet
- **Shelly Sergent**
  Somewhere In The Rainbow™ Toto, We're not in Kansas anymore!
  (A look at the celebrated The Somewhere In The Rainbow™ gem and jewellery collection)
- **Dr James Shigley**
  The evolving challenge of gem identification

EVENING SATURDAY 2 NOVEMBER

Anniversary Dinner

EVENING SUNDAY 3 NOVEMBER

Graduation Ceremony

- **Martin Rapaport** will present the Awards and give the address.

MONDAY 4 – TUESDAY 5 NOVEMBER

Exhibitions and Visits

Private viewings will be held at London museums, including the Cheapside Hoard at the Museum of London, the forthcoming Pearls exhibition at the V&A, and at the Natural History Museum. There will also be a private viewing of the Crown Jewels at the Tower of London.

To find out more about all of the above visit:
www.gem-a.com/news--events/gem-a-conference-2013.aspx

Proceedings of the Gemmological Association of Great Britain and Notices

New premises

Midsummer Day 2013 saw the departure of Gem-A from 27 Greville Street. The Gem Testing Laboratory first moved into part of no. 27 in 1982. They were joined by the Gemmological Association in 1990, with the second floor, fourth floor and basement being leased in subsequent years as they became available. Unfortunately recent negotiations to renew the lease broke down and the decision was taken to vacate the building, carrying out the necessary dilapidation work.

In April it was discovered that the freehold of 21 Ely Place was available and the Board of Trustees unanimously agreed to try to purchase this property. This was achieved at a price of £2.755 million plus VAT which was mitigated by the Association's charitable status and the use of much of the building for charitable purposes. By the same token Stamp Duty was also avoided due to the charitable status. The sale was completed on 11 June.

Built in 1775 on the site of the Bishop of Ely's London residence, no. 21 lies directly opposite a former home of the Association, Audrey House (named after St Audrey, the saint who founded the Abbey of Ely and after whom the thirteenth-century Chapel still standing in Ely Place is named; her Anglo-Saxon name St Etheldreda) which was bombed in 1941 causing our departure. Bomb damage repair can still be seen on no. 21.

The new building comprises 4250 sq ft over six floors including the basement. The top two floors will be used for administration while the remainder will be used for teaching and member services. The four classrooms on the lower floors have been named after prominent past members of the Association — Herbert Smith, Basil Anderson, Robert Webster and Eric Bruton.

For the first time in many years the Sir James Walton Memorial Library will be on display in its permanent new home on the first floor along with some of the Association's stone collection, and the book and stone collection of the South West Trust.

Editorship

This is the last issue of *The Journal of Gemmology* that will be presided over by Dr Roger Harding. He has been editor since 1994 and has done such an outstanding job that it has proved very hard to find a replacement. We thank Roger for his forbearance while we sought a suitable successor which has taken some time. Roger will remain on hand as advisory editor.

The new editor will be Brendan Laurs. Formerly editor of *Gems & Gemology* and having worked for GIA for almost 15 years, he is the ideal candidate to take on the role. He has many new ideas and would be very pleased to hear from anyone wishing to publish an article or with ideas about *The Journal*. He can be contacted at brendan@gem-a.com.

Brendan Laurs

Gem-A Awards

In the Gem-A examinations held in January 2013, 131 students qualified in the Gemmology Diploma Examination, including six with Distinction and ten with Merit, and in the Foundation Certificate in Gemmology Examination 182 qualified. In the Gem Diamond Examination 42 qualified, including five with Distinction and ten with Merit.

The names of the successful candidates are listed below.

Examinations in Gemmology

Gemmology Diploma

Qualified with Distinction

Dai Huiru, Beijing, P.R. China
Fazlali-Zadeh, Sonia Ariana, Barnes, London
Lu Siyu, Lanzhou, Gansu, P.R. China
Wang Dongqiu, Baoshan, Yunnan, P.R. China
Wang Sijia, Mudanjiang, Heilongjiang, P.R. China
Yin Bei, Shanghai, P.R. China

Qualified with Merit

Ai Qing, Jingzhou, Hubei, P.R. China
Huang Xudong, Shanghai, P.R. China
Huo Kaijie, Beijing, P.R. China
Lin Chun-Yu, New Taipei, Taiwan, R.O. China
Qu Meng, Beijing, P.R. China
Thiebaud, Mandy, Paris, France
Tsai Ko-Wei, Tainan, Taiwan, R.O. China
Venturelli, Adelmo, Morges, Switzerland
Yang Xiaowen, Beijing, P.R. China
Zheng Chen, Anqing, Anhui, P.R. China

Qualified

Alessandri, Matthias, Central, Hong Kong
Altobelli, Martha Claire, Austin, Texas, U.S.A.
Alvernhe, Paul, Nancy, France
An Xueying, Baotou, Inner Mongolia
Au Sui Keung, Shatin, Hong Kong
Bailey, Kate, Aberdeen, Aberdeenshire
Bondar, Ilona, Tooting, London
Bouchard, Claudie, Terrebonne, Quebec, Canada
Buckley, Amanda, Takapuna, North Shore, New Zealand
Chan Chi-Keong, Gene, New Taipei, Taiwan, R.O. China
Chan Hei Yiu, Pok Fu Lam, Hong Kong
Chan Kuan-Lang, Roger Jan, New Taipei, Taiwan, R.O. China
Chau Wai Ying, Tsuen Wan, Hong Kong
Chen Danlu, Shanghai, P.R. China
Chen Gong, Wuhan, Hubei, P.R. China
Chen Jiyi, Huangshi, Hubei, P.R. China
Chen Jizhou, Beijing, P.R. China
Chen Wen-Chi, Taichung, Taiwan, R.O. China
Chen Yin-Chen, Taipei, Taiwan, R.O. China
Chen Ying, Nanning, Guangxi, P.R. China
Cheng Ke, Beijing, P.R. China
Cheng See Sze, Cissy, Sai Kung, Hong Kong
Dai Yu-Ying, Stephanie, Taipei, Taiwan, R.O. China
Dang Ming Li, Suzhou, Jiangsu, P.R. China
Dodero, Stephanie, Asnières-sur-Seine, France
Dong Hai-Chen, Taipei, Taiwan, R.O. China
Dong Yi Ao, Wuhan, Hubei, P.R. China
Doraliyagoda, Kankanamge Rusiru, Mount Lavinia, Sri Lanka
Dryland, Davina, Barton-under-Needwood, Staffordshire
Du Li, Zaoyang, Hubei, P.R. China
Elamri, Tarek, Montréal, Quebec, Canada
Elliott, Beth Ann, Ledgewood, New Jersey, U.S.A.
Fan Pik Shan, Maggie, Tsim Sha Tsui, Hong Kong
Fong Sum Wing, Serena, Tai Koo Shing, Hong Kong
Fritz, Eric William, Taylorsville, North Carolina, U.S.A.
Gan Riyao, Guangxi, P.R. China
Gao Yanzhen, Shihezi, Xinjiang, P.R. China
Glenn, Alison, Chertsey, Surrey
Guo Difei, Shanghai, P.R. China
Heilio, Saara, Bromley, Kent
Herold, Doerte, Zurich, Switzerland
Hu Yuting, Xinyu Jiangxi, P.R. China
Huang Chunxian, Shantou, Guangdong, P.R. China
Huang Yu Ming, Guangzhou, Guangdong, P.R. China
Jezova, Olesia, London
Jiang Wenchao, Laizhou, Shandong, P.R. China
Johansson, Sandra, Kungsbacka, Sweden
Kang Weirui, Shihezi, Xinjiang, P.R. China
Kronenberg, Hugh, Paddington, New South Wales, Australia
Kuo Wen-Yu, Taipei, Taiwan, R.O. China
Lejman, Travis, New York, U.S.A.
Lents, Joshua D., New York, U.S.A.

Leung Yin Chun, Jeannie, Kowloon, Hong Kong
Li Xin, Tianjin, P.R. China
Liang Genmeng, Guangxi, P.R. China
Lin Jin, Taizhou City, Zhejiang, P.R. China
Liu Gaoming, Beijing, P.R. China
Liu Ting Ying, Beijing, P.R. China
Liu Tingjun, Beijing, P.R. China
Liu Xu, Beijing, P.R. China
Loong Suk Min, Stanley, Hong Kong
Lu Baifei, Liuzhou, Guangxi, P.R. China
Lu Biyue, Beijing, P.R. China
Lu Min-Ju, Taipei, Taiwan, R.O. China
Lv Yandi, Beijing, P.R. China
Ma Yunlu, Linfen, Shanxi, P.R. China
Marshall, Angela, Cambridge
Martin-Gutierrez, Francesca Maria, Bounds Green, London
McArley, Lisa Maree, St Kilda, Victoria, Australia
Mei Lin, Nanning, Guangxi, P.R. China
Moussa, Farida, Yangon, Myanmar
Ng Siu Kwai, Kwai Tsing, Hong Kong
Ng So Ching, Tseung Kwan O, Hong Kong
Niu Xiaowei, Beijing, P.R. China
Peng Kuo, Beijing, P.R. China
Peng Mian Yu, Shanghai, P.R. China
Peng Yu-Shin, Taichung, Taiwan, R.O. China
Pino, Orazio, Chiavari, Genoa, Italy
Qian Xiang, Shaoxing, Zhejiang, P.R. China
Quinney, Holly F., Verdun, Quebec, Canada
Raoul, Ando, Aubervilliers, France
Rembeault, Benjamin, Montréal, Quebec, Canada
Roden, Rhiannon, Allestree, Derbyshire
Santarsiere, Miguel Angel, Folkestone, Kent
Shen Tengjie, Shaoxing, Zhejiang, P.R. China
Shi Xianglai, Beijing, P.R. China
Shu Yunsheng, Beijing, P.R. China
Sun Jingxuan, Tianjin, P.R. China
Tang Jiazhen, Wuhan, Hubei, P.R. China
Tang Yali, Beijing, P.R. China
Tian Jia Lu, Shanghai, P.R. China
To Siu Lun, Wong Tai Sin, Hong Kong
Tong Xiaofei, Shanghai, P.R. China
Tsang Yuk Lung, Billie, Shatin, Hong Kong
Tuovinen, Riikka, Vantaa, Finland
Vahman, Sarira, Florence, Italy
Van Lenten, Andrea, Lexington, Kentucky, USA
Wa Sze Man, Winnie, Tseung Kwan O, Hong Kong
Wang Cheng, Beijing, P.R. China
Wang Yang, Beijing, P.R. China
Wang Zi, Beijing, P.R. China
Warner, Simon, Tring, Hertfordshire
Wei Ting, Ledu, Qinghai, P.R. China
Win Htet Naung, Yangon, Myanmar
Wong, Vannessa, Lam Tin, Hong Kong
Wong Wing Nga, Quarry Bay, Hong Kong
Wong Yi Sai, Gloria, Tsim Sha Tsui, Hong Kong
Wu, Anna, Karamay, Xinjiang, P.R. China
Wu Zheng Yuan, Haimen, Jiangsu, P.R. China
Xin Tong, Xi'an, Shanxi, P.R. China
Xu Xiaoya, Ezhou, Hubei, P.R. China
Yang Dongxiu, Beijing, P.R. China
Yang Fei, Beijing, P.R. China
Yao Qiong, Shanghai, P.R. China
Yeung Sin Yee, Sindy, Tin Shui Wai, Hong Kong
Yin Lisha, Jingmen, Hubei, P.R. China
Yu Choi Lin, Tsuen Wan, Hong Kong
Yu Ho Fai, Miranda, Sai Kung, Hong Kong
Zeng Piao, Tianmen, Hubei, P.R. China
Zhang Dan Qiong, Taiyuan, Shanxi, P.R. China
Zhang Shiyin, Chang Tou, Neimenggu, P.R. China
Zhang Ya Peng, Wuhan, Hubei, P.R. China
Zhang Yi Xin, Wuhan, Hubei, P.R. China
Zhang Yichi, Beijing, P.R. China
Zhang Yusheng, Dalian, Liaoning, P.R. China
Zhao Xiaohuan, Beijing, P.R. China
Zhao Zhizhe, Chengdu, Sichuan, P.R. China
Zheng Fangyi, Shanghai, P.R. China
Zhong Rui, Beijing, P.R. China
Zhou Wei, Basel, Switzerland
Zong Xiang, Beijing, P.R. China

Foundation Certificate in Gemmology

Backes, Karina, London
Bai Fangfang, Heze, Shandong, P.R. China
Bailey, Anneabell, Plymouth, Devon
Ban Yuansheng, Nanning, Guangxi, P.R. China
Bhowmik, Abhishek, London
Brown, Victoria, Dunfermline, Fife
Cai Changhua, Ziyuan, Guilin, Guangxi, P.R. China
Cavalier, Sophie, Streatham, London
Chan Ka Lok, Choi Hung, Hong Kong
Chan Kai Hing, Tai Po, Hong Kong
Chan Wai Yu, Tseung Kwan O, Hong Kong
Chan Ya-Ting, Taipei, Taiwan, R.O. China
Chang Hsueh-Pin, Taipei, Taiwan, R.O. China
Chao Ting, Taipei, Taiwan, R.O. China
Cheer, Peter, Somerton, Somerset
Chen Chun-Wen, Taipei, Taiwan, R.O. China
Chen Jingli, Liuzhou, Guangxi, P.R. China
Chen Lingyu, Shanghai, P.R. China
Chen Man Lung, Lam Tin, Hong Kong
Chen Xiaobin, Beijing, P.R. China
Chen Yi, Shanghai, P.R. China

Chen Ying, Nanning, Guangxi, P.R. China
Cheng Cheuk Yu, Tuen Mun, Hong Kong
Cheng Cho Luen, Kowloon, Hong Kong
Cheng Kwok Hoo, Quarry Bay, Hong Kong
Chong, Tanya, Croydon, Surrey
Chong Mui, Yim, Tseung Kwan O, Hong Kong
Chong Ting-Fung, Lannavaara, Sweden
Chou Chia Chia, Taipei, Taiwan, R.O. China
Chung Ching Man, Sheung Wan, Hong Kong
Colloud Aballe, Lydie, La Chaux-de-Fonds, Switzerland
Cope, Emma, London
Corbin, Marie-Hélène, Montreal, Quebec, Canada
Crowther, Lucy, London
Crump, Emma, Reading, Berkshire
Dai Qin, Shanghai, P.R. China
Deng Heng, Guilin, Guangxi, P.R. China
Ding Hai Ju, Tseung Kwan O, Hong Kong
Dix, Eleanor Charlotte, Harrogate, North Yorkshire
Dong Hai-Chen, Taipei, Taiwan, R.O. China
Drake, Florence, London
Dulay, Sundeep, Leamington Spa, Warwickshire
Earl, Jeremy, Kettering, Northamptonshire
Edmundson, Laura, Anerley, London
Elamri, Tarek, Montreal, Quebec, Canada
Fang Qiaoling, Hangzhou, Zhejiang, P.R. China
Fang Xiang, Shanghai, P.R. China
Farr-Barron, Hannah, Newton Abbot, Devon
Féral, Catherine, Paris, France
Finn, Riona, Castleknock, Dublin, Ireland
Floch, Edouard, Paris, France
Ford, Nicola, Ryde, Isle of Wight
Fu Minli, Xiaogan, Hubei, P.R. China
Gong Xiaowen, Shanghai, P.R. China
Grant, Leigh, Gillingham, Kent
Gu Bin Quan, Shanghai, P.R. China
Guo Jing, Shanghai, P.R. China
Guy, Angharad, London
Harrison, Katharine, Worcester
Hasselrot, William Anders, Stockholm, Sweden
He Huishi, Zhuji, Zhejiang, P.R. China
Hector, Liv, Lannavaara, Sweden
Hedström, Emma, Hallstahammar, Sweden
Ho Chun Wai, Hung Hom, Hong Kong
Hong, Bindi, Shanghai, P.R. China
Hopkins, Prudence, Happisburgh, Norfolk
Hrustic, Ibrahim, Marieholm, Sweden
Hu Yue, Shenzhen, Guangdong, P.R. China
Huang Hui Meng, Kaohsiung City, Taiwan, R.O. China
Huang Lilin, Beihai, Guangxi, P.R. China
Huang Liuyun, Guilin, Guangxi, P.R. China
Huang Qicheng, Guangzhou, Guangdong, P.R. China
Huang Shengling, Hepu, Guangxi, P.R. China
Huang Yang Ting, Kaohsiung City, Taiwan, R.O. China
Hucker, Louise, Great Blakenham, Suffolk
Hui Cheuk Fan, Tuen Mun, Hong Kong
Hui Ka Ching, Sha Tin, Hong Kong
Jayarathne, Rasika Waruna, Moratuwa, Sri Lanka
Jayawardena, S.A. Dhaneshi Thamalika, Colombo, Sri Lanka
Jhu Syuan-Rou, Taichung City, Taiwan, R.O. China
Jiang Huiyue, Shandong, P.R. China
Kang Xiao Feng, Shanghai, P.R. China
Kenyon, Janelle, Auckland, New Zealand
Khabrieva, Dilyara, London
Khan, Amina, Kowloon Tong, Hong Kong
Kim Ri Na, Seoul, South Korea
Ko Chih-Li, Taichung, Taiwan, R.O. China
Kolator, Barbara, London
Ku Yun An, New Taipei City, Taiwan, R.O. China
Kuo Chun-Han, Taipei, Taiwan, R.O. China
Kwok Man Yee, Kwai Chung, Hong Kong
Kwok Siu Mi, Kwai Chung, Hong Kong
Lagerstedt, Cecilia, Lannavaara, Sweden
Lai Ruoyun, Lanxi, Zhejiang, P.R. China
Lam Chi Him, Siu Sai Wan, Hong Kong
Lam Wai Ting, Quarry Bay, Hong Kong
Lammertse, Max M. R., Amsterdam, The Netherlands
Lau Chui Ting, Tin Shui Wai, Hong Kong
Leclerc, Charlotte, Paris, France
Lee Yu Bin, Seoul, South Korea
Lei Yaxiu, Xi'an, Shaanxi, P.R. China
Levy, Elsa, Boulogne-Billancourt, France
Li Pengfei, Kuitun, Xinjiang, P.R. China
Li Pingting, Wuhan, Hubei, P.R. China
Li Sum In, Sally, Causeway Bay, Hong Kong
Li Wenfeng, Tai'an, Shandong, P.R. China
Li Xiaofeng, Lianjiang, Fujian, P.R. China
Li Yi-Chen, Taipei, Taiwan, R.O. China
Lin Kai Yuan, New Taipei City, Taiwan, R.O. China
Lin Kun-Yan, Taipei, Taiwan, R.O. China
Liu Nianchuan, Yangzhou, Jiangsu, P.R. China
Lo Kuo-Feng, Zhongli City, Taiwan, R.O. China
Lo Siu Kian, Sha Tin, Hong Kong
Lou Ying, London
Lueviboonrat, Gunyasiree, London
Lui, Jo Weng Allan, Chai Wan, Hong Kong
Luk Tong Teng, Yuen Long, Hong Kong
Mak Shuk Kwan, Kowloon, Hong Kong
Malarin, Christian, Paris, France
Mancioppi, Laura, Genoa, Italy
Meng Mingqi, Guilin, Guangxi, P.R. China
Minelli, Adriana, Toronto, Ontario, Canada

Moore, Harriette, Newbury, Berkshire
Moorhead, Anna, London
Nassi, David, Norwalk, Connecticut, U.S.A.
Nayak, Asha, Egham, Surrey
Nyein Aye Than, Khin, Yangon, Myanmar
Orlova, Elena, Genoa, Italy
Ovesen, Hasanthi, London
Pan Ai, Taipei, Taiwan, R.O. China
Parkin, Charlotte, Caterham, Surrey
Petropoulou, Eleni, Athens, Greece
Philippe, Sophie, Paris, France
Prochniak, Ada, Barnet, Greater London
Qin Yayun, Yulin, Guangxi, P.R. China
Quinlivan, Melissa, Christchurch, New Zealand
Ramlov, Hans, Copenhagen, Denmark
Reading, Charlotte, Nuneaton, Warwickshire
Regan, Lisa, Collaroy, New South Wales, Australia
Rodwell, Nathalie, Earlsfield, London
Rykova, Elena, Yangon, Myanmar
Saksirisamphan Rimml, Phornthip, Näfels, Switzerland
Saleem, Melanie, Manchester, Greater Manchester
Schuler-Immoos, Gertrud, Gants Hill, Essex
Shen Yi, Changzhou, Jiangsu, P.R. China
Shin Gi Eun, Kyunggi-Do, South Korea
Soe Ye Htet, Yangon, Myanmar
Su Yung Chu, Kaohsiung City, Taiwan, R.O. China
Syn Hla Maw, Phyu, Yangon, Myanmar
Tam Yin Hung, Tseung Kwan O, Hong Kong
Tang Tiankai, London
Tanswell, Thomas, Rochester, Kent
Than Oo, Bo Bo, Yangon, Myanmar
Thierrin, Laure-Anne, Porrentruy, Switzerland
Tiegler, Thomas, Sante Fe, New Mexico, U.S.A.
Tsang Lan, Kim, Tuen Mun, Hong Kong
Tung Jen-Hao, Taichung, Taiwan, R.O. China
Wang Lin, Xuzhou, Jiangsu, P.R. China
Weldon, Tamara, Whitefield, Greater Manchester
White, Holly, Shepton Mallet, Somerset
Wong Cheung, Kwai Chung, Hong Kong
Wong Fang, Singapore
Wong Fu Wing, Cheung Sha Wan, Hong Kong
Wong Mei Sze, Tseung Kwan O, Hong Kong
Wong Nga Ting, Tuen Mun, Hong Kong
Wong Yu Ting, Tai Po, Hong Kong
Woo Kyung Hee, Seoul, South Korea
Wright, Abby, New Plymouth, New Zealand
Xu Xinhang, Guilin, Guangxi, P.R. China
Yang Jiong, Tai'an, Shandong, P.R. China
Yang Qiujing, Singapore
Yeah Chia Kai, Singapore
Yeung Ming Wai, Percy, Kowloon, Hong Kong
Yung Hoi Yan, Central, Hong Kong
Zhang Mengyi, Shanghai, P.R. China
Zhang Ruxiang, Shanghai, P.R. China
Zhang Yun, Weihai, Shandong, P.R. China
Zhao Junlong, Wulumuqi, Xinjiang, P.R. China
Zhao Yijia, Shaoxing, Zhejiang, P.R. China
Zheng Juanjuan, Laibin, Guangxi, P.R. China
Zhou Qianmin, Jieshou Town, Guangxi, P.R. China
Zhou Yonghang, Jinhua, Zhejiang, P.R. China

Diamond Diploma examination

Qualified with Distinction

Higgo, Emma, Hindhead, Surrey
Li Wenli, Beijing, P.R. China
Li Ziyue, Zhuhai, Guangdong, P.R. China
Stevens, Sophie, Kingston-upon-Thames, Surrey
Tsang Yuet Ming, Tuen Mun, Hong Kong

Qualified with Merit

Bratek, Elizabeth Jane, Romford, Essex
Burden, Maxwell, Birmingham, West Midlands
Chiang Cheng-Hsien, New Taipei, Taiwan, R.O. China
Evans, Rachel Mary, Stebbing, Essex
Fung Hoi Ching, Yuen Long, Hong Kong
Leung Ho Chin, Taikoo Shing, Hong Kong
Lou Hongwei, Beijing, P.R. China
Mak Ka Wai, Kowloon, Hong Kong
Xie Chenyu, Beijing, P.R. China
Yates, Elspeth, Aberdeen, Aberdeenshire

Qualified

Anand, Shraddha, Uttaranchal, India
Armstrong, Larisa, London
Brar, Denesha, Hounslow, Middlesex
Chan Hoi Ping, Tsim Sha Tsui, Hong Kong
Chau Wai Yuk, Kowloon, Hong Kong
Chen Jing, Zhujiang New Town, Guangzhou, P.R. China
Chou Yun-Wen, Taipei, Taiwan, R.O. China
Chu Wai Hung, Kowloon, Hong Kong
Chui Kwan Fung, Kowloon, Hong Kong
Feng Wei, Guangzhou, Guangdong, R.O. China
Hui Sin Kam, Tseung Kwan O, Hong Kong
Kanda, Sonia, Farnham Royal, Buckinghamshire
King, Chantiel, London
Ku Yee Ling, Tsing Yi, Hong Kong
Kwok Hei Tung, Hung Shui Kiu, Hong Kong
Law Pui Lun, Sham Tseng, Hong Kong
Legros, Maria, London

Li Wenjie, Zhujiang New Town, Guangzhou, P.R. China
Lin Dongyu, Zhujiang New Town, Guangzhou, P.R. China
Lin Yi Ping, Taipei, Taiwan, R.O. China
Liu Jian Yi, Guangdong, Guangzhou, P.R. China
Lui Sin Ting, Fiona, Tsuen Wan, Hong Kong
Ma Yaqi, Beijing, P.R. China
McWhirter, Hannah Maeve, Bury St Edmunds, Suffolk
Mok Ka Yan, Kowloon, Hong Kong
Nadal, Cynthia, London
Ng Wai Fong, Kowloon, Hong Kong
Ng Yat Sen, Natalie, Hong Kong
Robinson, Kristin, Wanstead, London
Tang Ying, Xiangyang, Hubei, P.R. China
Tsai Ko-Wei, Tainan, Taiwan, R.O. China
Valle, David, Tunbridge Wells, Kent
Wang Jing, Beijing, P.R. China
Wang Shuishui, Beijing, R.O. China
Wang Xiaohan, Beijing, P.R. China
White, Lucy, Virginia Water, Surrey
Wilding, Mark, St Helens, Merseyside
Wong Hing Yee, Yuen Long, Hong Kong
Wu Shih-Yu, Taipei, Taiwan, R.O. China
Xu Min Min, Pok Fu Lam, Hong Kong
Yeung Woon Ying, Maggie, Kwai Chung, Hong Kong
Zhao Yichen, Beijing, P.R. China

Annual General Meeting

The Annual General Meeting was held on Wednesday 3 July 2013 at the Naval Club, London W1J 5NS. The meeting was chaired by Harry Levy, the President of the Association. The Annual Report and Accounts were approved. Brian Jackson and Cally Oldershaw who retired from the Council by rotation, and Paul Greer, Nigel Israel and Stephen Whittaker who had been appointed by the Council since the 2012 Annual General Meeting. were re-elected.

Hazlems Fenton were re-appointed as auditors for the year.

The AGM was followed by a talk by James Riley entitled 'One hundred not out', on the Gem-A Gemmology Diploma which celebrates its centenary this year.

Membership

During the period January to June 2013, the Council approved the election to Membership of the following:

Fellowship and Diamond Membership (FGA DGA)

Wong, Winnie, Tsimshatsui, Hong Kong

Fellowship (FGA)

Alessandri, Matthias, Central, Hong Kong
Boisserand, Anne, Fréjus, France
Bruyère, Manon-Océane, L'Isle-sur-la-Sorgue, France
De Wit Sandstrom, Ida Marianne, Dalby, Sweden
Dryland, Davina, Burton-upon-Trent, Staffordshire
Forsner, Christina, Södra Sandby , Sweden
Frederick, Helen, Wellington, New Zealand
Fremy, Pierre, Bois-Colombes, France
Glenn, Alison, Chertsey, Surrey
Huang Yuan, Birmingham, West Midlands
Jayawardene, D. M. Dulip, Peradeniya, Sri Lanka
Lavoie, Martine, Montreal, Quebec, Canada
Li Qi, Guilin, Guangxi, P.R. China
Marshall, Angela, Cambridge
Negus, Patricia, Ushaw Moor, County Durham
Perry, Charles, Ampthill, Bedfordshire
Porter, Rex, Hook, Hampshire
Roden, Rhiannon, Allestree, Derby
Sanders, Esmee, Amsterdam, The Netherlands
Venturelli, Adelmo, Morges , Switzerland
Verdoorn-De Vrede, Veronica, Dordrecht, The Netherlands
Yang Mingyu, Jinan, Shandong, P.R. China

Diamond Membership (DGA)

Burden, Maxwell, Birmingham, West Midlands
Thomas, Jade, London
Valle, David, Tunbridge Wells, Kent
Wilding, Mark, Ecclestone, Merseyside
Wong Yu Ting, Tai Po, Hong Kong

Associate Members

Bekker, Alina, Haywards Heath, West Sussex
Burley, Lorraine, Hythe, Cornwall
Hendry, David, Oakland, California, U.S.A.
McReynolds, Meghan, Evansville, Indiana, U.S.A.
Williamson, Eleanor, London

Gold Corporate Membership

Carl's Japan Inc., Takamatsu City, Kagawa, Japan
GemLab Jewellery Valuers, Auckland, New Zealand
Japan Germany Gemmological Laboratory, Kofu, Yamanashi, Japan

Gifts and Donations to the Association

The Association is most grateful to the following for their gifts and donations for research and teaching purposes:

Joanna Angelett, London, for a sample of rough rough stromatolite.

Jeffrey Lee Bergman, Las Vegas, Nevada, U.S.A., for a copy of *An Emerald Encryption – The Abhaya Emerald Buddha* by Cameron Cooper and Pascal Butel, and three cabochon-cut trapiche sapphires.

Bezalel Gems Ltd, London, for faceted diffusion-treated sapphires.

Chao-Ming Wu FGA DGA, Taipei, Tiawan, R.O. China, for a piece of nephrite from Hualian, Taiwan.

Dr Tanya Chong, Croydon, Surrey, for a twinned gypsum crystal.

Eiko Ito FGA DGA, Jewellery Craft School, Tokyo, Japan, for a copy of *Practical Wax Modeling : Advanced Techniques for Wax Modelers* by Hiroshi Tsuyuki and Yoko Ohba.

Charles M. Ellias GG, Palladot Inc., Clawson, Michigan, U.S.A., for an assorted collection of pallasite peridot crystals and cut stones.

John Greatwood FGA, Mitcham, Surrey, for a black synthetic moissanite simulating black diamond.

Bill Kasso, Eagle Creek Opals, Queensland, Australia, for samples of opal replacement of coral and wood in rock.

John Kessler, J.A. Kessler Ltd, London, for a large quantity of assorted stones (see *Gems&Jewellery,* **22**(4), June 2013, page 9).

Bart Krijger FGA, The Hague, The Netherlands, for a selection of artificial and synthetic gemstones, including glass, plastic, doublets, synthetic spinel and synthetic corundum. Mr Krijger donated the stones in celebration of 40 years as a Fellow of the Association; he was awarded his Gemmology Diploma with Distinction in 1973.

Shawn Maddox Gem Cutting, Austin, Texas, U.S.A., for a sphere of andradite displaying cat's-eye from Southern Diablo range, San Benito, California.

MRD Import-Export GmbH, Vienna, Austria, for rough and faceted demantoid garnet from Green Dragon mine, Erongo, Namibia.

Renee Newman GG, Los Angeles, California, U.S.A., for a copy of her book *Gold, Platinum, Palladium, Silver and Other Jewelry Metals*.

Helen Serras-Herman FGA, Rio Rico, Arizona, U.S.A., for a piece of galactic jade (black jadeite with pyrite) and a slab of pink angel skin chalcedony from Graham County, Arizona.

E.A. Thomson Gems Ltd., London, for a large number of faceted green soude stones.

Ray Zajicek, Equatorian Imports Inc., Dallas, Texas, U.S.A., for red beryls from the Wah Wah mountains, Utah, including crystals on the host rock and faceted stones.

Monetary donations were gratefully received from:

Vincenzo De Michele, Milan, Italy
James C. Finlayson FGA, Stoke-on-Trent, Staffordshire
Gwyn Green FGA DGA, Barnt Green, Birmingham, West Midlands
Barbara Kolator, London
Torbjorn Lindwall FGA DGA, Lannavaara, Sweden
Elaine Rowley FGA DGA, London
Moe Moe Shwe FGA, Singapore
Wanda Hoi Chi Wat FGA, Kowloon, Hong Kong
Jiewen Zhang DGA, Shanghai, P.R. China

Corporate Membership

M&J Gems Ltd , Birmingham, West Midlands

Transfers

Fellowship to Fellowship and Diamond Membership (FGA DGA)

Evans, Rachel, Stebbing, Essex
McWhirter, Hannah Maeve, Bury St Edmunds, Suffolk
Stevens, Sophie, Kingston-upon-Thames, Surrey
White, Lucy, Virginia Water, Surrey

Diamond Membership to Fellowship and Diamond Membership (FGA DGA)

Warner, Simon, Tring, Hertfordshire

Associate Membership to Fellowship (FGA)

Drucker, Richard, Glenview, Illinois, U.S.A.
Herold, Dorte, Zürich, Switzerland
Kronenberg, Hugh, Paddington, New South Wales, Australia
Matlins, Antoinette, Woodstock, Vermont, U.S.A.
Riley, James, Knutsford, Cheshire
Williams, Bear, Jefferson City, Missouri, U.S.A.

Obituary

Michael Ngan FGA DGA (D. 2004), Hong Kong, died recently.

Manuel Maria Ramos Pinto Rosas FGA (D. 1949 with Distinction), Porto, Portugal, died in December 2012. He was the first person in Portugal to qualify in the Gemmology Diploma examination, and was involved in the selection and setting of the gems in the Portuguese Crown Jewels.

Joseph W. Tenhagen FGA (D.1969), Miami, Florida, U.S.A., died 27 April 2013 at the age of 79.

Joseph (Joe) was involved in the gem and jewellery trade for over 40 years as an appraiser and consultant, and was actively involved in a number of trade organizations. He was a member of the Accredited Gemologists Association (AGA) and was appointed president from 1981 to 1984. Joseph joined the National Association of Jewelry Appraisers (NAJA) in 1992 and served as its associate director. He was also a charter member, past president and past secretary of the Diamond Dealers Club of Florida until 2005. Joe published the *Diamond Value Index* from 1995 to 1998, and many of his articles appeared in trade journals.

Joseph Tenhagen was a keen and much-valued supporter of Gem-A education. Over the years he donated large quantities of rough and cut gemstones for use in our courses and examinations. During a trip to the UK in 2002 he gave a presentation to Gem-A members entitled 'New aspects of cut in round brilliant-cut diamonds'.

Said Antoinette Matlins of AGA: "Joe was a close friend of AGA founder, Tony Bonanno, and the two made an awesome team! They were part of that special generation — that unique 'breed' of gemmologists — who helped determine the very course of gemmology in the USA, and the role that gemmologists would serve in raising the ethical and professional standards within the broader jewellery world."

Joe will be sadly missed by all who had the pleasure to know him. He leaves his wife Mary, a son and two grandchildren.

Lord Ian Balfour

21 December 1924 – 14 April 2013

The Hon. Ian Balfour, 2nd Baron of Inchrye — Ian to his friends and people he knew — died on 14 April 2013.

Balfour, diamond expert, author, composer, will be missed by many as a kind and loyal friend. Born on 21 December 1924, he succeeded his father in September 1988, entering the House of Lords as a Cross Bencher. Educated at Eton, he served in the Royal Navy during the Second World War and on his release went up to Magdalen College, Oxford, to read modern languages and music.

Coming down from university, he worked for a while at Anglo American. This did not tax him greatly and he went to work at the Diamond Trading Company (DTC), the selling arm of De Beers. There he sat at a bench like any other trainee and sorted diamonds. He was a burst of fresh air into the rather formal working conditions there. A great practical joker, he was not averse to bringing them into the office; a great peal of laughter would come from his bench as someone fell for one of his japes.

His sorting days came to an end when, as he once put it: "Catastrophe struck. All the trays were laid out for the right handed, but I am left handed. One day I caught my tweezers on something and all the contents went haywire."

This happened at a time when the press and the public were beginning to want to know more about diamonds. A knowledgeable person was required to do this and he was given the job. He settled into his new task producing a 'Glossary of Terms used in Sorting', a first of its kind. A copy is in the library of the Gemmological Association.

In collaboration with Norman Harper he wrote the first diamond courses for the Gemmological Association and, together with Professor Tolansky, Professor of Physics at London University, was an examiner.

It was around this time that his exhaustive research into famous diamonds bore fruit with a compilation in 1959 entitled *Notes on Famous Diamonds*. This was followed by two booklets on the subject. Further study was undertaken culminating in the production of the first edition of *Famous Diamonds* in 1987, which he dedicated to his wife Maria, whom he married in November 1953.

This was a labour of love and thought by some to come from his close association with Sir Ernest Oppenheimer, whose love of diamonds was well known.

Leaving the DTC, he joined Hennigs, the prestigious firm of diamond brokers. Established in 1890 it brokered the purchase of the Jonkers in 1935 and the Star of Sierra Leone in 1970, the third largest diamond found, weighing 968.9 ct (or nearly half a pound avoirdupois).

His easy manner and friendly attitude made him a great success with the clients, both when they came to London to the De Beers' Sights and when he visited them in their cutting centres.

In addition to his work in diamonds, researching new material for his next edition of *Famous Diamonds*, he also found time for his other love, music. He composed nine operas and a number of orchestral and vocal pieces, which were performed in a number of cities throughout the world. After thirty years in diamonds he retired and became a consultant. He was working on the sixth edition of his book when a car accident resulted in a broken collar bone. From then on his health deteriorated and he died on 14 April 2013. With his death the title became extinct. He is survived by his daughter Roxane, born in September 1955.

On page 48 of the first edition of *Famous Diamonds*, Ian had written: "All who write about the history of diamonds must forever remain grateful to Jean Baptiste Tavernier." A reviewer of the book at that time wrote: "Today, the same can be said about Ian Balfour." Never was a truer word written, for today he has left a monumental work which will be a boon for scholars for many years to come.

Johnny Roux

Gem-A

THE GEMMOLOGICAL ASSOCIATION OF GREAT BRITAIN

50 YEARS OF THE FIRST DIAMOND DIPLOMA

50

– Gem-A celebrates –

100

100 YEARS OF THE FIRST GEMMOLOGY DIPLOMA

Achieve your potential

Gem-A Gemmology and Diamond Courses

A strong knowledge of gemstones and diamonds will increase customer confidence and boost your sales. Gain that knowledge by studying with the world's longest established educator in gemmology. Graduates may apply for election to Fellowship or Diamond membership of the Association enabling them to use initials FGA or DGA after their name.

GEM-A COURSES

- Gemmology Foundation*
- Gemmology Diploma*
- Diamond Diploma

* Course notes are available in Simplified and Traditional Chinese, Japanese and French as well as in English.

STUDY OPTIONS

As well as attending day or evening classes at our headquarters in London, students may study worldwide with the following study options:

- Open Distance Learning — Study online with a wealth of online resources
- Accredited Teaching Centres (ATC) — Study at one of our ATCs
- Gem-A Approved Practice Providers GAPP — ODL students may visit a GAPP for the practical lab class
- Blended Learning – Online and on-site at our London headquarters

Full details of all courses are given at www.gem-a.com/education.aspx or call +44 (0)20 7404 3334 email education@gem-a.com

Understanding Gems™

Visit www.gem-a.com

The Journal of
Gemmology
2013 / Volume 33 / Nos. 5–6

Contents

Cover Picture: Multiphase vapour-liquid-solid inclusions in unheated tanzanite from Merelani, Tanzania. (See 'Liquid hydrogen sulphide (H_2S) fluid inclusions in unheated tanzanites (zoisite) from Merelani, Tanzania: Part 2. Influence on gem integrity during and after heat treatment', page 161.)

The Gemmological Association of Great Britain

21 Ely Place, London EC1N 6TD, UK
T: +44 (0)20 7404 3334 **F**: +44 (0)20 7404 8843
E: information@gem-a.com **W**: www.gem-a.com

Printed by DG3 (Europe) Ltd
ISSN: 1355-4565